THEORETICAL AND SIMULATION STUDY ON OGSTON SIEVING OF BIOMOLECULES USING CONTINUUM TRANSPORT THEORY

LI ZIRUI

(M. Eng, NUS)

A THESIS SUBMITTED

FOR THE DEGREE OF DOCTOR OF PHILOSOPHY

DEPARTMENT OF MECHANICAL ENGINEERING

NATIONAL UNIVERSITY OF SINGAPORE

2008

Acknowledgements

I would like to express my deepest gratitude to my supervisor, Prof. Liu Gui Rong, for providing me with this invaluable opportunity for my Ph.D. study, and for his invaluable guidance and continuous support throughout all these years. His profound knowledge, enthusiasm in research and the passion to excel have been the most important sources of my strength and will continue to influence me for the whole life. I would also like to extend my gratitude to professors who are working on the same project, Prof. Jongyoon Han (MIT), Prof. Chen Yu Zong, Prof. Wang Jian-Sheng, Prof. Nicolas Hadjiconstantinou (MIT) for numerous valuable advices, comments and suggestions for my research work and for paper publications. I am grateful to former NUS professor Nikolai K. Kocherginsky for his helpful advices and continuous encouragements. The membrane transport theory he taught me in his class served as the starting point for my research.

Many thanks are conveyed to my fellow colleagues and friends in Center for ACES, Dr. Zhang Guiyong, Dr. Deng Bin, Dr. Kee Buck Tong, Dr. Cheng Yuan and Mr. Song Cheng Xiang. Their friendship and encouragement are important beyond words. I am extremely grateful to my wife, Zhang Xin and my son, Li Zuo Wei. Being constant source of love and encouragement, they have been supporting me silently for all these years.

Finally, this work was supported by Singapore-MIT Alliance (SMA)-II, Computational Engineering (CE) program.

Table of Contents

Summary

Separation of biomolecules using polymeric gels is one of the most important tasks and has become a standard routine practice in various biological or medical applications. Although such processes are performed everyday all over the world, the physical mechanisms behind them remain far from clear, especially those involving the entropic effect due to the loss of the configurational degree of freedom. Recently a number of microfabricated nanofilter devices have been developed as the potential substitute for the gels for research and industrial purposes.

This thesis studies electrophoretic separation of the rod-like short DNA molecules over repeated regular nanofilter arrays consisting of alternative deep and shallow regions. Unlike most methods based on stochastic modeling, this thesis reports a theoretical study based on macroscopic continuum transport theory. In this study, an entropy term that represents the equilibrium dynamics of rotational degree of freedom is inserted to the macroscopic transport equations. Analytical formulas are derived from a one-dimensional simplified description and numerical methods are developed to solve the general three-dimensional nanofiltration problem. It is demonstrated that the complex partitioning of rod-like DNA molecules of different sizes over the nanofilter array can be well described by the continuum transport theory with the orientational entropy and confinement induced anisotropic transport parameters properly quantified.

The first part of the thesis is devoted to the mechanisms and quantification of orientational entropy of the rod-like DNA in aqueous solution and in the confined space. Configurational entropy and the flux caused by entropic differences are derived

from the equilibrium theory of rotational and translational diffusions.

The second part contributes to the development of a simplified one-dimensional transport model, from which important analytical expressions of the mobility and the dispersion are obtained. Effects of all the considered factors are explicitly given. A method for the assessment and optimization of the nanofilter arrays is proposed. It is expected to serve as the handy theoretical tool for the experimentalists to predict the performance of the nanofilters.

The last part of the thesis describes a more complex three-dimensional model in which the non-uniform electric field and the anisotropic flux of the molecules are considered. Effects of the confinement on the transport parameters of the DNA in the shallow channels are calculated. Numerical methods to solve the anisotropic transport equations are developed based on the smoothed particle hydrodynamics formulation. The results of simulation are compared with the experimental data.

The most important contributions of this thesis to the field of nanofiltration are highlighted as follows: (1) It is demonstrated that the macroscopic continuum model is capable of description of Ogston sieving process in nanoscale filtration systems, as long as the microscopic physics that are averaged to zero in macroscopic scale are restored appropriately. (2) Using a simplified one-dimensional model, analytical expressions for the mobility and dispersion in nanofiltration systems are obtained. These formulas describe the effects of several physical mechanisms explicitly. They are currently the only tools that experimentalists can rely on to assess and optimize their nanofilters. (3) The role of the rotational diffusion of an anisotropic particle on its partition near a solid wall are realized and quantified. Better understanding might be achieved when this effect is considered in analysis of nanoscale transport problems.

Nomenclature

a	radius of a DNA
A_I	anisotropy factor
$\bar{c}$	averaged concentration of DNA in the well
C	concentration
C_{gel}	gel concentration
d	diameter of a DNA
d_d, d_s	depths of the deep and the shallow regions of the nanofilter
$\mathcal{D}^d(\Theta)$	anisotropic diffusion coefficient in DNA's local coordinate system
$\mathbf{D^d(r)}$	diffusion coefficient tensor in at **r** global coordinate system
D^d	free-solution translational diffusion coefficient (experimental result)
$D_{//}$, $D_{\perp}$	translational diffusion coefficients along, perpendicular to the axis of DNA
D'_j	relative effective diffusion coefficient in coordinate direction j
D^r	rotational diffusion coefficient of DNA
E_{av}	external field strength.
E_d, E_s	external field in deep and shallow regions of the nanofilter.
ϵ	Electro-chemical potential of DNA
f	fraction free volume
f_r	rotational friction coefficient
H	plate height

$\mathbf{J}(\mathbf{r}), J(x)$	three-dimensional and one-dimensional fluxes of DNA
k_B	Boltzmann constant
K	partition coefficient between shallow and deep regions
K_d, K_s	partition coefficient in the shallow and deep regions
l_s, l_d	lengths of shallow region and deep region of the nanofilter
l_r	repeat length of nanofilter array
L	length of DNA
$\widetilde{L}$	total length of the nanochannel
M	analyte molecular size
n	repeat number of nanochannel
$\widetilde{n}$	amount of solute;
$\mathbf{n}$	normal vector of the channel surface
N	base pair number of the DNA
N_θ	frictional torque on a DNA rod
$P(\mathbf{r},t)$	probability that the tip of rotational DNA is located at $\mathbf{r}$ at time t
$p(\mathbf{\Theta} \mid \mathbf{r})$	probability that a molecule is not oriented at $\mathbf{\Theta}$ when it's located at $\mathbf{r}$
q	net charge of an electrolyte
$\tilde{q}$	effective charge of a DNA molecule
$\mathbf{r}$	position of the center of DNA in global system
R	gas constant
R_h	hydrodynamic radius
r_t	translational distance in diffusion
S	general entropy

S_Θ	orientational entropy
T	absolute temperature
$U(x)$	potential of DNA in the nanochannel.
U^S	mobility to "entropic force"
U^d	the mobility of DNA rods in translational diffusion
$U^e, \overline{U}^e$	isotropic free-solution electrophoretic mobility (experimental result)
$U_{//}, U_\perp$	mobility of DNA when the rod is parallel, perpendicular to electric field
U_{EEO}	electro-osmotic mobility
U'_j	relative diffusion coefficients in coordinate direction j
$\boldsymbol{\mathcal{U}}^e(\boldsymbol{\Theta})$	anisotropic electric mobility in DNA's local coordinate system
$\mathbf{U}^e(\mathbf{r})$	electric mobility at $\mathbf{r}$ global coordinate system
$\widetilde{V}$	one-dimensional apparent translation velocity
w	width of the nanofilter
$W(r)$	smooth function
ΔW	potential energy barrier
y_m	reduced electric potential
γ, δ, ν_c	correction terms in calculating diffusion coefficient or mobility of DNA
ν	ratio of depths of shallow and deep region of the nanofilter
η_0	the viscosity of the solvent
κ_D	Debye-Hückel parameter, κ_D^{-1} is the Debye length
$\kappa(\mathbf{r})$	local partition function
$\rho_\Theta(\mathbf{r})$	probability that a molecule is not intersected by the channel wall

σ_T^2	spatial variance of DNA band
λ_p	the effective persistence length
τ_r	rotational correlation time
τ_{travel}	travelling time of electrolyte over nanofilter without entropy barrier
τ_{trap}	trapping time of electrolyte by nanofilter due to entropy barrier
μ	mobility in the device
μ^0	standard-state chemical potential
μ^*	reduced mobility
μ_0	free-solution electrophoretic mobility
ζ	friction coefficient
ζ^d	friction coefficients for diffusion
$\zeta_{//}^d, \zeta_{\perp}^d$	translational hydrodynamic friction coefficients along, perpendicular to the axis of a cylinder under diffusion
ζ^e	friction coefficients for electric driven motion
$\zeta_{//}^e, \zeta_{\perp}^e$	translational hydrodynamic friction coefficients along, perpendicular to the axis of DNA in electric field
Ω_r	angular velocity of DNA rod
$\Omega(\mathbf{r})$	accessible microscopic orientation state integrals at location $\mathbf{r}$
Φ	external electric potential
Γ	zone broadening rate
$\boldsymbol{\Theta}=(\theta,\phi)$	spherical polar coordinates

List of figures

1 Introduction

1.1 Background

As the carrier of the heredity, deoxyribonucleic acid (DNA) is a highly complex macro-molecule. It contains all the necessary information responsible for the biological identity of a specific species and for a particular individual in this species. Naturally, DNA is a long thin thread-like molecule made of nucleotides constructed from the bases adenine (A), thymine (T), guanine (G) and cytosine (C). Two complementary strands are kept together by the hydrogen bonds between the A-T and C-G nucleotide pairs (see Fig. 1.1). Because DNA molecules go by pairs that are exactly complement of each other, they are able to replicate. The sequence of nucleotides contains the codes for the synthesis of all the proteins and other biomolecules. Segments of DNA encoding specific proteins are called genes.

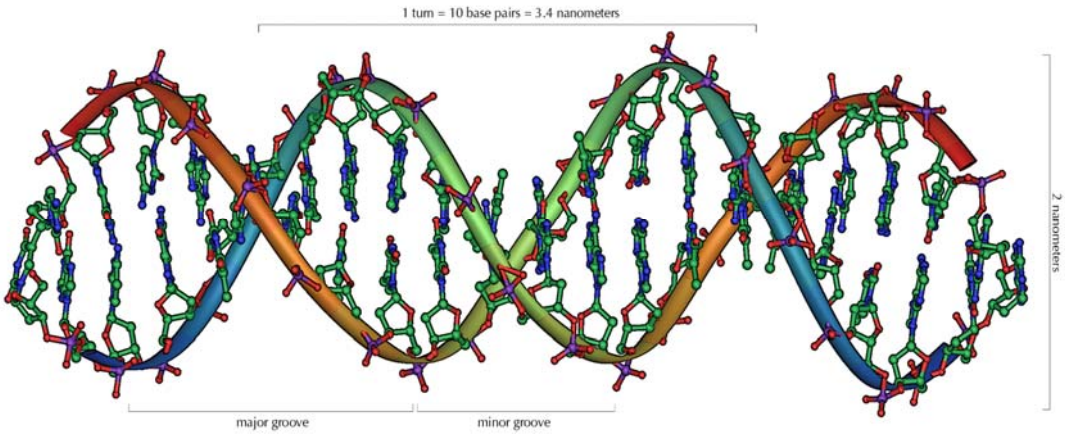

Fig. 1.1. The structure of a double stranded DNA molecule (image courtesy of http://en.wikipedia.org/wiki/DNA). The two stands of the DNA are compliment to each other. An adenine (A) forms a pair with thymine (T) and guanine (G) forms pair with cytosine (C).

Deciphering genes by determining the DNA sequences and their generic functions is therefore the first step to the understanding of life and is the core task in basic research studying fundamental biological processes. Practically, in the genome sequencing process, short pieces of chromosomes are broken down into a set of DNA fragments that differ in length from each other. The fragments in this set are separated according to their lengths, which enables the identification of the sequence of bases of each fragment. The sequences of the chromosome pieces (DNA segments) from which these fragments are generated are then obtained.

As one of the most important step in the above processes, separation of DNA molecules by size has become one of the most essential techniques in the analysis of restriction endonuclease digests of genomic DNA and polymerase chain reaction (PCR) products. The separation of DNA molecules are normally performed through application of an electric field. A DNA backbone has one dissociable proton per phosphate group. Ionization of phosphate causes the negative charge on DNA. This negative charge provides electrostatic force to DNA molecules in the solution. The free-solution electrophoretic mobility, which characterizes the speed of a DNA obtained in free solution when a unit electric field is applied, is found to be independent of sizes of DNA if the DNA molecules are longer than a few hundred base pairs. This feature is due to the balance between the hydrodynamics drag of the polymer and the opposing counterions forces (Muthukumar, 1997). As a result, DNA molecules can not be fractioned in free solution. However, DNA molecules of different size can be separated through gels because of the combined effects of electric force, interaction with the surrounding fluid and steric forces exerted by the gel fibers. Longer DNA molecules have decreased electrophoretic mobility due to increased collisions with the gel matrix. Similarly, a narrower gel pore also reduces

the electrophoretic mobility of the molecules passing through it. Apart from DNA molecules, other types of polyelectrolytes including RNAs, denatured proteins, most polysaccharides and synthetic polyelectrolytes can also be separated in gel. Nowadays, gel electrophoresis is performed everyday as standard process in many industrial applications and research projects (Viovy 2000).

As the foundation of gel electrophoresis theory, Ogston-Morris-Rodbard-Chrambach (OMRC) model (Ogston, 1958; Rodbard and Chrambach, 1970; Morris,1966) states that the gel electrophoretic mobility of biomolecules is determined by the ratio of the characteristic size of the random porous network and that of molecules in solution. It is found later that OMRC model is only applicable to the cases of small molecule electrophoresis with low electrical fields and low gel concentrations. For more complicated situations, more sophisticated models and extensive calculations are required (Locke and Trinh, 1999). Although a large number of modifications have been suggested for OMRC model trying to address the problem of hindered transport of biomolecules with arbitrary shapes through porous gels, the interpretation of experimental data for even simple, rod-like cylindrical molecules is still far from satisfactory (Allison et al., 2002). It has been realized that, in addition to the characteristic sizes of the molecule and the gel pore, comprehensive interpretation of experimental data for systems involving anisotropic solutes requires information about entropic barrier that originates from reduction of the orientational freedom of polyelectrolytes in small pores of polymeric gels (Yuan et al., 2006). Since the experimental situations using gels are very complex and many factors contribute to the observed phenomena, the explanation of experimental results is difficult. One of the main obstacles is the disorder present in the gels, which plays an essential, but very unpredictable, role in gel electrophoresis.

To achieve better understanding of the sieving process involved in gel electrophoresis and identify effect of various specific factors, quantitative characterization on a well characterized model system is desirable. Patterned periodic regular sieving structures are ideal for study of molecular dynamics of electromigration of polyelectrolytes because the dimension of obstacles and channels can be easily controlled (Muthukumar and Baumgartner, 1989; Muthukumar, 2007).

The development of artificial electrophoresis sieving media is a major step to optimize DNA separation methods. Arrays of micro- or nano-sized obstacles are etched on the surface of a silicon wafer. Examples of artificial sieving structures include matrices of poles (Turner et al., 1998; Chou et al., 2000; Volkmuth 1992), alternated shallow slits and deep wells (Han et al., 1999; Han and Craighead, 2000; Fu et al., 2005; Fu et al., 2006), etc. The main advantages of artificial structures are the flexibility and precision in geometry of sieving system. In addition to these experimental efforts, simulation studies have also contributed very much into the understanding of such processes, some of which are difficult to achieve by experimental means.

A shown in Fig. 1.2, the microfabricated filtration device developed by Han and his group consists of regions of two different depths. This kind of devices have been used to study the migration of long DNA (Han et al., 1999; Han et al., 2000), rod-like short DNA (Fu et al., 2006; Fu et al., 2007) and small proteins (Fu et al., 2005). For typical nanofilter array, the depths of the wells are in the scale of 1μm while those of the slits are less than 100nm. As the effective sizes of the migrating molecules (rod length of the short DNA) are in the same order or larger than the depth of the slits (nanofilter gap size), the entry into the restricted nanofilter slits requires the DNA molecules to be positioned and oriented properly without interfering with the nanofilter wall. This

steric constraint forms an orientational entropy barrier for the transport of DNA and plays a major role in the electrophoretic separation of DNAs over such repeated nanofilter arrays. Theoretical size selectivity of such nanochannels has been addressed empirically based on experimental observations and the basic equilibrium models (Fu et al., 2006). However, optimization of the nanofilter separation system would require an efficient computational model that can estimate the performance of different device structures in terms of both separation selectivity (partitioning) and dispersion. Simulations of the same system, based on dissipative particle dynamics (Fan et al., 2006; Duong-Hong et al., 2007) and Brownian dynamics (Laachi et al., 2007), have recently been reported. However, these types of stochastic modeling techniques tend to be computationally expensive. Also, these simulations often track only a single molecule in the nanochannel system, and therefore are not well-suited for modeling the peak dispersion behavior, which is another important figure of merit of the nanofilter separation systems.

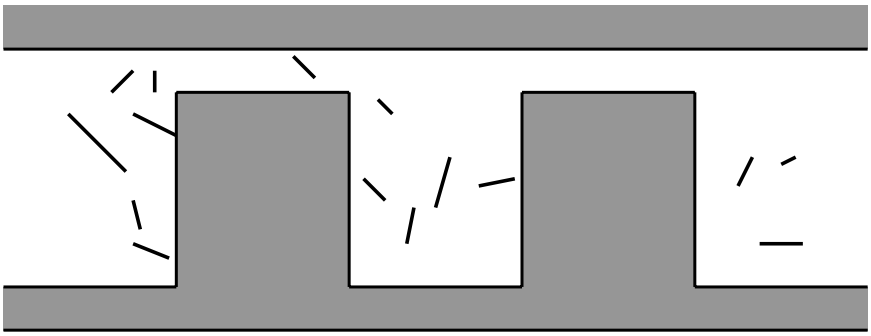

Fig. 1.2. The nanofilter array that consists of regions of two different depths designed for separation of the charged biomolecules.

1.2 Literature review

Study of the detailed dynamics of single macromolecules such as DNA and proteins in solvent environment is essential to understanding of their fundamental properties and biological functions. The experimental and theoretical progress made from both macroscopic and molecular-level points of view has significantly enriched our understanding of the structure, mechanics, and thermodynamics of DNA in aqueous solution.

1.2.1 Free volume model of gel electrophoresis of globular particles

The electrophoretic migration of polyelectrolyte in polymeric gels forms the foundation of gel separation of biomolecules. It has become one of the essential tools for separation, quantification and characterization of various biological polyelectrolytes including DNAs and proteins. It is the most widely used owing to its low cost, wide availability and ease of performing.

A straightforward approach to analyses of gel electrophoresis process is to treat the gel as a sieve with a certain distribution of pore sizes and the separation as an electric field driven filtration. Under this formulation, the result of electrophoresis fractionalization is determined by characteristic size of the random porous network and that of molecules in solution. Basically, the scaled or reduced mobility, which is the ratio of the electrophoretic mobility in the gel (μ) relative to the free-solution mobility μ_0, is assumed to be equal to the fractional volume (f) available to the particle in the gel

$$\mu^* = \frac{\mu}{\mu_0} = f(C_{gel}, M). \tag{1.1}$$

Fraction free volume (f) is a function of gel concentration (C_{gel}) and the analyte molecular size (M). Fraction free volume has been calculated for spheres in suspension of obstacles of various geometries by Ogston (1958), Morris (1966), Rodbard and Chrambach (1970, 1971). This model is known as Ogston-Morris-Rodbard-Chrambach (OMRC) model. It has been the dominant approach for interpreting the experimental data of gel electrophoresis mobilities semi-quantitatively for several decades. However, OMRC model has been shown unsuccessful in explaining many experimental results. In such cases, precise structure of the sieving matrix and the properties of the analyte should be taken into account. Also, this model fails in explanation of the mobility dependence on the electric field in a medium-to-high field strength in its original form (Slater et al., 2002; Viovy, 2000). To solve these problems, there have been a large number of modified approaches based on OMRC model trying to address the problem of hindered transport of more general polyelectrolytes through porous gels. For example, a few models have been proposed in order to take into account effects ignored in OMRC model, such as hydrodynamic interactions (Lumpkin, 1984), nonuniform local electric field (Locke, 1998). However, the relationship between gel electrophoresis mobility and the geometrical parameters of the anisotropic analyte geometry remain very difficult to characterize quantitatively. Up to now, the interpretation of experimental data for even the rod-like cylindrical molecules is still far from satisfactory (Allison et al., 2002). The main reason lies in the complexity in the experimental situations. The polymeric gels used in electrophoresis are complicated random structures. Statistical characterization of irregularity in geometry of random pores of the polymeric gel is difficult. In addition, comprehensive interpretation of experimental data for such systems requires information about entropic barrier that originates from reduction of the orientational

freedom of polyelectrolytes in small pores of polymeric gels (Yuan et al., 2006).

1.2.2 Effects of entropy barriers on DNA transport

Apart from the complexity in describing the random gel structure, the anisotropy of the polyelectrolyte causes additional difficulty in analyses results of gel electrophoresis experiments. When an anisotropic analyte enters the narrow pore of the gel, the analyte's orientation freedom is reduced due to the spatial confinement from the wall. This reduction causes an entropy loss of the molecule and results in an increase in the chain free energy. This entropic barrier will become significant if the longest dimension of the analyte is comparable of larger than the diameter of the pore. If the external electric potential is weaker than the entropic trapping, the mobility is significantly reduced. As the polymers of different lengths have different entropy barriers, these polymers are trapped for different time. Separation of the polyelectrolytes is achievable although their free-solution electrophoretic mobility might be the same. Although the physics involved in these processes are quite straight forward to understand, quantitative analysis has been shown extremely difficult.

Yuan et al. (2006) proposed a model for gel electrophoretic mobility that considers the effect of entropy barrier in addition to the usual excluded-volume contribution. Their reduced mobility is the multiplication of the reduced mobility from OMRC model and an entropic factor that decays exponentially with of the characteristic length of the analyte and the pore size. Their predictions agreed much favorably with the experimental data for linear and three-armed branched rigid DNA molecules than OMRC model.

Muthukumar and Baumgartner studied the effects of entropic barriers on chain diffusion of polymer in random porous media (Baumgartner and Muthukumar, 1987)

and in a well-characterized cubic cavity with gates at the center of walls of the cavity (Muthukumar and Baumgartner, 1989) using Monte Carlo simulations. The found the dependences of the reduced diffusion coefficient (D) on the length of polymer (N) are different in random porous media and the regular arrays. In a random media, D decays in the form of $D \sim N^{-2.9}$. However, in the regular cubic cavity, D decays exponentially with N if the cross section of the gate is large while in the small gate regime, D is determined by the gate size but independent of N.

Dorfman and Brenner (2002) employed generalized Taylor-Aris dispersion (macro-transport) theory for spatially periodic networks to derive analytical expressions for transport parameters, including the solute dispersion, number of theoretical plates, and separation resolution etc. Their expressions are in qualitative agreement with experimental data.

1.2.3 Simulation study on gel electrophoresis

Simulation of gel electrophoresis process is important in understanding the physical mechanism and in developing new methods or devices. Unfortunately, the computational analysis of polymer dynamics is also extremely difficult. In one hand, the macroscopic hydrodynamic models are thought not applicable because that the size of the DNA molecule is comparable to the size of the space it can reside, and thermal fluctuations are not negligible. In the other hand, the tools that are suitable in the molecular scale remain prohibitive to currently available computational resources.

Although there have been some full-atom molecular dynamics (MD) simulations, for example, on the translocation of DNA through synthetic nanopores (Heng et al., 2006; Aksimentiev et al., 2004). such molecular dynamics analysis is still infeasible.

Currently, typical simulation time of MD is at most in the scale of nanosecond, while the translocation over the nanopore happens in the scale of milliseconds. Furthermore, the MD model is also too idealized in the description of structure and the physical interactions involved in the actual experimental systems. The relation between the MD simulation results and experimental data are quite difficult to establish. Therefore it is necessary to develop coarse-grained models to capture the slow coarse-scale features accurately while fast fine-scale dynamics are assumed to remain at local equilibrium.

The most popular coarse-grained models are Brownian dynamics (BD) (Larson et al., 1999; Hur et al., 2000; Hur et al., 2002; Doyle and Underhill, 2005,) and dissipative particle dynamics (DPD) (Español and Warren, 1995; Groot and Warren 1997; Fan et al., 2006). Such methods discretize the problem domain using a set of point particles, each of which represents a collection of molecules that move together. These particles interact with each other through a set of prescribed forces. In BD, the forces that drive the motion of the particle include: a conservative force calculated from the particle interaction potentials; a velocity-dependent friction; and a Brownian force term. In DPD for fluid dynamics, these forces include a purely repulsive conservative force (pressure force), a dissipative force that tries to reduce velocity differences between the particles (viscous force) and a stochastic force directed along the line joining the centre of the particles (random force) (Español, 2003). The amplitude of these forces are dictated by a Fluctuation-Dissipation theorem (Español and Warren, 1995) to conserve the momentum and to reproduce the macroscopic diffusive behavior.

To simulate the dynamics of the suspensions of polymeric macromolecules such as DNA and RNA, the simple BD or DPD particles are usually used to model the solvent, while the coarse-grained bead-rod or bead spring models are used to characterize the

dynamics of polymers. DNA molecule in an aqueous solution takes random coil conformation as a result of thermal fluctuation. Such a fluctuation shortens the end-to-end distance of the polymer, even against an applied force. This *elasticity* against stretching is purely entopic. In the Kramer's bead-rod model (Kramers, 1946), the polymer chain is modeled as a series of beads connected by rigid links where the beads are the points experiencing the viscous drag force and are also under constant thermal bombardment by solvent molecules whereas the rods serve to hold the beads apart at constant distance. As each rod represents a fixed length (one Kuhn length, the smallest rigid length scale of the polymer when there is no excluded volume effect) of the macromolecule, the number of rods needed to represent a polymer molecule is proportionally with the molecular contour length. Therefore, it is not applicable to long DNA molecules. In a bead-spring system, beads are distributed uniformly along the backbone of chain and linked together by springs. All the forces experienced by the polymer including the viscous force, pressure force, electric forces and the random forces are applied on the beads. The spring accounts for the entropy- induced elasticity which describes the force-extension relationship. Because one single spring can represent varied (large) number of Kuhn steps through changing the spring force parameters. Therefore number of the beads can be significantly reduced as long as it can describe in sufficient detail the distribution of configurations (Larson, 2004). It should be noted that it is assumed that the elasticity of submolecule represented by the spring is identical to that of the whole molecule. This assumption is only valid when each spring is representing a sufficient number (>10) of Kuhn length of DNA, and therefore set an upper limit of the beads number used to represent a DNA (Larson, 2004).

There have been a lot of force model for the springs such as the Hookean dumbbell

model (Kuhn and Grün, 1942), the Rouse model (1953) and the Zimm model (1956), the finitely extensible nonlinear elastic (FENE) dumbbell model (Bird, 1987; Wedgewood et al., 1991), the worm-like chain (WLC) model (Vologodskii, 1994; Marko and Siggia, 1995), and the inverse Langevin chain model (Hur, 2000), etc. Among all these models, the WLC model is found exellent in approximation of the entropic elasticity of DNA at low and intermediate forces. In WLC, the molecule is treated as a flexible rod of length L that curves smoothly as a result of thermal fluctuation. The force F required to induce an end-to-end distance extension of x in a chain of contour length L is given by (Vologodskii, 1994; Marko and Siggia, 1995),

$$\frac{F\lambda_p}{k_B T} = \frac{1}{4}\left(1-\frac{x}{L}\right)^{-2} - \frac{1}{4} + \frac{x}{L}, \tag{1.2}$$

where k_B is Boltzmann constant, T is the absolute temperature, and λ_p is the effective persistence length. According to (Smith et al., 1992), the effective persistence length can be set as $\lambda_p = 50 \sim 53$ nm under most biophysical or experimental conditions. Although (1.2) is derived from force-extension relationship of the whole molecule, it is expected to be applicable also to subsections as long as the length of the pieces of DNA corresponding to a single spring is much greater than the persist length of DNA (Hur et al., 2000).The spring forces in these models are always attractive. They are balanced by the pressure force, viscous force and other external forces.

Mesoscopic simulation methods, such as BD and DPD, along with suitable polymer model facilitate the studies of the dynamics of long DNA under various conditions by representing the long polymer using a sequence of bead-spring segments.

The most difficult problem in the study of the dynamics of polymers arises from the

complex coupling of factors including viscous force, entropic elasticity, Brownian forces, hydrodynamic interactions, excluded-volume interactions ,internal viscosity and self-entanglement, etc. (Larson, 2005). These forces and interactions are strongly coupled with each other through complicated atomic level interactions among the polymer and surrounding solvent molecules. Due to the oversimplification of coarse-grained particle interactions, most of BD and DPD implementations consider only the effect of the viscous drag, entropic elasticity and Brownian forces.

In addition, as these methods are stochastic, the simulation processes are normally very slow. To obtain reliable results, a number of simulations are required, the results of which are averaged to obtain the final results. In addition, there are no established methods to determine the parameters such as the viscosity of the fluid, the physical length and time scales which are required by these methods as input (Español, 2003).

1.3 Objective and significance of the study

In this thesis, electrophoresis filtration of short double stranded DNA segments is studied. Without special declaration, all the DNA molecules studied in this thesis are double stranded. The short DNA molecules is chosen here because the persistence length of DNA is ~50 nm in physiological conditions which means that it is quite safe the treat DNA molecules shorter than ~50nm as the rigid rod. This simplification permits one to focus on the role of entropic barrier in such process without considering the deformation of DNA molecules.

The theoretical model that will be developed for the analyses of the electrophoretic separation of rod-like DNA molecules in the patterned nanofilter arrays is based on continuum transport theory. In this theory, the degree of freedom in a DNA's

orientations is projected into an orientational entropy term, using statistical theory for the equilibrium distribution of rigid cylindrical molecules near solid channel walls. The effect of the orientational entropy on the partition and migration of DNA molecules is quantified as a single entropy driven transport term in the master flux equation. One-dimensional analytical formulas of the electrophoretic mobility and peak desperation will be derived. Theses analytical formulas provide handy tools for experimentalist to predict the results of separation and optimize the task-specific structure of the nanofiltration devices.

In addition, the effects of the spatial confinement of nanochannel to the DNA's mobility and translational diffusion coefficient will also be quantified using statistical theory for the equilibrium distribution. As the analytical solution to the anisotropic transport problem is not available. Numerical analysis is performed using a model nanofilter array consisting of a small number of repeated unit cells. From the translation and broadening of peaks over these repeats, the results of separation of the DNA molecules passing through the full-length channel, which may consists of tens of thousands repeats, are estimated using one-dimensional unified separation theory. It will be shown that the entropic barrier effect, combined with the modified anisotropic transport parameters in the confined nanofilter space, accounts for the fractionation of the DNA molecules of different sizes.

Unlike all the previous simulations, this continuum theory provides a platform to fully describe sieving, diffusion and convection of a band of biomolecules passing through a repeated array of nanofilters.

1.4 Organization of the thesis

This thesis is composed of 8 chapters, the contents of which are listed as follows.

In Chapter 1, the background of the DNA electrophoresis over random polymeric gels and the regular nanoarrays are provided. The review includes the established knowledge on the experimental, theoretical and simulation aspects of the electrophoresis of polyelectrolytes, especially those related to the entropic barrier mechanism. The objective and significance of this study are also provided.

Chapter 2 constitutes a brief introduction of the transport properties of the rod-like DNA molecules in free solution. Experimentally determined formulas or curves for free-solution diffusion coefficient and free-solution electrophoretic mobility of short rod-like DNAs are given. As one of the main objectives, the rotational diffusion of the DNA rods is presented to provide basis for calculation of entropy barriers, and analysis of other transport problems.

Chapter 3 describes the physics of rod-like DNA molecules in confined space. Orientational entropy is quantified using statistical mechanics theory. In addition, the mobility corresponding to the interactive force from the solid wall, which is referred to as entropic force, is also obtained.

In chapter 4, principles of membrane transport theory is applied to develop an exact analytical solution for the mobility and dispersion of DNA molecules migrating in the nanofilter array. This model is based on equilibrium partition theory using isotropic transport parameters. The physical mechanisms of electric field driven transport and trapping time induced by entropy barrier are elucidated clearly. Method to assess and optimize the structure of the nanofilter and selection of the electric field is proposed.

In Chapter 5, the model for anisotropic transport of DNA molecules is developed, followed by the numerical solutions to the anisotropic transport equations as described in Chapter 6. These approaches serve as more accurate tools to analyze more complicated phenomena, especially for the cases with nonuniform electric field.

The results and discussions are given in Chapter 7. Using the experimental specifications of the nanochannel structure and the well-established values of transport parameters, reproduction of the experimental results for mobility is achieved faithfully. In addition, band dispersion is also estimated, which is far more difficult in other stochastic simulation methods.

Last, in Chapter 8 the conclusions are drawn and some future work to extend this study is given.

2 Rod-like DNA molecules in aqueous solution

Double stranded DNA molecules are relatively stiff polymer, with a persistence length of ~50nm, corresponding to ~150 base pairs (bp). Geometrically, short DNA molecules of a few hundred base pairs normally behave as rigid rod of diameter ~2 nm in solutions. As a polyelectrolyte with $2e^-$ charge per base pair, a DNA is subject to an electrostatic force if it is located in an electric field. A short DNA rod also undergoes high-speed random translational and rotational thermal motions.

The dynamics of DNA molecules in aqueous solution are traditionally characterized by free-solution (translational) diffusion (D^d) and free-solution electrophoretic mobility (U^e). The first two sections of this chapter briefly outline the formula and data that have been established by experiments, followed by a section discussing the relationship between D^d and U^e, *i. e.* the Nernst-Einstein relation. Although the analysis of rotational motion of DNA rod is not necessary in free solution electrophoresis (because all the orientations are equally accessible, DNA molecules can be treated as isotropic), the random rotation of DNA molecules has to be studied here to provide proofs of validity of our approaches.

2.1 Free-solution diffusion coefficient of rod-like DNA

Diffusion of particles in a solution from a region of high concentration to regions of low concentration is a spontaneous process caused by the Brownian motion of the particles. Starting from a point in three-dimensional space, the variance of distance

($< r_t^2 >$) that a particle travel in time duration τ is described by diffusion coefficient (D^d) such that,

$$< r_t^2 >= 2D^d\tau \,. \tag{2.1}$$

Free-solution diffusion coefficient of short DNA molecules of length L and diameter d has been extensively studied and well established (Allison and Mazur, 1998; Eimer and Pecora, 1991; Tirado et al., 1984). For short rod-like DNA molecules, diffusion coefficient D^d is given by

$$D^d = \frac{k_B T}{3\pi\eta_0 L}\left(\ln(\frac{L}{d}) + \nu_c\right) \tag{2.2}$$

where η_0 is the viscosity of the solvent, and

$$\nu_c = 0.312 + 0.565d / L + 0.010d^2 / L^2 \tag{2.3}$$

represents the correction term for the end effect of short DNA molecules (Tirado et al., 1984).

2.2 Free-solution electrophoretic mobility of DNA

The free-solution electrophoretic mobility (U^e) characterizes the drift velocity of an electrolyte in the solution under a unit external electric field. It is experimentally established that the free-solution electrophoretic mobility of DNA is independent of molecular weight for DNA molecule longer than a threshold value of ~400bp (Stellwagen et al., 1997; Stellwagen and Stellwagen 2002). For these molecules free-solution separation is impossible. Although the mobility of shorter DNA molecule is size dependant, the range of mobility differences for 10-400bp DNAs is less than 15%. This minor difference made the free-solution separation impractical even for short

DNA molecules.

The free-solution electrophoretic mobility of a polyelectrolyte is dependent on many factors including the ionic strength, temperature etc. In this thesis, the experimental curves established by Stellwagen et al. (1997) is adopted because their experimental conditions are similar to those for the DNA filtration studied here.

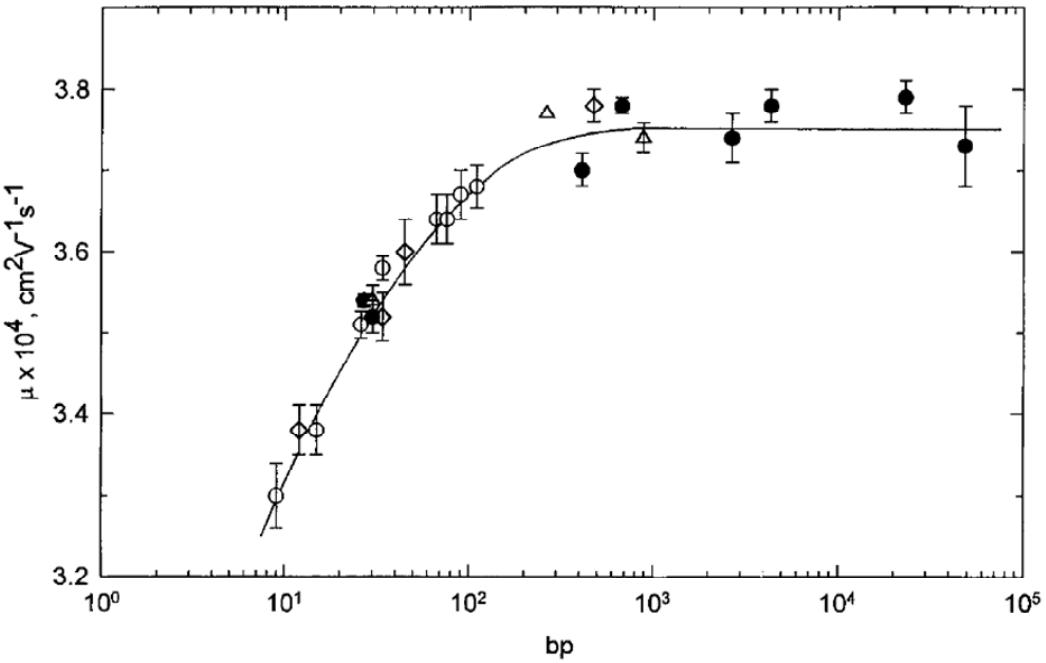

Fig. 2.1. Size dependence of the free-solution electrophoretic mobility of DNA molecules (reproduced from Fig. 7 of Stellwagen et al., 1997.)

2.3 Validity of Nernst-Einstein relation

For small spherical solute particles, the hydrodynamic friction coefficients for translational diffusion and the electric field driven motion would be identical. Let ζ be the friction coefficient that relates the drifting velocity $\tilde{V}$ and the force applied to the particle F by

$$F = \zeta \tilde{V} . \qquad (2.4)$$

This means that the translational diffusion coefficient of the particle is equal to

$$D^d = \frac{k_B T}{\zeta}, \tag{2.5}$$

while electric mobility is

$$U^e = \frac{ze}{\zeta}. \tag{2.6}$$

where z is the charge number of the charged particle.

In this case, Nernst-Einstein relation

$$D^d / U^e = k_B T / ze \tag{2.7}$$

would be valid.

For the Nernst-Einstein relation holds for the DNA molecules, the dependences of D^d and U^e on molecule size N should be characterized by the same form of functions. However, it is well known that free-solution mobility for DNA longer than ~400bp is independent of N, i.e. $U^e \sim N^0$ (Stellwagen et al., 1997; Stellwagen and Stellwagen, 2002; Stellwagen et al., 2003). On the other hand, diffusion coefficient of long DNA molecules changes with molecule size by $D^d \sim N^{-\upsilon}$, with $\upsilon = 0.5 \sim 0.75$ depending on theoretical or experimental conditions (Nkodo et al., 2001; Smith et al., 1996; Lukacs et al., 2000; Sorlie and Pecora, 1990; Stellwagen et al., 2003). It is apparent that the Nernst-Einstein relationship is generally not valid for DNA molecules (Nkodo et al. 2001, Mercier and Slater, 2006).

As an exception to this result, it is claimed that Nernst-Einstein relation is valid for short DNA molecules smaller or shorter than the persistence length (Mercier and Slater, 2006). However, when one analyzes the experimental data of diffusion coefficient and the free-solution electrophoretic mobility, it is found that Nernst-

Einstein relation does not hold for molecules even as short as 10-100bp. To show this the free-solution electrophoretic mobility is calculated from Nernst-Einstein equation and the formula of diffusion coefficient. If the Nernst-Einstein relation is valid, the calculated data should reproduce the experimental curves as shown in Fig. 2.1 at least approximately.

If the Nernst-Einstein relation (2.7) holds for short DNA, the free-solution electrophoretic mobility of N -bp DNA can be calculated as

$$U_e \propto \frac{2Ne}{k_B T} D^d . \tag{2.8}$$

Substituting the expression for diffusion coefficient Eq. (2.2) to (2.8), one has

$$U^e \propto \frac{2Ne}{3\pi\eta_0 L}\left(\ln(\frac{L}{d}) + \nu_c \right). \tag{2.9}$$

Equation (2.9) tells that the free-solution electrophoretic mobility U^e has to be proportional to

$$U' = \frac{N}{L}\left(\ln(\frac{L}{d}) + \nu_c \right) \tag{2.10}$$

if the Nernst-Einstein relation is valid for short molecules.

Fig. 2.2 shows the curves of U' for short DNA with $d = 2\,\text{nm}$ and L calculated from Kratky-Porod model (Kratky and Porod 1949; Marko and Siggia, 1995)

$$L = \left\{ 2l\lambda_p [1 - \frac{\lambda_p}{l}(1 - e^{-l/\lambda_p})] \right\}^{1/2} . \tag{2.11}$$

This curve departs seriously from the data shown in Fig. 2.1 by Stellwagen et al. (1997) and it does not fit into the free draining DNA electrophoresis mobility (which is independent of the length). For the molecules between 10-100bp, the change in

experimentally obtained free-solution electrophoretic mobility is rather small (about 10%), while U' (derived here from Nernst-Einstein relationship) is about 200%. Similarly, for molecules between 100-300bp, the change in mobility is about 20%, while that in U' is about 50%. Based on these arguments, one can conclude that Nernst-Einstein relationship is not valid for DNA in any range of lengths.

The reason for this, as explained partly by Nkodo et al. (2001) and Stellwagen et al. (2003), is because the frictional constants involved in the electric driven motion and the diffusion are different. Einstein's relation only focuses on the molecule itself and the surrounding neutral fluid, but the electrophoresis is also determined by the friction between DNA and counterion (with opposite charges). Since the counterions are also charged and are driven by electric field as well, the friction constant will be different.

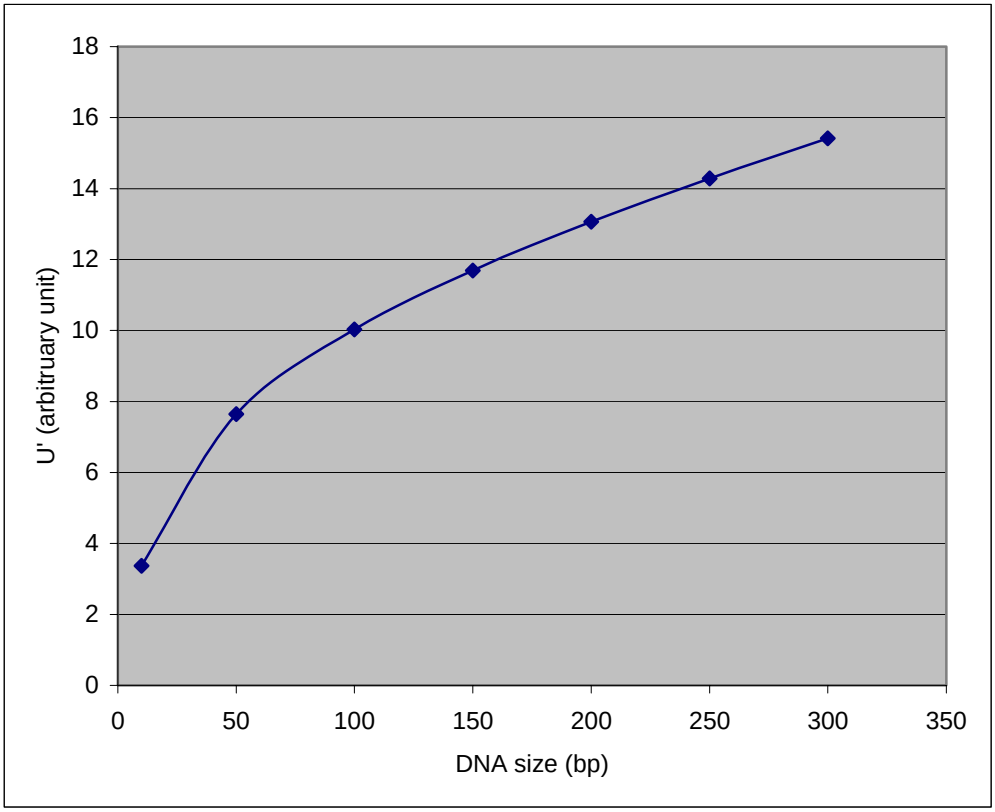

Fig. 2.2. Electrophoretic mobility of rod-like DNA predicted from the diffusion coefficient and the Nernst-Einstein relation. If the Nernst-Einstein relation is valid, this curve should reproduce the experimental

data approximately.

2.4 Rotational diffusion of a DNA rod

As a short cylindrical rod, a DNA molecule is a highly anisotropic molecule. The non-interacting Brownian rotation of rod-like DNA molecules causes a continuous reorientation, which gives rise to rotational diffusion. For short DNA rods, this rotational diffusion is much faster than its translational diffusion or electric field driven migration, so much so that at any point during the migration, all the orientations are accessed many times with equal probabilities. This fact allows for a simplification of modeling and calculation by removing the rotational degree of freedom as performed in the later chapters of this thesis. In this section, the process of rotational diffusion of rod-like DNA molecules will be analyzed in order to provide the basis for the calculation of the entropy barrier and other transport quantities.

2.4.1 Stokes-Einstein-Debye model

The main focus of theory on rotational Brownian motion is the calculation of the probability density function for the orientation. The first theory of rotational Brownian motion was developed by Debye (1929) and is the rotational analog of the simple translational diffusion. The fundamental assumption of this theory is that collisions between the DNA and the surrounding liquid molecules are so frequent that DNA molecule can rotate only through a very small angle before suffering the next reorientation collision. The direction of the next rotation is independent of its current orientation.

The orientation of DNA rod can be specified by the unit vector $u(t)$ with spherical polar coordinates (θ, ϕ) as shown in Fig. 2.3a. During the rotation, the two ends of

DNA rod remain on the surface of a sphere of unit radius as the length of the rod is constant. Therefore, the reorientation of the molecule corresponds to a random trajectory on the surface of the unit sphere. An example is shown in Fig. 2.3b, where the orientation angle of a rod changes from $u(0)$ at time 0 to $u(t)$ at time t though rotational random walks. In a sufficiently long run, this random trajectory will cover the whole sphere surface uniformly, which means that the DNA molecule samples all the possible orientation equally.

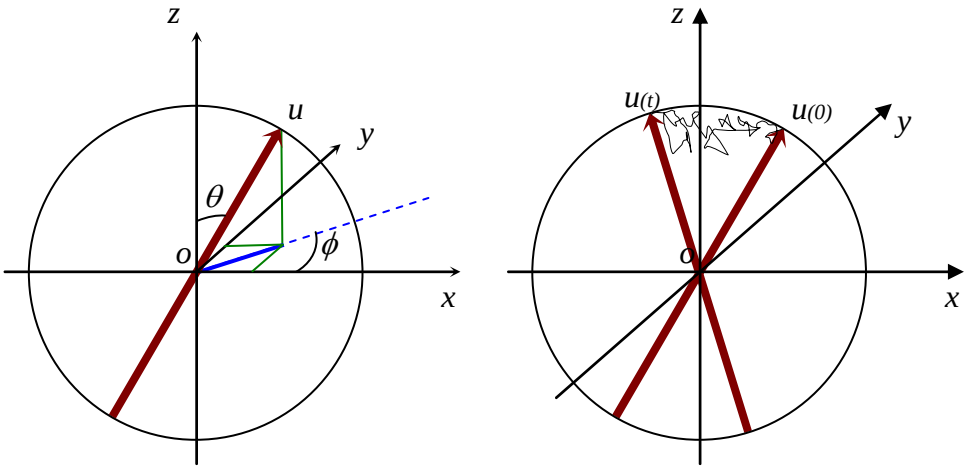

Fig. 2.3. The orientation and reorientation of the rod-like DNA molecules. (a) Orientation of the rod-like DNA is represented by a unit vector u. (b) the reorientation of the rod corresponding to a random trajectory on the surface of the unit sphere.

The basic assumption of the Debye theory indicate that the random rotation of rod-like DNA molecule is equivalent to a particle (attached to the tip of DNA rod) randomly moving on the surface of a unit sphere. Microscopic particles in solution have an average kinetic energy associated with rotation about any axis of $k_B T/2$, which are equal to the average kinetic energy associated with translation along any axis. Corresponding to the viscous drag force which is proportional to the velocity in

translation, the frictional torque N_θ is also assumed to be proportional to angular velocity Ω_r of the particle with a friction coefficient f_r by

$$N_\theta = \Omega_r f_r . \tag{2.12}$$

As a result, the relationship between the rotational diffusion coefficient and rotational friction coefficient is described by Stokes-Einstein-Debye equation (Stokes, 1856; Einstein, 1906; Debye, 1929)

$$D^r = \frac{k_B T}{f_r}. \tag{2.13}$$

The mean square angular random deviation of the infinitesimal angle $\Delta\theta$ by which a vector rotates during an infinitesimal time interval Δt is

$$< \Delta\theta^2 >= 4D^r \Delta t . \tag{2.14}$$

The rotational diffusion coefficient of a rod-like DNA of length L and diameter d was has been established by Tirado et al. (1984)

$$D^r = \frac{3k_B T}{\pi\eta_0 L^3}\left(\ln(\frac{L}{d}) + \delta \right), \tag{2.15}$$

where the end effect correction term δ is given by

$$\delta = -0.662 + 0.917 d / L - 0.050 d^2 / L^2 . \tag{2.16}$$

Equation (2.14) is valid for only very short time. This is because in contrast to the three-dimensional translational diffusion in the infinite domain, the rotational diffusion takes place in a periodic angular space. For a cylindrical DNA rod, the recognizable rotation angle lies in a very small range of $0 \sim \pi / 2$. A more accurate description is given in the next subsection.

2.4.2 Time dependent angular distribution

The governing equation for rotational diffusion can be derived from the governing equation for the translational diffusion

$$\frac{\partial P(\mathbf{r},t)}{\partial r} = D^r \nabla^2 P(\mathbf{r},t) \tag{2.17}$$

by representing the Laplacian operator ∇^2 in spherical coordinate system (r,θ,ϕ),

$$\nabla^2 = \frac{1}{r^2}\frac{\partial}{\partial r}(r^2\frac{\partial}{\partial r}) + \frac{1}{r^2\sin\theta}\frac{\partial}{\partial\theta}(\sin\theta\frac{\partial}{\partial\theta}) + \frac{1}{r^2\sin^2\theta}\frac{\partial^2}{\partial^2\phi}, \tag{2.18}$$

where $P(\mathbf{r},t)$ is the probability that the tip DNA molecule is located at point **r** at time t.

On a unit sphere surface, r is equal to 1, and all the derivatives respect to r are 0. Therefore, the Laplacian operator reduces to,

$$\nabla^2 = \frac{1}{\sin\theta}\frac{\partial}{\partial\theta}(\sin\theta\frac{\partial}{\partial\theta}) + \frac{1}{\sin^2\theta}\frac{\partial^2}{\partial^2\phi}. \tag{2.19}$$

Substituting expression (2.19) to (2.17), one gets the rotational diffusion equation in spherical coordinate system,

$$\frac{\partial P(\theta,\phi,t)}{\partial t} = D^r\left(\frac{1}{\sin\theta}\frac{\partial}{\partial\theta}(\sin\theta\frac{\partial P(\theta,\phi,t)}{\partial\theta}) + \frac{1}{\sin^2\theta}\frac{\partial^2 P(\theta,\phi,t)}{\partial^2\phi}\right). \tag{2.20}$$

Let us consider a special case where a fixed number of molecules were released instantaneously at $\theta = 0$ at $t = 0$ (all the molecules are aligned in z direction as shown in Fig. 2.3). At any time $t > 0$, the distribution of orientation is independent of ϕ. Therefore, all the derivatives of $P(\theta,\phi,t)$ with respective to ϕ are zero. The rotational diffusion equation (2.20) becomes,

$$\frac{\partial P(\theta,\phi,t)}{\partial t} = D^r \left(\frac{\cos\theta}{\sin\theta} \frac{\partial P(\theta,\phi,t)}{\partial \theta}) + \frac{\partial^2 P(\theta,\phi,t)}{\partial \theta^2}) \right). \quad (2.21)$$

Using numerical method, this mater equation for rotation diffusion is solved with the initial condition at $t = 0$

$$P(\theta,\phi,0) = \begin{cases} 1 & \theta = 0 \\ 0 & \theta \neq 0 \end{cases}, \quad (2.22)$$

to obtain the probability density function $P(\theta,\phi,t)$ at any time.

Integrating the probability density over ϕ, the probability of the rod oriented with angle θ is,

$$P_\theta(\theta,t) = 2\pi \sin\theta \, P(\theta,\phi,t) . \quad (2.23)$$

Subsequently, angular variance $< \Delta\theta^2 >$ and anisotropy parameter A_I are obtained by,

$$< \Delta\theta^2 >= \int_0^\pi \theta^2 P_\theta(\theta,t) d\theta , \quad (2.24)$$

and (Carrington and McLachlan, 1967; Lavalette et al., 1999)

$$A_I =< \frac{3\cos^2\theta - 1}{2} >= \frac{3}{2}\int_0^\pi \cos^2\theta P_\theta(\theta,t) d\theta - \frac{1}{2} \quad (2.25)$$

respectively. The anisotropy parameter described by Eq.(2.25) decays exponentially with time t,

$$A_I(t) = \exp(-6D^r t) = \exp(-t/\tau_r) , \quad (2.26)$$

with τ_r being the rotational correlation time given by

$$\tau_r = \frac{1}{6D^r} . \quad (2.27)$$

The relationship described by Eq. (2.14) works well when the diffusion time is

smaller than the critical residing time

$$\tau_r^c = \frac{1}{4D^r}, \tag{2.28}$$

which satisfies

$$< \Delta\theta^2 >= 1\,\mathrm{rad}^2 . \tag{2.29}$$

when equation (2.14) is used to calculate the angular variance in rotational diffusion.

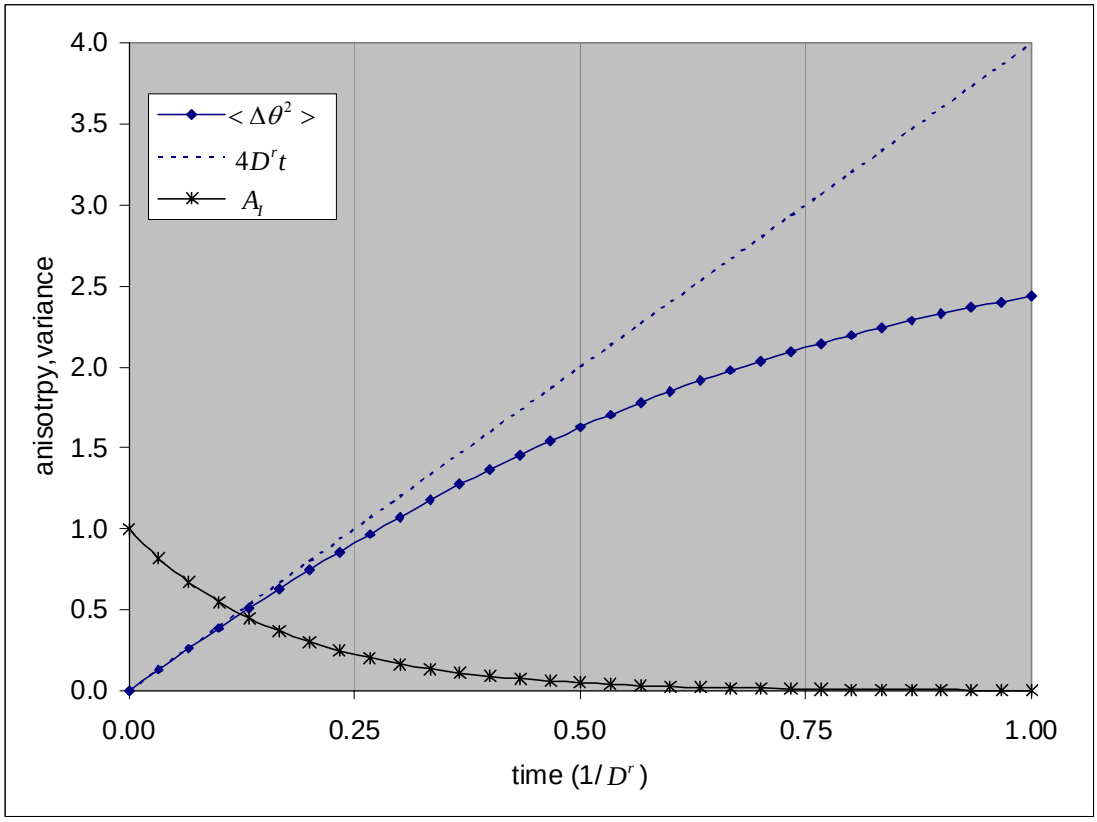

Fig. 2.4. The angular variance and the anisotropy factor changing with time. Estimation of angular variance using $< \Delta\theta^2 >= 4D^r t$ is generally accurate for $t \le \tau_r^c = 1/4D^r$ ($1/D^r$ =0.25). At $t = \tau_r^c$ the anisotropy factor is less than 0.2, meaning that the orientation of an anisotropic particle is almost uniformly distributed regardless of its initial orientation.

In practice, τ_r^c serves at the threshold value in judging the dependence of the orientational distribution on the initial state. If a particle resides at a point for a time

longer than τ_r^c, all its orientations would occur in approximately equal probability, regardless of its original orientation. This can be confirmed from the simulation results shown in Fig. 2.4. In this figure, the anisotropic factor is less than 0.2 at time $t = \tau_r^c$. It is also noteworthy that τ_r^c also serves as the threshold time for the validity of Eq. (2.14). For $t \le \tau_r^c$, $< \Delta\theta^2 >$ is approximately equal to $4D^r t$. Beyond the critical value, Eq. (2.14) is not valid anymore.

Now let us look at the short DNA molecules migrating in the regular nanofilter array. At room temperature, the rotational diffusion coefficients for 50-300bp DNA molecules are in the order of $10^4 \sim 10^6 rad^2/s$. The critical residing times are within the range of $0.1 \sim 10 \mu s$. Actually, the mean residing time of DNA molecules in one unit of nanofilter (repeat length $1.0\ \mu m$) under typical electric field strengths (14-57V/cm) is about 0.05~0.1s. This residing time is far more higher than the critical threshold value, therefore a DNA molecule is able to sample all accessible orientations many times. It is quite safe to assume that there exists an orientational equilibrium at all points of the nanofilter. The orientational degrees of freedom of the DNA rod can be eliminated by averaging of the orientation dependent quantities with their Boltzmann probabilities.

3 Rod-like DNA in confined space

When a DNA rod is located in a confined space, some of its orientations are forbidden due to the presence of solid channel walls. This reduction in configurational accessibility causes an entropy loss which has been shown to play an essential role in transport of the biomolecules through pores in various biological membranes. This entropy reduction is also responsible to the separation of rod-like DNA through the nanofilter array device studied in this thesis. In this chapter, configurational entropy DNA rod is quantified using the theory of equilibrium statistical mechanics. In addition, the confinement in the orientational space made the transport of DNA molecules anisotropic (the flux caused by the thermal motion or the electrostatic force is direction dependent). The anisotropic transport parameters will also be calculated based on the experimental data for free-solution isotropic cases.

3.1 Probability of orientation for a DNA rod in confined space

As shown in Fig. 3.1, vector **r** denotes the position of center of the DNA (O') in global coordinate system *Oxyz*. The orientation of rod is represented by a vector $\mathbf{\Theta} = (\theta, \phi)$ ($|O'A| = 1$) that is locked into the DNA rod ($|O'B| = L/2$, L is the length of the rod) and lies along the rod's long axis. The surface of the unit sphere is represented by S, representing all the possible orientations of the rod.

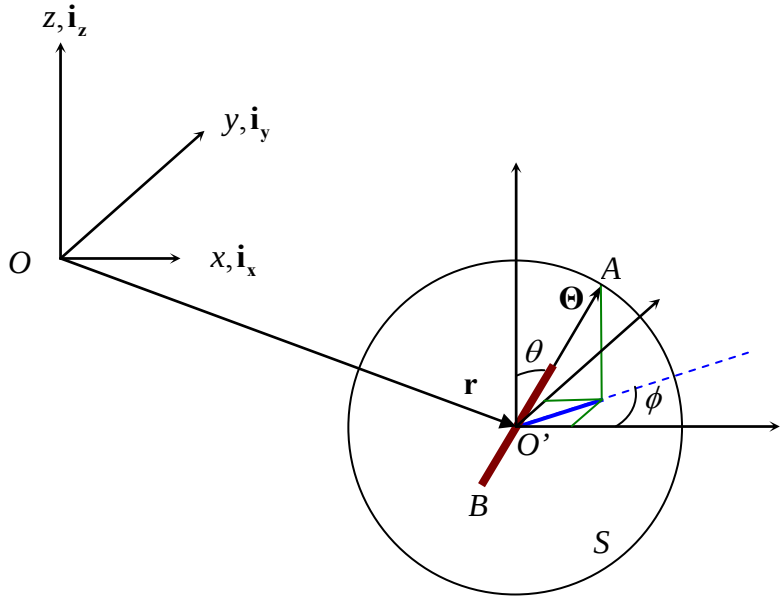

Fig. 3.1. The position and orientation of a DNA rod. The position of DNA is defined by a vector **r** in the global system Oxyz, while the orientation of the DNA rod is represented by vector $\mathbf{\Theta} = (\theta, \phi)$.

Based on the discussions presented in Section 2.4, one may assume that all the orientations of DNA rod in free solution are equally accessible due to fast rotational diffusion. Because the surface area of a unit sphere is equal to 4π, the probability density of the rod oriented at $\mathbf{\Theta}$ is

$$p_0(\mathbf{\Theta}) = \frac{1}{4\pi}. \tag{3.1}$$

Now let us consider the case when the centre of DNA rod O' is located at **r** near a solid wall as shown in

Fig. 3.2. Some orientations are not accessible because the DNA rod would intersect with the solid wall at these orientations. Such inaccessible orientations correspond to the domain represented by the dashed curves on the surface of unit sphere as shown in Fig. 3.2. Other orientations, which are permissible, are represented by domain S' on

the surface in solid curves. The ratio of the number of permissible orientations to the total number of orientations of a DNA rod centered at is $\mathbf{r}$ given by

$$\rho_{\Theta}(\mathbf{r}) = \iint_{S'} (4\pi)^{-1} d^2\mathbf{\Theta} . \tag{3.2}$$

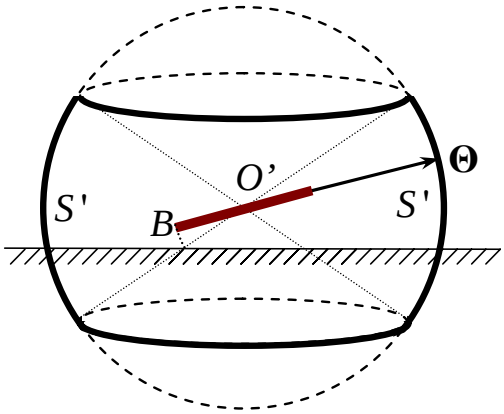

Fig. 3.2. Permissible and forbidden orientations of the DNA rod near a solid wall. The surface represented by S' corresponds to permissible orientations while the others (S-S') shown by dashed curves are forbidden.

The ratio $\rho_{\Theta}(\mathbf{r})$ describes how much of the rod's orientational space is accessible at position $\mathbf{r}$. It has a maximum value of 1.0 meaning that all orientations are permissible (as in the free-solution), and a minimum value of 0.0 which means that the rod intersects with the solid wall at all orientations.

3.2 Orientational entropy of the rod-like DNA in confined space

The interactions between a rigid boundary and a rigid molecule imply a hard-wall potential. The interactive energy between the DNA rod and solid boundary is $\varepsilon_{Mb} = \infty$ if the molecule and boundary overlap and $\varepsilon_{Mb} = 0$ if they do not overlap. The Boltzmann factor of the molecule boundary interactive energy,

$\exp[-\varepsilon_{Mb}(\lambda)/kT]$, is there fore either 1 (for all molecular orientations free from boundary overlap) or 0 (for all overlapping orientations). It is very straightforward to find that in the hard-wall approximation, the Boltzmann factor is equivalent to $\rho_{\Theta}(\mathbf{r})$, the probability of no intersection with boundary walls at given location $\mathbf{r}$.

For the purpose of rigid DNA transport, only orientational entropy needs to be calculated as other type of entropies does not affect the flux of DNA over the nanochannel structure. According to statistical theory, orientational entropy of rigid molecules is defined as

$$\Delta S(\mathbf{r}) = -R \ln \Omega(\mathbf{r}), \tag{3.3}$$

where $\Omega(\mathbf{r})$ is the accessible microscopic orientation state integrals at location $\mathbf{r}$ (Giddings et al., 1968).

For the rod-like rigid DNA molecules specifically, the orientational entropy of interest can be rather simply expressed by

$$S_{\Theta}(\mathbf{r}) = k_B \ln \kappa(\mathbf{r}). \tag{3.4}$$

where the subscript $\boldsymbol{\Theta}$ indicates that the entropy S_{Θ} is induced by the loss of orientational freedom, $\kappa(\mathbf{r})$ is the local partition function (defined as the ratio of number of accessible microscopic configurations at $\mathbf{r}$ near the solid wall to those in the bulk liquid, Giddings et al., 1968). As this $\kappa(\mathbf{r})$ is exactly the ratio $\rho_{\Theta}(\mathbf{r})$ given by Eq. (3.2), the entropy is given by

$$S_{\Theta}(\mathbf{r}) = k_B \ln \rho_{\Theta}(\mathbf{r}). \tag{3.5}$$

Based on this formulation, a DNA molecule acquires maximum entropy of value 0 when it is located in the bulk solution. As the DNA is located close to a solid wall, a

portion of its orientational space is not accessible and therefore the orientational entropy decreases to a negative value. A negative entropy causes no problem here as only the gradient of entropy enters the expression of the flux of DNA molecules as studied in next chapter. This definition of orientational entropy of a rod-like DNA molecule is based on the assumption that all the possible orientations occur in equal probabilities. This assumption is valid when electric force exerted on the electrolyte is much smaller than the random thermal force, and the molecule has enough time to sample all the available orientations at any location of domain.

3.3 Mobility of DNA rod for entropic force

Another important parameter is the mobility associated with the entropic force. By definition, U^S corresponds to the velocity of a rigid DNA obtained if 1 newton of "entropic force" is applied to 1mol of DNA molecules. Although this quantity is not available through experimental observation, one can derive it based on some qualitative assumptions.

The entropic force in this thesis is originated from the reactive force that the solid wall applies to a rigid rod when this rod hits the solid wall through rotational motion starting from a permissible orientation. As the energy of thermal fluctuation in each dimension is $k_B T/2$ for both rotational and translational diffusions, the expression of U^S is derived through the comparison between the speeds of the motion at the centre of a rod caused by these two types of diffusions.

The free-solution diffusion coefficient and the rotational diffusion coefficient of the short rod-like DNA molecules are given by (Tirado et al., 1984)

$$D^d = \frac{k_B T}{3\pi\eta_0 L}\left(\ln(\frac{L}{d}) + \nu_c\right) \quad (2.2)$$

and

$$D^r = \frac{3k_B T}{\pi\eta_0 L^3}\left(\ln(\frac{L}{d}) + \delta\right), \quad (2.15)$$

respectively. The parameters ν_c and δ represent the correction terms as the end effect for DNA rods. Neglecting the end effect terms δ and ν in Eq. (2.2) and (2.15), the relationship between D^d and D^r is

$$D^r = 9D^d / L^2 . \quad (3.6)$$

Within a typical time duration τ, the one-dimensional average diffusion angle of the DNA rod in bulk solution is

$$< \alpha >= (2D^r \tau)^{1/2}, \quad (3.7)$$

corresponding to an effective angular velocity (Berg, 1983)

$$< \dot{\alpha} >= (2D^r / \tau)^{1/2} . \quad (3.8)$$

When one end of a DNA molecule hits the solid wall during rotation, it is assumed that the tip of this end stops instantaneously and the other portions of the rod rotate at the same speed as that before hitting (Fig. 3.3). This assumption is based on the nature of the near-wall thermal diffusions of nanoparticles (Kihm et al. 2004). The amplitudes of the thermal fluctuations of solid particles and the surrounding fluids decrease when they approach the wall. The particles or the portions of an object that are further from the solid wall will are subject to a higher degree of thermal motion, while motions of those on the solid surface are hindered.

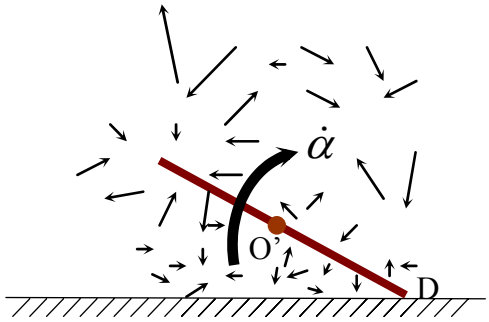

Fig. 3.3. Interaction between the rotational rod and the solid wall. When one end of a DNA rod (*D*) hits the wall at rotational velocity ($\dot{\alpha}$, shown by thick arrow) during rotational Brownian motion, that end stops instantaneously as its motion is hindered in all directions while other portions of the rod retain their original rotational velocities owing to the sustained random thermal fluctuations of the surrounding fluid molecules (shown by the irregular thin arrows).

As shown in Fig. 3.3 , at the moment when one end of the DNA (end *D*) hits the wall at a rotational velocity, the motion of end *D* is hindered in *xy*-plane by stationary fluid (no-slip boundary condition), -*z* by solid wall. The motion in +z direction is also not possible at this moment because of the momentum of the whole rod. Therefore *D* is treated as fixed instantaneously. As long as the thermal fluctuations of surrounding fluids are not affected by the event that the DNA hits the wall, the fluids will continue to push the other portions of the rod to rotate at its original velocity $\dot{\alpha}$ and induces a translational motion for the center of the DNA. Consequently the translational velocity at the centre of the rod is

$$< \dot{r}_r >=< \dot{\alpha} > L/2\,, \tag{3.9}$$

which can be further expressed as

$$< \dot{r}_r > = (9D^d / 2\tau)^{1/2}\,. \tag{3.10}$$

From the translational diffusion point of view, during the same time duration of τ , the

one-dimensional average translational diffusion speed is

$$< \dot{r}_t >= (2D^d / \tau)^{1/2} . \tag{3.11}$$

Comparing the velocity of the centre of the rod caused by hindered rotational diffusion and that induced by translational diffusion, one can find the relationship of

$$< \dot{r}_r >= 9 < \dot{r}_t > / 4 . \tag{3.12}$$

This relationship tells that the speed caused by the rotational diffusion near the solid wall (entropic force) is 9/4 times that of the translational diffusion. Therefore one has

$$U^S = 9D^d / 4RT , \tag{3.13}$$

The orientational entropy S and the entropic mobility U^S enable one to incorporate the effect of orientational confinement in shallow channels to the expression of traditional unified electrochemical potentials and the flux developed for continuum transport of small spherical particles.

4 One-dimensional isotropic transport theory

In this chapter, a theoretical model is developed for the analysis of Ogston sieving of anisotropic polyelectrolytes in patterned nanofilter arrays based on steady state transport theory. In this model, the electric field driven migration of the polyelectrolytes is formulated as the transport of point-sized charged particles in the aqueous solutions, owing to the fact that there exists an equilibrium state in the rotational degree of freedom, as discussed Chapter 2 and Chapter 3. In addition, the three-dimensional transport problem will be transformed into a one-dimensional one through appropriate projections. Formula for the electrophoretic mobility and the dispersion of the polyelectrolytes across rectangle-shaped barrier will be derived analytically and the theoretical results are compared with experimental data. A method of designing the sieving structure and the electric field strengths will also be proposed.

4.1 Dynamically effective charged of rodlike DNA

In an aqueous solution, the electrostatic force that a polyelectrolyte is subjected to under an external electric field E is balanced by the viscous friction through

$$qE = \tilde{V}\varsigma^{e} \tag{4.1}$$

where q is the net charge, $\tilde{V}$ is the drifting velocity, and ς^{e} is the hydrodynamic friction coefficient for electric field driven motion. Free-solution electrophoretic mobility, which characterizes the velocity an electrolyte obtained under unit electric

field strength, is related to the friction coefficient by

$$U^e = \tilde{V} / E = q / \varsigma^e . \tag{4.2}$$

Apart from the electric field driven migration, polyelectrolytes in aqueous solution undergo random Brownian motions which magnify as translational diffusions. The translational diffusion coefficient is related to the translational diffusion coefficient by,

$$D^d = k_B T / \varsigma^d \tag{4.3}$$

where ς^d denotes the hydrodynamic friction coefficient for diffusion (Berg 1993). As discussed in Section 2.3, the friction coefficients ς^e and ς^d may take different values because the friction to diffusive motion and that to the electric field driven motion are associated with different physical phenomena (Mercier and Slater, 2006; Stellwagen et al., 2003). When a polyelectrolyte is moving due to non-electrostatic forces such as random kicks in diffusion, its surrounding counterions may move with it, while in the electric field, the counterions will be driven by the electric field to move in the opposite direction to that of the polyelectrolyte. In order to unify the flux caused by these diverse phenomena, so that the flux is dependent solely on the gradient of a unified energy (a force) and a unified friction coefficient (ς) regardless of the physical forces involved, a dynamically effective charge $\tilde{q}$ of the polyelectrolyte is introduced as

$$\tilde{q} = \frac{k_B T U^e}{D^d} . \tag{4.4}$$

This effective charge satisfies the relationship

$$\tilde{q} / \varsigma^d = q / \varsigma^e = U^e , \tag{4.5}$$

and it does not change the mobility of the electrolyte.

The introduction of $\tilde{q}$ permits one to reproduce the dynamics caused by the diffusion and electric field driven motion simultaneously without the need to deal with the two phenomena separately. Therefore one can use the transport model established for small spherical charged particles to analyze the electrophoretic dynamics of DNA molecule.

4.2 Partition coefficient between the shallow and the deep regions of the nanofilter

Let $C(\mathbf{r})$ be the concentration of an electrolyte at a point $\mathbf{r}=(x,y,z)$ in three-dimensional space. The partition function in a domain V at equilibrium state is defined by Giddings et al. (1968)

$$K=\frac{\iiint_V C(\mathbf{r})d\mathbf{r}}{\iiint_V c_0 d\mathbf{r}}, \tag{4.6}$$

where c_0 is the reference concentration in the bulk solution.

For the field free partition of anisotropic particles in the nanochannel space, $C(\mathbf{r})$ is determined by the balance between the steady state flux caused by diffusion

$$J_d=-D^d\frac{dC(\mathbf{r})}{d\mathbf{r}} \tag{4.7}$$

and that caused by the difference of orientational entropy

$$J_S=U^s C(\mathbf{r})\frac{dS_\Theta(\mathbf{r})}{d\mathbf{r}}. \tag{4.8}$$

At equilibrium state, J_d and J_S canceled each other such that

$$J_d + J_s = 0 . \tag{4.9}$$

Substituting the formulas of the orientational entropy and the entropic mobility as described in Chapter 3,

$$S_\Theta(\mathbf{r}) = k_B \ln \rho_\Theta(\mathbf{r}) \tag{3.5}$$

and

$$U^S = 9D^d / 4RT , \tag{3.13}$$

to Eq. (4.9), $C(\mathbf{r})$ is obtained as a function of $\rho_\Theta(\mathbf{r})$, which is

$$C(\mathbf{r}) = c_0 \rho_\Theta^{9/4}(\mathbf{r}) . \tag{4.10}$$

One may calculate the value of $\rho_\Theta(\mathbf{r})$ of a DNA rod at point $\mathbf{r}$ in the deep wells and shallow slits of the nanofilter numerically. Subsequently, the partition functions at the deep and shallow regions (K_d and K_s) can be obtained from Eqs. (4.6) and (4.10) .

The partition coefficient between the shallow region and the deep region is then

$$K = K_s / K_d . \tag{4.11}$$

This partition coefficient describes the distribution of anisotropic particles in the shallow and deep regions of the nanofilter caused by the difference of orientational entropies in these regions. It is noteworthy that this partition coefficient is defined in terms of the concentration in three-dimensional space. For particles whose sizes are significantly smaller than the channel dimension, the partition function is 1.0.

4.3 Projection of nanofilter to an equivalent channel with uniform cross sections

Because the transport of DNA molecules happens mainly in the direction of the

channel axis (x) direction, the degree in the depth (y) and width (z) directions of the channel can be eliminated by proper approximations. By this means, flux or migration in y - and z - directions are eliminated, one may formulate on the dynamics of DNA in the channel as one-dimensional transport problem (in x direction).

Let $C_a(x)$ be the averaged concentration over the cross section of the nanofilter at x,

$$C_a(x) = \frac{\iint_A C(x,y,z)dydz}{\iint_A dydz} \tag{4.12}$$

where A is the cross section of the channel. Here $C_a(x)$, which has a unit of $mol \cdot m^{-3}$, is still the concentration in three-dimensional space.

Because the area of the cross sections of the shallow and the deep regions

$$\iint_{A_S} dydz = w \cdot d_s \tag{4.13}$$

and

$$\iint_{A_d} dydz = w \cdot d_d \tag{4.14}$$

are different, variables that are related to the areas of cross section are all different for these two regions. For example, the amount of the molecules in deep region and that in shallow regions are given by

$$n_d = w \cdot d_d \int_{well} C_a(x)dx \tag{4.15}$$

and

$$n_s = w \cdot d_s \int_{slit} C_a(x)dx \tag{4.16}$$

respectively, where w is the width of the nanochannel.

Similarly, the amount of particles passing through the cross section of the deep region and that passing through the cross section of the shallow region are

$$N_d = w \cdot d_d J_d(x) \tag{4.17}$$

and

$$N_s = w \cdot d_s J_s(x) \tag{4.18}$$

respectively. At a steady state, the conservation of the mass requires that

$$N_d = N_s \tag{4.19}$$

meaning that

$$J_d(x) = \frac{d_s}{d_d} J_s(x). \tag{4.20}$$

The cross section difference causes unnecessary complications to the description of the problem when the three-dimensional description is projected to one-dimensional one. For simplification, the nanofilter is transformed to an equivalent imaginary channel with the uniform cross sections (width w and depth d_d) as shown in Fig. 4.1b. In this equivalent channel, the concentration of the electrolytes in the shallow and deep regions are defined as

$$C(x) = \begin{cases} \varepsilon C_a(x) & \text{if } x \text{ belongs to the slit} \\ C_a(x) & \text{if } x \text{ belongs to the well} \end{cases} \tag{4.21}$$

where

$$\varepsilon = d_s / d_d \tag{4.22}$$

is the depth ratio between the shallow and deep regions. It could be found easily that the steady state flux is constant over this imaginary channel, which is consistent to the conventional expressions.

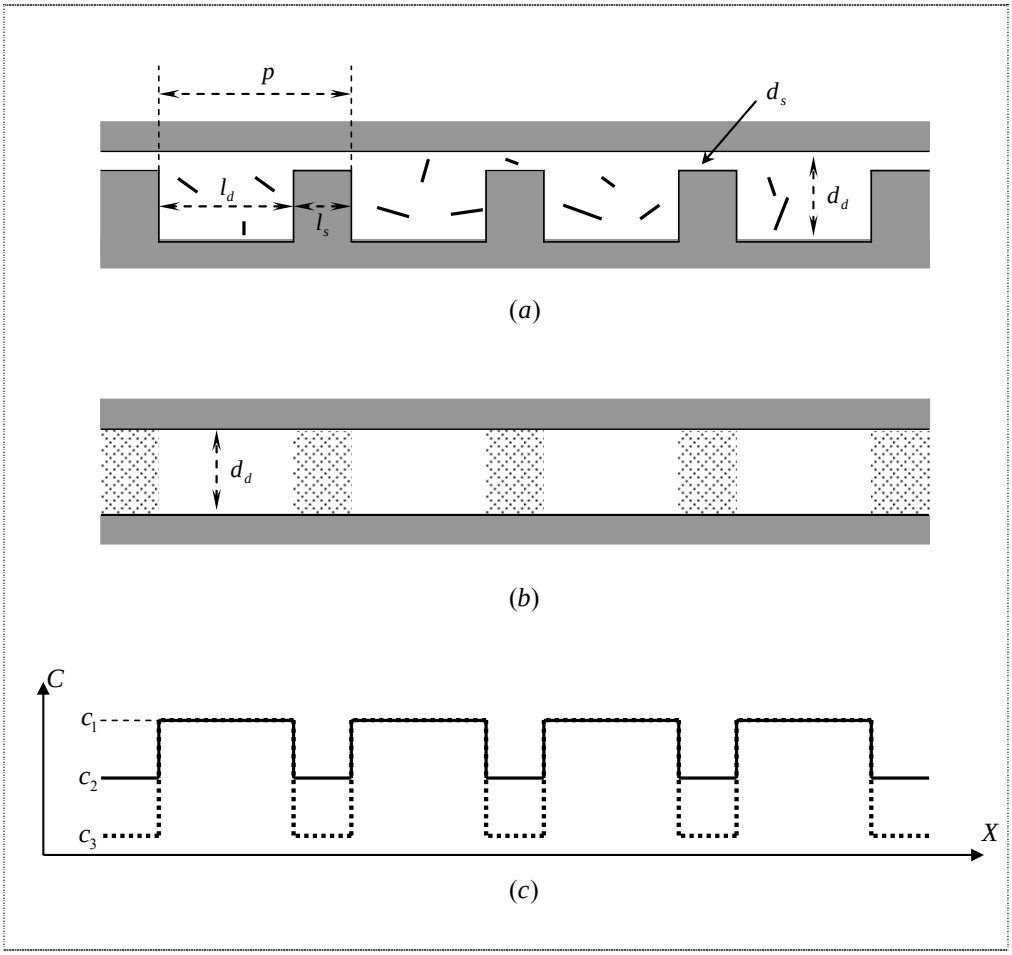

Fig. 4.1. Projection of the nanofilter array to an equivalent channel with uniform cross sections. (a) The nanofilter array. (b) The equivalent channel with uniform cross sections. (c) Partitions of molecules between shallow and deep regions in a field-free equilibrium state in the nanofilter array (solid lines) and in the equivalent channel (dotted lines). The coefficient $K = c_2 / c_1$ reflects the partition effect induced by configurational entropy. The ratio $K_\varepsilon = c_3 / c_2$ is the partition coefficient caused by projection.

Actually, the projection from the three-dimensional channel to the equivalent one-dimensional one through Eqs. (4.12) and (4.21) constitutes a new partition coefficient between regions representing the slit and the well of the nanofilter in this equivalent one-dimensional channel

$$K_\varepsilon = \varepsilon . \tag{4.23}$$

For example, let us consider an equilibrium state of a solution of ion where ion

concentration is a constant (c_0) in the whole channel space without an electric field. In this situation, K is equal to 1 because there is no configurational entropy effect. The values of $C_a(x)$ at deep and the shallow regions calculated using Eq. (4.12) are the same (both are equal to c_0). When one transforms these concentrations to the equivalent one-dimensional channel as shown in Fig. 4.1b, $C(x)$ in deep regions is equal to c_0 while $C(x)$ in shallow regions is εc_0. There arises a partition between these two regions (= ε) in this equivalent one-dimensional channel. The same reasoning holds for the cases where the orientational entropy exists ($K \neq 1$). Fig. 4.1c illustrates the typical concentration profile in the nanofilter array (solid lines) and that in the equivalent channel (dotted lines) at the field-free equilibrium state. The difference in the concentrations in the shallow and deep regions ($c_2 / c_1 = K$) is caused by the partition effect induced by configurational entropy. As one studies the distribution of the concentration in the imaginary one-dimensional channel, the partition coefficient is $c_3 / c_1 = \varepsilon K$. The ratio $K_\varepsilon = c_3 / c_2 = \varepsilon$ is the result of projection.

4.4 The potential energy landscape

The potential energy of a rigid anisotropic electrolyte in the nanofilter as shown in Fig. 4.2a is determined by the electric potential and the entropy. Based on the effective charge calculated in the Section 4.1, the dynamically unified potential in the equivalent channel as shown in Fig. 4.2b is given by

$$U(x) = \tilde{q}\Phi(x) - TS(x) \tag{4.24}$$

where $\Phi(x)$ is the electric potential, and $S(x)$ is the entropy. The entropy $S(x)$

accounts for the partitions caused by both the orientational entropy and the contraction in the channel width in the shallow regions.

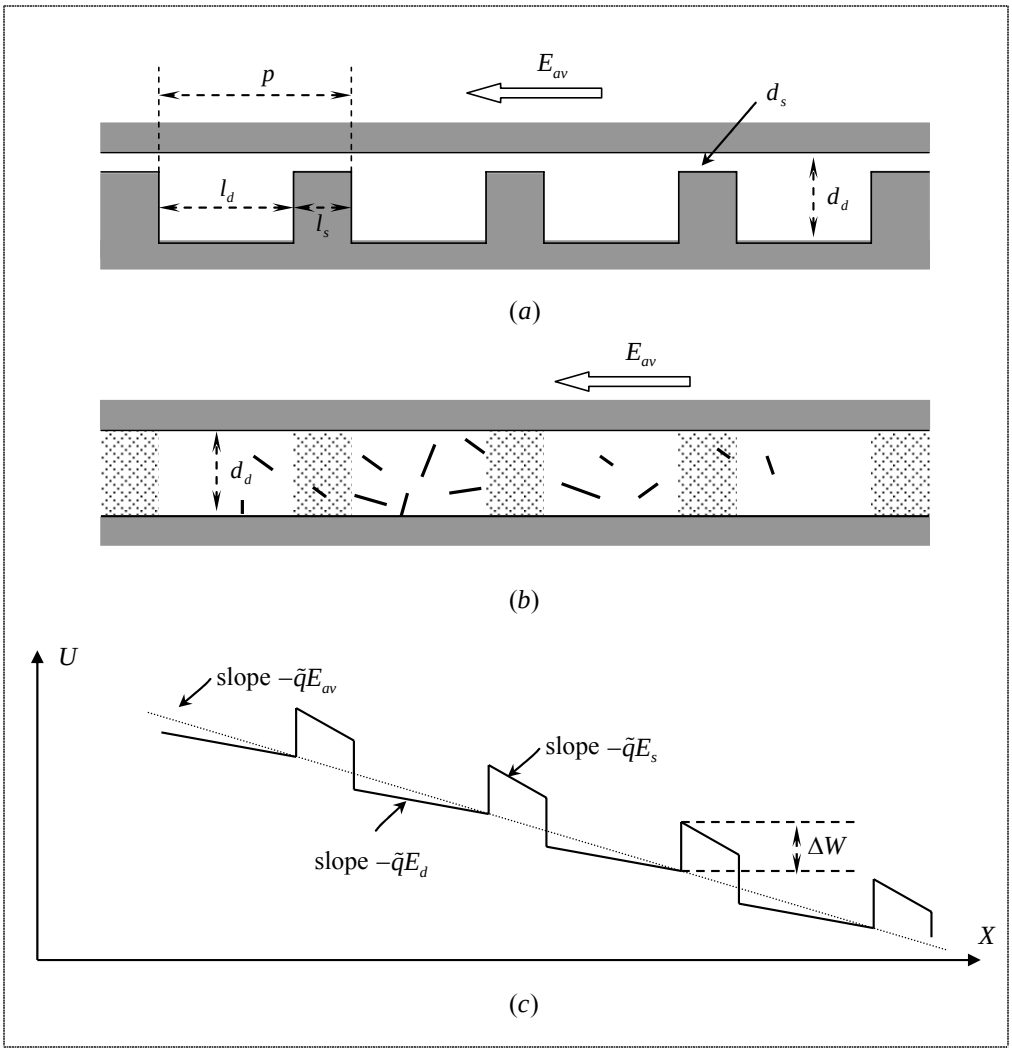

Fig. 4.2. The potential energy landscape of a rodlike DNA molecule along the nanofilter channel under an electric field. Under external electric field E_{av}, the overall slope of the energy landscape is $-\tilde{q}E_{av}$. The energy barrier ΔW is determined by the geometry of the nanofilter and the partition coefficient by $\Delta W = -k_B T \ln \varepsilon K$.

A typical potential energy landscape is show in Fig. 4.2c. This energy landscape has an overall slope of $-\tilde{q}E_{av}$, superimposed on which are a step function of entropic barrier and the variation of electric field in the deep and shallow regions.

The energy barrier at the junction of the well and the slit is

$$\Delta W = -T\Delta S = -k_B T \ln \varepsilon K . \tag{4.25}$$

Meanwhile, the electric field strength in the direction of channel axis in deep and shallow regions are given by

$$E_d = \frac{(l_s + l_d)d_s}{d_s l_d + l_s d_d} E_{av} \tag{4.26}$$

and

$$E_s = \frac{(l_s + l_d)d_d}{d_s l_d + l_s d_d} E_{av} \tag{4.27}$$

respectively.

The energy landscape $U(x)$ permits one to calculate the migrating speed of the electrolytes under appropriate assumptions. For example one can estimate the flux of charged particles using the Kramer's model, which states that the rate of transition from one potential well to the next well is determined by the height of the energy barrier between them in an exponential way. This method has been adopted widely to study the hindered transport problems (Stockmayer,1976; Ajdari and Prost, 1991). However, Kramer's model works only when the energy barriers are sufficiently high. In this thesis, the same problem will be solved using membrane theory. This method does not differentiate between the energy barrier and energy well and it can give the most accurate results under all range of electric fields.

4.5 Flux of electrolytes across the imaginary membrane with boundaries of fixed concentrations

Suppose there is an imaginary membrane separating the two deep regions. The thickness of this membrane is equal to the repeat length. The time for the solutes to

travel from one side of this imaginary membrane to the other side is exactly the trapping time in a well in Kramer's model. Based on the potential energy within this membrane, one can calculate the flux of particles at the steady state given the concentrations at the left side and the right one. The concentration within the membrane at steady state is determined by Boltzmann factor. By packing these imaginary membranes one exactly touching another (representing the repeats of the nanofilter array), non-steady-state evolution of concentration is described by changing of the concentrations at the interface between these membranes. In this case, the concentrations within the whole channel satisfy Boltzmann distribution piecewisely.

Fig. 4.3 shows the energy landscape and the concentration profile of the electrolytes across the imaginary membrane representing a unit of nanofilter. The values of concentration ($C \equiv C(x)$) at the left side and the right side of the membrane are c_A and c_B respectively. If the speed of electric motion is significantly smaller than that of translational diffusion, the steady state net flux of charged Brownian particles across the potential energy landscape ($U \equiv U(x)$) is given by (Stockmayer,1976)

$$J = -\frac{k_B T}{\varsigma}\nabla C - \frac{1}{\varsigma} C \nabla U \ . \tag{4.28}$$

By multiplying $e^{U/k_B T}$ to both sides of Eq. (4.28), one has

$$J e^{U/k_B T} = -\frac{k_B T}{\varsigma}\nabla (C e^{U/k_B T}) \tag{4.29}$$

At steady state, the flux J is independent of x. Therefore, the flux J can be calculated simply by spatial integration of both sides of Eq. (4.29) over the thickness of the membrane (x), which is (Cooper et al., 1985; Kocherginsky and Zhang, 2003)

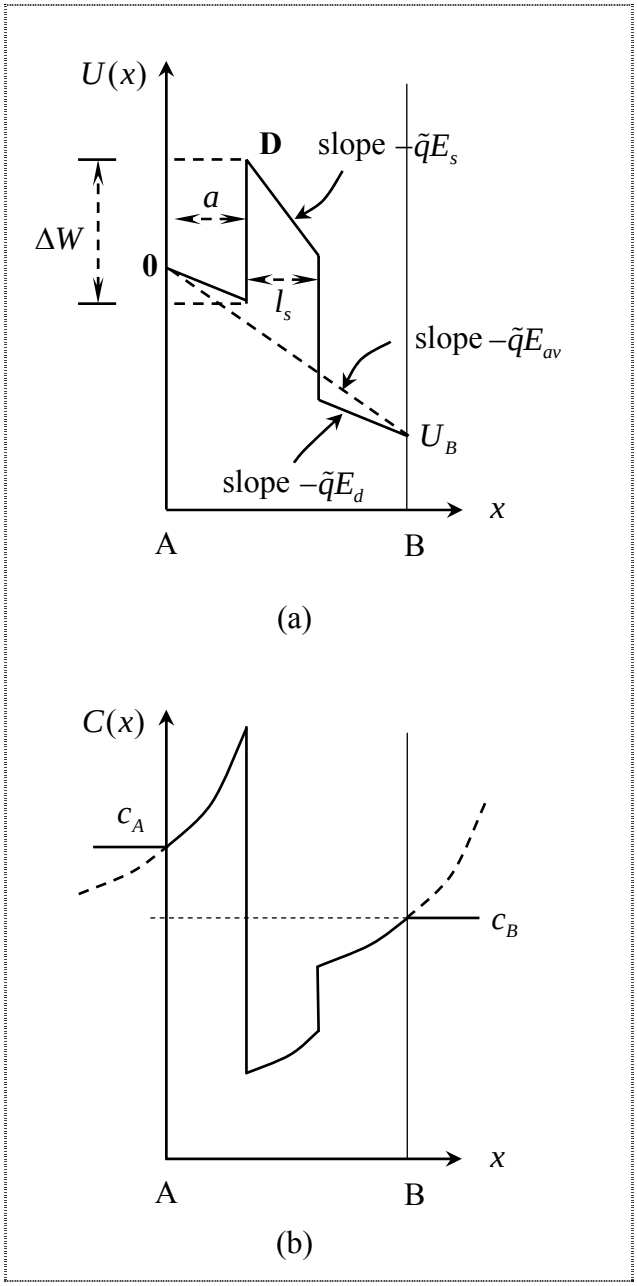

Fig. 4.3. The profile of potential and the concentration of a rod like DNA over a unit of a nanofilter. A and B are two corresponding points in the deep wells of two adjacent repeats (both of them are of distance $a \le l_d$ from the right wall of the well). (a) The potential profile of the DNA over the nanofilter under an average external electric filed E_{av}. E_s and E_d are electric fields in the slits and the wells, respectively. $\tilde{q}$ is the effective charge of the electrolyte. (b) Concentration of the electrolyte in the steady state when the concentrations at points A and B are maintained as c_A and c_B respectively.

$$J = -\frac{k_B T}{\varsigma}\left(c_B e^{U_B/k_B T} - c_A e^{U_A/k_B T}\right) / \int_A^B e^{U(x)/k_B T} dx . \tag{4.30}$$

With reference to Fig. 4.3a, if the reference energy at A is set as zero, the potential energy is given by

$$U(x) = \begin{cases} -\tilde{q}E_d x & 0 \le x < a \\ -\tilde{q}E_d a + \Delta W - \tilde{q}E_s (x-a) & a \le x < ls + a \\ -\tilde{q}E_{av} p + E_d (p-x) & ls + a \le x \le p. \end{cases} \tag{4.31}$$

Integration of the denominator of (4.30) yields,

$$J = -\frac{k_B T}{\varsigma}(c_A - c_B e^{-y_m})\frac{\varepsilon y_m (1+\nu)}{(\varepsilon+\nu)p}\left\{[1 - e^{-y_m} + (\varepsilon e^{\hbar} - 1)\eta]\right\}^{-1}. \tag{4.32}$$

Here the dimensionless parameters

$$\nu = l_s / l_d , \tag{4.33}$$

$$y_m = U_B / k_B T , \tag{4.34}$$

and

$$\hbar = \Delta W / k_B T = -\ln \varepsilon K \tag{4.35}$$

are the ratio of length of the slits to that of the wells, the reduced electric potential, and the reduced energy barrier, respectively. Parameters

$$\lambda = a / l_d , \tag{4.36}$$

and

$$\eta = (1 - e^{-\frac{\nu}{\varepsilon+\nu} y_m}) \delta e^{-\frac{\varepsilon\lambda}{\varepsilon+\nu} y_m} \tag{4.37}$$

are introduced for simplicity in expression. Substituting Eqs (4.4), (4.5), (4.31) and (4.35) to Eq. (4.32), one gets the expression of J in terms of mobility and electric field strength,

$$J = U^e E_{av}(c_A - c_B e^{-y_m}) \frac{\varepsilon(1+\nu)}{(\varepsilon+\nu)} \left\{[1 - e^{-y_m} + (K^{-1}-1)\eta]\right\}^{-1}. \quad (4.38)$$

4.6 The mobility of an electrolyte across the imaginary membrane

From the flux of particles under various conditions, transport parameters such as the electrophoretic mobility in the device and the dispersion rate can be obtained. To obtain the expression of the mobility in the nanofilter, one needs only to supply the electrolyte with constant concentration at one end and let them pass out at the other end. In the long run, a steady state is established such that the concentration profiles in every repeat are exactly the same. In such a steady state, the diffusion across the nanofilters is cancelled each other. The effective mobility can be obtained accordingly. By setting $c_A = c_B$ in Eq. (4.38), the effective mobility of anisotropic charged particles migrating across the imaginary membrane is derived as

$$\mu = \frac{1 - e^{-y_m}}{1 - e^{-y_m} + (K^{-1}-1)\eta} \frac{\varepsilon(1+\nu)}{\varepsilon+\nu} \bar{U}^e. \quad (4.39)$$

This mobility characterizes the average speed an electrolyte obtained under unit electric field strength when it migrates across the imaginary membrane representing one unit cell the nanofilter (From A to B in Fig. 4.3a). It is in accordance with the expectations that this mobility of anisotropic electrolyte is dependent on the electrolyte's free-solution ($\bar{U}^e$), the geometry of the nanofilter (ε, ν), the partition coefficient due to orientational entropy (K) and the electric field strength (y_m). However, it is quite counterintuitive to find that this mobility is dependant on the starting point of migration (η in Eq. (4.39), which is a function of distance a in Fig. 4.3a). This paradoxical fact arises from the nonuniform distribution of concentration of electrolyte in the well. At steady state, electrolytes are distributed such that the net

flux

$$J = \tilde{V}(x)C(x) \tag{4.40}$$

is constant at any value of x. The varied concentration $C(x)$ along the channel axis means that the average migrating velocity $\tilde{V}(x)$ in the channel differs at different points. The result is that the mobility of electrolytes over the membrane derived from $\tilde{V}(x)$ is dependent on the location of the starting point or boundary conditions. Calculating the effective mobility using $\tilde{V}(x)/E_{av}$ will surely produce a function of x.

4.7 The mobility of an electrolyte across a nanofilter cell

To derive the expression of the mobility for the nanofilter, one needs to have a further look into the problem. In the special case shown in Fig. 4.4, each well contains an amount of n_A electrolytes and the concentration profiles in all the repeats are identical. The average concentration in the well is given by

$$\overline{c} = \frac{n_A}{w l_d d_d}. \tag{4.41}$$

At the steady state, the distribution of the concentration $C(x)$ in the wells (and in the slits) is determined the Boltzmann factor and the constant flux requirements.

If one sets the left wall of the well at $x = 0$ (the right wall at $x = l_d$) the concentration $C(x)$ and the flux J at steady state can be obtained as,

$$C(x) = \frac{\varepsilon y_m \overline{c} \left\{ (e^{\frac{\nu y_m}{\varepsilon+\nu}} - 1) e^{\frac{\varepsilon y_m}{\varepsilon+\nu}\frac{x}{l_d}} (1-K) + K(e^{y_m} - 1) \right\}}{(1 - e^{\frac{\varepsilon y_m}{\varepsilon+\nu}})(1 - e^{\frac{\nu y_m}{\varepsilon+\nu}})(1-K)(\varepsilon+\nu) + \varepsilon(e^{y_m} - 1)K y_m} \tag{4.42}$$

and

$$J = \frac{\bar{c}\bar{U}^e E_{av}(1-e^{-y_m})\varepsilon^2(1+\nu)y_m}{(\varepsilon+\nu)^2\left\{(1-e^{-\frac{\varepsilon}{\varepsilon+\nu}y_m})(1-e^{-\frac{\nu}{\varepsilon+\nu}y_m})(\frac{1}{K}-1)+\frac{\varepsilon}{\varepsilon+\nu}y_m(1-e^{-y_m})\right\}} \tag{4.43}$$

respectively. From the value of steady state flux, one can obtain the average speed ($\bar{V}$) of all the n_A electrolytes in the well (the concentration is $\bar{c}$) migrating over the nanofilter as

$$\bar{V} = J / \bar{c} \,. \tag{4.44}$$

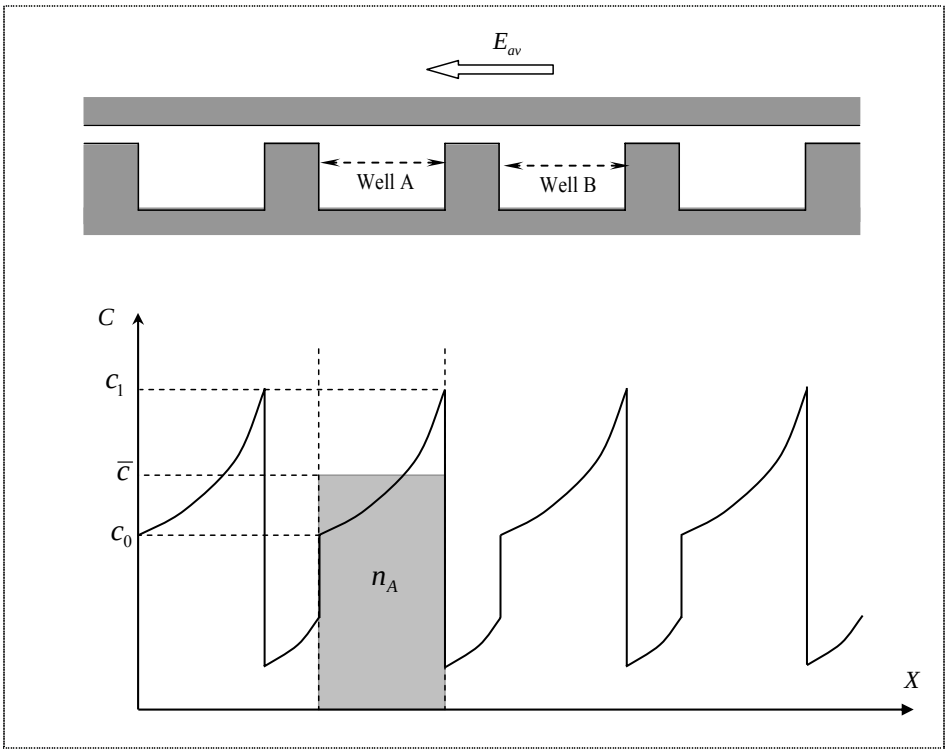

Fig. 4.4. Concentration profile over the nanofilter array at the steady state. As the concentration profiles in all repeats of nanoarray are identical, the net flux is entirely due to the motion driven by the electric field, from which the mobility can be obtained. The mobility of the electrolytes is based on the average speed for all the n_A electrolytes in well (A) to migrate to the next well (B).

Corresponding to the migration of solutions of electrolytes in the flat channel at the same speed $\bar{V}$ under electric field E_{av}, the mobility of a electrolyte over the nanofilter is given by

$$\mu = \frac{(1-e^{-y_m})\varepsilon^2(1+\nu)y_m}{(\varepsilon+\nu)^2\left\{(1-e^{-\frac{\varepsilon}{\varepsilon+\nu}y_m})(1-e^{-\frac{\nu}{\varepsilon+\nu}y_m})(\frac{1}{K}-1)+\frac{\varepsilon}{\varepsilon+\nu}y_m(1-e^{-y_m})\right\}}\bar{U}^e. \quad (4.45)$$

This mobility is an average value of the mobilities of a group molecules passing through the nanofilter arrays. It directly corresponds to the data obtained from experiments. In addition, unlike the previous models based on Kramer's model, which are valid approximately for low field cases, this mobility is valid in all ranges of electric fields.

4.8 Effect of electroosmotic flow

The finite charge of the solid channel wall leads to the electro-osmotic flow of the solution (Pennathur and Santiago, 2005a; Pennathur and Santiago, 2005b). As the surface properties of the solid channel and the depth of the Debye layer are difficult to obtain, the electro-osmotic mobility is difficult to determine *ab initio*. Fortunately, it is well known that, in the limit of thin Debye layer (under high ionic strength conditions) and low electric field, the profile of electroosmotic flow is similar to that of the electric field (Cummings et al., 2000; Duong-Hong et al., 2008). The result is that the effect of such an electro-osmotic flow can be modeled through modification of electrophoretic mobility of DNA molecules. Under such formulation, one needs to replace free-solution electrophoretic mobility $\bar{U}^e$ in expressions of mobility (and the dispersions described in Section 4.10) to incorporate the effect of the effect of electroosmotic flow.

4.9 Properties of the mobility of anisotropic electrolytes in the nanofilter array

The expression of the mobility of an anisotropic electrolyte over a nanofilter given be Eq. (4.45)) looks very complicated. It can be reduced to all known results or observations in the simpler cases.

4.9.1 Flat channel

If $\varepsilon = 1$ ($d_s = d_d$) or $\nu = 0$ ($l_s = 0$), the nanofilter reduces to a flat channel of depth d_d. The mobility in Eq. (4.45) will become

$$\mu_1 = \bar{U}^e. \tag{4.46}$$

Here the subscript "1" (and also the number in subscripts in the following subsections) means nothing but to indicate this is a special case (case 1) of the general mobility. This is in agreement with the expectation that the mobility of an electrolyte is equal to that of free-solution value when the hydrodynamic friction between the electrolyte and the channel wall is not considered due to presence of electroosmotic flow.

4.9.2 Transport of small ions

For small ions, the size of the particle is negligible to that of the channel. Because there is no orientational entropy effect, the partition functions due to orientation loss is $K_s = K_d = 1$. Substituting $K = 1$ to Eq. (4.45) yields

$$\mu_2 = \frac{\varepsilon(1+\nu)}{\varepsilon+\nu}\bar{U}^e. \tag{4.47}$$

This mobility for point-sized ions is the maximum mobility for an electrolyte to

migrate over a nanofilter array. It is often referred to as the maximum sieving free mobility $\mu_{\max}$, against which the mobilities of different electrolytes are compared to evaluate result of separation.

4.9.3 To mimic the channel to a gel membrane

The difference in the depths of the well and that of the slit of nanofilter (characterized by parameter ε), has two roles in the nanofiltration system: (1) to determine the size of the pore for the electrolytes to pass though (taking effect along with K), and (2) to distribute the electric potential gradients between the well and the slit (this role takes effect only in the insulate channel). To compare the mobility of electrolytes over insulate nanofilter with formula for the conducting gels, ε must be set as 1.0 ($d_s = d_d$) in order to ensure the same electric field in the regions with and without gel fibers. In this case, the shallow slit corresponds to a porous gel structure with partition coefficient K, while the deep well represents the open space filled with the solution. With reference to Fig. 4.3a, because the gel corresponds only to slits of the nanofilter, the length of the deep well has to be 0, which means $\nu >> 1$.

Under low electric field, where the mobility can be obtained by substitution of $e^{-y_m} \approx 1 - y_m$, $\varepsilon = 1$ and $\nu >> 1$ to Eq. (4.45), which gives

$$\mu_3 \approx K\bar{U}^e . \tag{4.48}$$

This is exactly the free volume model, which states that electrophoretic mobility of molecules in a porous system is simply equal to partition coefficient, or the ratio of the volume available to the molecule and the total gel volume (Ogston, 1958; Rodbard and Chrambach, 1970; Morris,1966).

4.9.4 Loss of entropic barrier effect under high field

Under high electric fields, with $e^{-y_m} \approx 0$, the mobility approaches

$$\mu_4 \approx \frac{\varepsilon(1+\nu)}{(\varepsilon+\nu)}\bar{U}^e . \tag{4.49}$$

This expression tells that under high electric field, the role of orientational entropy barrier (partition function K in Eq. (4.45)) becomes negligible. This phenomenon has been observed in both experimental observations (Fu et al. 2005) and stochastic model simulations (Lacchi et al, 2007). They contribute this finding to the lack of time for the DNA rods to sample all the orientations. However, based on the approximate equality between expression (4.49) (under high electric field and orientational entropy considered) and Eq. (4.47) (under any field strength, without orientational entropy), it can be established that even if the molecule has enough time to establish its orientational equilibrium state, the entropy barrier will still be overcome by the strong electric field.

4.10 Trapping time due to entropic barrier

The average time for an electrolyte molecule to travel from one repeat to the next one is obtained from the mobility μ

$$\tau = \frac{p}{\bar{V}} = \frac{p}{\mu E_{av}} \tag{4.50}$$

This time corresponds to the transition time from one state to the other across an energy barrier in Kramer's model. Substituting the Eq. (4.45) to (4.50), one gets the transition time being the sum of two terms,

$$\tau_{travel} = \frac{(\varepsilon+\nu)}{\varepsilon(1+\nu)}\tau_0 \tag{4.51}$$

and

$$\tau_{trap} = \frac{(\varepsilon+\nu)(1-e^{-\frac{\varepsilon}{\varepsilon+\nu}y_m})(1-e^{-\frac{\nu}{\varepsilon+\nu}y_m})}{\varepsilon(1-e^{-y_m})y_m}\frac{(1-K)}{K}\tau_{travel} \tag{4.52}$$

where $\tau_0 = p/\mu_0 E_{av}$ is the traveling time of the electrolyte in flat channel.

The drift time τ_{travel} in Eq. (4.51) describes the traveling time of an electrolyte without orientation entropic barrier. It is the time for a group of ions with mobility $\bar{U}^e$ to migrate across a unit nanofilter. Because the average electric field in the well is $E_d = E_{av}\varepsilon(1+\nu)/(\varepsilon+\nu)$, τ_{travel} of these ions in the nanofilter is prolonged by a factor of E_{av}/E_d, meaning that these ions migrate at an average speed of a speed $\bar{U}^e E_d$ over the nanofilter.

The trapping time τ_{trap} in Eq. (4.52) is the average time for the anisotropic particles to find their permissible orientations and travel across the slit of the nanofilter. Among all the n_A particles, Kn_A of them are at permissible orientations and passed without being trapped. The other $(1-K)n_A$ particles need a time duration $1/K$ times longer to find their permissible orientations, meaning that $\tau_{trap} \propto (1-K)/K$. The first factor in Eq. (4.52) reflects the focusing effect, which accumulates the electrolytes near the orientational entropy barrier and reduces τ_{trap}. This can be clearly seen at an intermediate or high voltages with $e^{-y_m} \sim 0$ and $e^{-\nu y_m/(\varepsilon+\nu)} \sim 0$. In such cases, introducing $\lambda = E_d l_d / E_{av} l_r$ as the fractional voltage in deep region, the first factor in τ_{trap} is approximately $(1-e^{-\lambda y_m})/\lambda y_m$, which is exactly the ratio of to $\bar{c}_d / C(l_d)$. A

higher the electric field in the deep region induces higher concentrations of electrolytes in the junction, which facilitates a higher number of them enter the slit. Therefore average trapping time is reduced.

4.11 Diffusion coefficient of electrolyte in the nanofilter

By comparison of the diffusion-induced flux is in the presence of the entropic barrier ($\varepsilon < 1$) and electric field (using(4.43)), and the corresponding flux in a flat channel ($\varepsilon = 1$ in Eq. using(4.43)), the effective diffusion coefficient in the nanofilter is obtained as,

$$D_{eff} = \frac{U_{eff}^{e}}{\bar{U}^{e}} \bar{D}^{d} . \tag{4.53}$$

Spatial variance of the diffusive dispersion over one nanofilter unit is therefore

$$\sigma_{diffu}^{2} = 2D_{eff}\tau = 2\bar{D}^{d}\tau_{0} , \tag{4.54}$$

where τ_0 is the times required for a particle to travel in flat channel for distance l_r. In addition to the diffusive dispersion, there is a convective dispersion arising from the exponential decay of concentration with time in a deep well**.** The mean and standard deviation of transition time (t_p) from one well (A) to the next (B) are $< t^{p} >= \tau$ and $< t_{p}^{2} >= 2\tau^{2}$, respectively(Ajdari and Prost, 1991). The variances in spatial space observed at B is $\sigma_{conv}^{2} = p^{2}$. The total variance of band dispersion over the n-repeat nanofilter array is

$$\sigma_{T}^{2} = np^{2} + 2n\bar{D}^{d}\tau_{0} . \tag{4.55}$$

This implies that in an electric field, the diffusive dispersion is not affected by the presence of the entropic barrier. The convective dispersion is dependent solely on the

structure of the nanofilter.

4.12 Design of task-specific nanofilter array

The analytical expression of the mobility permits one to assess the performance of a nanofilter without expensive experiments and time consuming numerical simulations. Specifically, $\mu - K$ plots can be drawn for different electrolytes under various electric field strengths for the designed nanofilters as shown in Fig. 4.5. Generally, the mobility μ of electrolytes increases with partition function K, approaching $\mu_{\max}$ with a rate dependent on the strength of the electric field. In a specific nanofilter, DNA rods of different sizes take different partition function values. The optimization of the nanofilter structure and the electric field is achieved when the mobilities of molecules with various lengths are well separated from each other.

Fig. 4.5 (solid markers) shows the computed mobilities of short DNA rods in a nanofilter with geometric parameters $l_s = l_d = 0.5\mu m$, $d_s = 60nm$ and $d_d = 240nm$ (referred to as 60/240 structure), and the comparison of these results with our experimental data. In the calculation, the electro-osmotic mobility U_{eeo} is used as the single free parameter to fit the predicted data to the experimental ones.

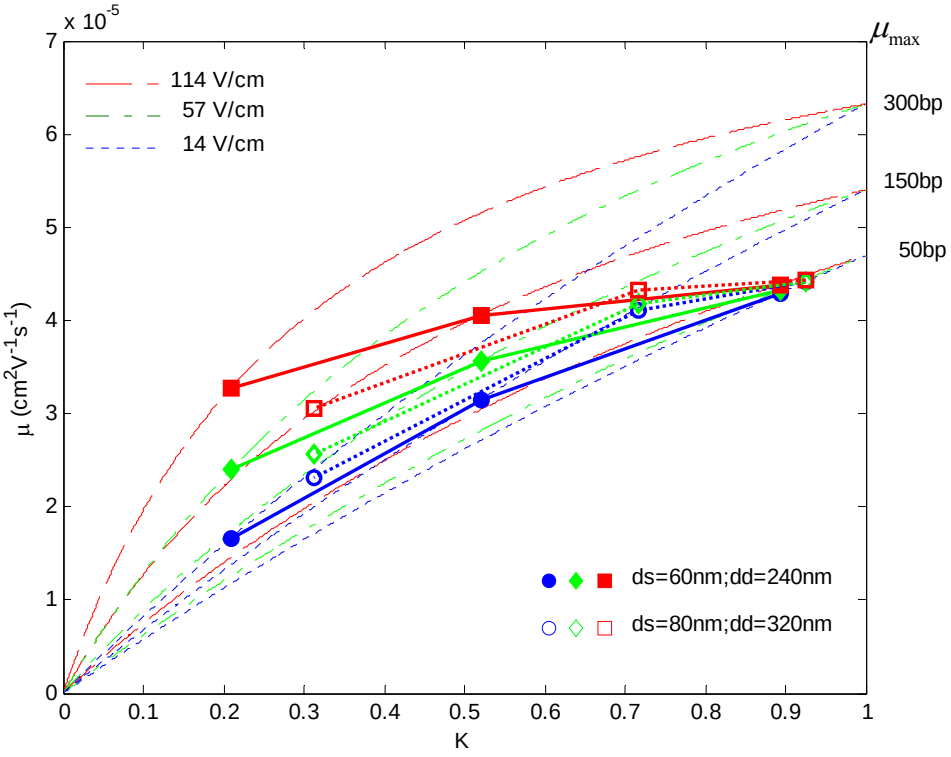

Fig. 4.5. The dependence of mobility μ on the partition coefficient K of DNA molecules of different sizes under varied electric field strengths. Colors of the curves represent the electric fields (red 114V/cm, green 57V/cm, and blue 14V/cm). For a specific DNA molecule, different nanoarray structures vary in the partition coefficients, indicated by solid (60/240) and unfilled (80/320) markers respectively. Thick lines connecting the solid or unfilled markers correspond to the experimentally obtained curves of mobility. The selectivity is optimized (by choosing the nanofilter and the selection of electric field) if the mobilities of DNA molecules of different sizes are well separated from each other in a given structure under a specific electric field.

Among voltages investigated here, 14V/cm electric field yields the best selectivity between 50bp, 100bp and 300bp DNA molecules. In addition to the 60/240 structure, Fig. 4.5 also shows $\mu - K$ plots of these DNA molecules over a wider nanofilter $d_s = 80nm$ and $d_d = 320nm$ (80/320) under the same electric fields. These two structures take the same values of ε and ν, therefore they produce the same

maximum mobility μ_{max} for a specific DNA. The $\mu - K$ curves for these two structures are also the same under a specific electric field. However, for a given DNA molecule, its partition coefficient K takes different values, and therefore its mobilities in these two structures are different. For example, a 300bp DNA has partition coefficient ~0.22 in 60/240 structure, while in 80/320 one, this value is ~0.42. It could be found from Fig. 4.5 that the selectivity for 50-300bp DNA in 80/320 structure is lower than that in 60/240 one under low electric field strengths. Under the electric field of 57 V/cm for 80/320 structure and that of 114V/cm for 60/240 structure, the separation is difficult as the mobilities of different molecules are close to each other in these cases. All these results agree well with our experimental observations. It is noteworthy that the mobility of DNA under high electric field strengths is close to the μ_{max} at all levels of K, meaning that the effect of entropy barrier becomes insignificant. In the previous study, this phenomenon was interpreted in terms of the aligning of DNA molecules along the electric field (Laachi et al., 2007).

4.13 Discussions

As the most important contribution to the theory of electrophoretic separation utilizing the entropy barrier in the nanofilter array, the formulas of the mobility and dispersion are established. Important insights into the mechanisms involved in this kind of separation process are obtained from these formulas. It provides valuable tools for design and analysis of the separation devices.

The analytical expressions in this chapter, including the mobilities, trapping times and the dispersions *etc.*, are derived from the over-simplified one-dimensional continuous

transport equation. Factors such as the nonuniform distribution of the electric field in the well, deformation of the electrolytes, the variations in the channel thickness and channel wall angles, non-zero depth of Debye layer, Joule heating and a lot of others are ignored, although some of them may have significant impacts on the separation results in the practice of experiments. Precautions must be taken in comparing the analytical results with the experimental data.

Despite of all these over-simplifications, the theoretical solutions obtained in this chapter are the only solution that is currently available for the experimentalists. To conduct more complicated simulations studies such as BD, DPD considering some of these factors are practically very computational expensive. Even the continuum model as described in the next two chapters is not easy for experimentalists. In addition, the physics involving the factors that have been neglected in this chapter are mostly not well established in the nanoscale. Analyzing the effect of these factors is not expected to be ubiquitously successful through any modeling approaches.

The dynamics of DNA electrophoresis in this chapter (and all through this thesis) is described in terms of behavior of a group of molecules. However, some physical parameters, such as the electrophoretic mobility and the trapping time, are normally defined and presented in a particle-based way. It seems that the group behavior should be different from that of the single molecule. For example, the time for a single molecule to migrate across a small pore of size that is comparable to the size of the particle is definitely different from that for a large group of molecules. However, this impression is not necessarily to be correct when the particle is subjected to some random forces and its dynamics has to be described stochastically.

Actually, the relationship between the dynamics of the group and that of a particle is that the group behavior is just average value of the dynamics single particles. This

average can be carried out in either time or spatial domain. The stochastic dynamics of a single molecule in the very long run should be the same as the dynamics of the group, which are characterized by dynamics of the group. Similarly, if one calculates the stochastic dynamics of a large number of particles concurrently, the averaged quantities of these dynamics should be the same as those obtained from group description. Specific to the problem of electrophoretic separation studied in this chapter, expectation of mobility of single molecule (particle-based description) should be the equal to that computed from the flux of a group of molecules (the group behavior).

The above justification works also for the definition of transition time. The average amount of time required for a group of molecules trapped in one trap to move on to the next trap is equal to the average time required for a single molecule. That is why concentration does not appear in the expressions of the mobility in Eq. (4.45) or transition times in Eqs. (4.51) and (4.52).

5 Three-dimensional anisotropic transport model

The one-dimensional theoretical formulation developed in Chapter 4 provides a simple analytical solution to the mobility and dispersion of anisotropic electrolytes migrating over the nanofilter array. It helps one to identify the effect of the nanofilter geometries and the electric field strengths without consideration of many other factors which are often very difficult to describe. In this chapter, a more complicated scenario is considered that includes the effect of some complicated factors such as the inhomogeneous electric field, the anisotropic transport parameters etc. For this purpose, the master differential equations for the flux and the concentration will be developed in three-dimensional space using anisotropic transport theory. These differential equations are to solved numerically (details to be described in the next chapter) to obtain the concentration profile of the electrolytes at any time in the channel.

5.1 Anisotropic transport equation

Let $C \equiv C(\mathbf{r},t)$ denote the concentration of DNA molecules at a point $\mathbf{r} = (x, y, z)$ at time t, a unified electrochemical potential $\epsilon \equiv \epsilon(\mathbf{r},t)$ of an electrolyte in an aqueous solution can be expressed as (Kocherginsky and Zhang, 2003)

$$\epsilon = \epsilon^0 + RT \ln C + q\Phi - TS . \tag{5.1}$$

Here ϵ^0, R, T, q and $\Phi \equiv \Phi(\mathbf{r})$ denote the reference standard-state potential, the gas constant, the absolute temperature, the effective charge of the DNA and the external

electric filed potential, respectively. Scalar field function $S \equiv S(\mathbf{r})$ represents the orientational entropy of the rigid DNA rod which captures the stochastic distribution of its orientations in the presence of solid channel walls. The spatial gradient of this unified potential $\nabla \epsilon$ constitutes a driving force that generates a flux of the DNA in the solvent. According to Eq. (5.1), $\nabla \epsilon$ consists of forces from three independent factors, namely thermal fluctuation, electric force and entropic gradient respectively. The fluxes induced by these forces are the sum of their respective contributions, *i. e.*

$$\mathbf{J} = -\left(\mathbf{D}^{\mathbf{d}} \nabla C + \mathbf{U}^{e} C \nabla \Phi - U^{S} C T \nabla \mathrm{S}\right), \tag{5.2}$$

where $\mathbf{D}^{\mathbf{d}} \equiv \mathbf{D}^{\mathbf{d}}(\mathbf{r})$ and $\mathbf{U}^{e} \equiv \mathbf{U}^{e}(\mathbf{r})$ are the tensors of diffusion coefficient (in unit of $cm^2 s^{-1}$) and electrophoretic mobility (in $\mathrm{ms^{-1}V^{-1}}$) respectively. The scalar U^S, which is referred to as *entropic mobility* in this thesis, represents the mobility associated with the gradient of orientational entropy (an *entropic force*). This mobility captures the stochastic interactions of a DNA with the solid wall. It has a unit of $m \cdot s^{-1} mol^{-1} N^{-1}$ and equals to the velocity of a DNA rod obtained if 1 newton of force is applied to 1mol of DNA molecules. The evolution of the concentration of DNA is governed by the mass conservation law

$$\frac{\partial C}{\partial t} = -\nabla \cdot \mathbf{J} . \tag{5.3}$$

The solution of master equations (5.2) and (5.3) with no-flux boundary conditions describes the electrophoretic transport of the rod-like DNA molecules in the nanofilter array.

5.2 Electric field in the nanofilter

The channel walls studied in this thesis are made of insulate silicon-based material.

When an external electric field E_{av} is applied over a nanochannel with length $\tilde{L}$, the electric filed is distributed according to Laplace equation

$$\nabla^2\Phi = 0\,, \tag{5.4}$$

with boundary conditions

$$\begin{aligned}&\Phi(0, y, z) = 0\\ &\Phi(\tilde{L}, y, z) = -\tilde{L}\tilde{q}E_{av}\,,\\ &\frac{\partial\Phi}{\partial\mathbf{n}} = 0\end{aligned} \tag{5.5}$$

where **n** represents the normal vector of surface of the channel wall. Because the analytical solutions of the electric potential Φ and its gradient $\nabla\Phi$ not available, they are obtained numerically (as described in the next chapters).

5.3 Anisotropic diffusion coefficient and electrophoretic mobility

A DNA rod has two different translational hydrodynamic friction coefficients, denoted by $\zeta_{//}^{d}$ and $\zeta_{\perp}^{d}$, respectively, for the motion parallel and perpendicular to its long axis under thermal fluctuation, gravity and other non-electrostatic forces (Brenner, 1979; Han et al., 2006; Berg 1993). As a result, the translational diffusion coefficient is orientation dependent. When the same force is applied to two identical DNA rods with different orientations, the speeds that these DNA acquired will be different.

When a DNA is oriented at $\mathbf{\Theta} = (\theta, \phi)$ as shown in Fig. 5.1, its translational diffusion coefficient is given by tensors (Brenner, 1979)

$$\boldsymbol{\mathcal{D}}^{\boldsymbol{d}}(\mathbf{\Theta}) = D_{//}^{d}\mathbf{\Theta}\mathbf{\Theta} + D_{\perp}^{d}(\mathbf{I} - \mathbf{\Theta}\mathbf{\Theta})\,, \tag{5.6}$$

where

$$D_{//}^{d} = k_B T / \zeta_{//}^{d} \tag{5.7}$$

and

$$D_{\perp}^{d} = k_B T / \zeta_{\perp}^{d} \tag{5.8}$$

are the coefficients of the rod for translational diffusion parallel and perpendicular to the rod's axis, respectively. The expression

$$\mathbf{I} = \mathbf{i}_x\mathbf{i}_x + \mathbf{i}_y\mathbf{i}_y + \mathbf{i}_z\mathbf{i}_z \tag{5.9}$$

denotes the physical space identity tensor.

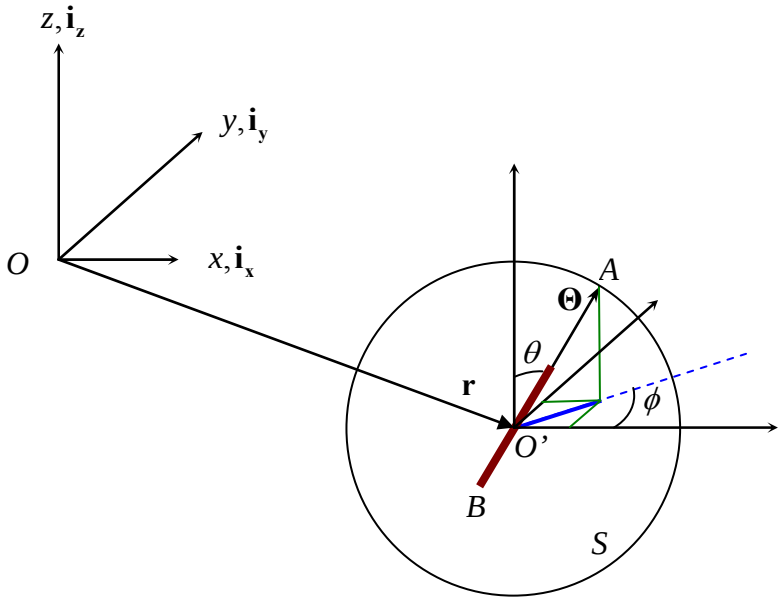

Fig. 5.1. The position and orientation of a DNA rod. Axes *Oxyz* represent a global system. Vector **r** denotes the position of center of the DNA. Vector $\mathbf{\Theta} = (\theta, \phi)$ represents the unit vector ($|O'A| = 1$) locked into the DNA rod ($|O'B| = L/2$) and lies along the rod's long axis. The surface of the unit sphere is represented by S, corresponding to all the possible orientations of the rod.

Similarly, the orientation dependent electrophoretic mobility is given by,

$$\boldsymbol{\mathcal{U}}^{e}(\mathbf{\Theta}) = U_{//}^{e}\mathbf{\Theta}\mathbf{\Theta} + U_{\perp}^{e}(\mathbf{I} - \mathbf{\Theta}\mathbf{\Theta}), \tag{5.10}$$

where

$$U_{//}^{e} = q / \zeta_{//}^{e}, \tag{5.11}$$

and

$$U_{\perp}^{e} = q / \zeta_{//}^{e} \tag{5.12}$$

are the coefficients of the rod for electric field driven motion parallel and perpendicular to the rod's axis, respectively. Here translational hydrodynamic friction coefficients for electric field driven motion, $\zeta_{//}^{e}$ and $\zeta_{\perp}^{e}$, are not necessarily equal to their corresponding values for diffusion, $\zeta_{//}^{d}$ and $\zeta_{\perp}^{d}$ respectively. The reason is that these two are different physical phenomena (Mercier and Slater 2006; Stellwagen et al., 2003). When a DNA is diffusing or moving due to non-electrostatic forces, its surrounding counterions will move with it, while in the electric field, the counterions will be driven by the electric field to move in the opposite direction.

At the rotational equilibrium state, the mean translational diffusion coefficient $\mathbf{D}^{\mathbf{d}}(\mathbf{r})$ and the mean electrophoretic mobility $\mathbf{U}^{\mathbf{e}}(\mathbf{r})$ at position $\mathbf{r}$ are given by the weighted summation of orientation dependent tensors ($\boldsymbol{\mathcal{D}}^{d}(\boldsymbol{\Theta})$ and $\boldsymbol{\mathcal{U}}^{e}(\boldsymbol{\Theta})$), such that

$$\mathbf{D}^{\mathbf{d}}(\mathbf{r}) = \iint_{S} p(\boldsymbol{\Theta} \mid \mathbf{r}) \boldsymbol{\mathcal{D}}^{d}(\boldsymbol{\Theta}) d^{2}\boldsymbol{\Theta} \tag{5.13}$$

and

$$\mathbf{U}^{\mathbf{e}}(\mathbf{r}) = \iint_{S} p(\boldsymbol{\Theta} \mid \mathbf{r}) \boldsymbol{\mathcal{U}}^{e}(\boldsymbol{\Theta}) d^{2}\boldsymbol{\Theta}, \tag{5.14}$$

respectively. Here the areal element on the surface of the unit sphere $S = \{0 \le \theta < \pi; 0 \le \phi < 2\pi\}$ is

$$d^{2}\boldsymbol{\Theta} = \sin\theta d\theta d\phi, \tag{5.15}$$

and $p(\mathbf{\Theta}\,|\,\mathbf{r})$ is the probability that the rod is orientated at $\mathbf{\Theta}$ when its center is located at point $\mathbf{r}$.

When the DNA lies in the bulk solution, or when it is located such that there is no intersection between the rod and the wall at any orientation, all its orientations are accessible at an equal probability of

$$p(\mathbf{\Theta}\,|\,\mathbf{r}) = (4\pi)^{-1}. \tag{5.16}$$

On the other hand, if the DNA rod is in a confined space, some of its orientations is not accessible. The occurrence of the orientation $\mathbf{\Theta}$ is determined by the requirement that the summation of the probabilities of the permissible orientations be equal to unity, which yields,

$$p(\mathbf{\Theta}\,|\,\mathbf{r}) = \begin{cases} [4\pi\rho_{\Theta}(\mathbf{r})]^{-1} & \text{if orientation } \mathbf{\Theta} \text{ is permissible at } \mathbf{r} \\ 0 & \text{otherwise} \end{cases}. \tag{5.17}$$

For the calculation of $\mathbf{D^d}(\mathbf{r})$ and $\mathbf{U^e}(\mathbf{r})$, parameters $D^d_{//}$, $D^d_{\perp}$, $U^e_{//}$ and $U^e_{\perp}$ have to be determined. These values can be obtained approximately from the free-solution diffusion coefficient and free-solution electrophoretic mobility using methods as described below.

In the bulk solution, the mean diffusion coefficient and the mean electrophoretic mobility are isotropic (Brenner, 1979). The tensors $\bar{\mathbf{D}}^{\mathbf{d}}$ and $\bar{\mathbf{U}}^{\mathbf{e}}$ are given by

$$\bar{\mathbf{D}}^{\mathbf{d}} = \mathbf{I}D^d \tag{5.18}$$

and

$$\bar{\mathbf{U}}^{\mathbf{e}} = \mathbf{I}U^e, \tag{5.19}$$

respectively. The scalars

$$D^d = (D^d_{//} + 2D^d_{\perp})/3 \tag{5.20}$$

and

$$U^e = (U^e_{//} + 2U^e_{\perp})/3 \tag{5.21}$$

correspond to the diffusion coefficient and the free-solution electrophoretic mobility that are obtained experimentally (Stellwagen and Stellwagen, 2002; Allison and Mazur 1998; Eimer and Pecora, 1991; Tirado et al., 1984; Tinland et al., 2000; Arvanitidou and Hoagland, 1991; Stellwagen et al., 1997).

Equations (5.20) and (5.21) permit one to estimate the values of $D^d_{//}$, $D^d_{\perp}$, $U^e_{//}$ and $U^e_{\perp}$ from $\bar{D}^d$ and $\bar{U}^e$ directly using the established relationships $D^d_{//} \approx 2D^d_{\perp}$ (Happel and Brenner, 1991) and $U^e_{//} \approx 2U^e_{\perp}$ (Ohshima, 1996),

$$D^d_{//} \approx 2D^d_{\perp} \approx \frac{3}{2} D^d \tag{5.22}$$

and

$$U^e_{//} \approx 2U^e_{\perp} \approx \frac{3}{2} U^e . \tag{5.23}$$

To determine $D^d_{//}$, $D^d_{\perp}$, $U^e_{//}$ and $U^e_{\perp}$ using the experiment data relieves one from the complicated task of determining the hydrodynamic coefficients and effective charges for the DNA molecules (Levine et al., 2004; Nkodo et al., 2001).

It should be noted that while the relationship between $D^d_{//}$ and $D^d_{\perp}$ is well-established (Happel and Brenner, 1991), the relationship between the $U^e_{//}$ and $U^e_{\perp}$ is not so simple. It has been shown that $U^e_{\perp}$ is dependent on $\kappa_D a$ (κ_D is the Debye-Hückel parameter and a is the radius of the DNA) in contrast to $U^e_{//}$, which is $\kappa_D a$ independent

(Ohshima,1996). In the low $\kappa_D a$ regime, Debye length κ_D^{-1} is comparable or larger than the width of the DNA (a), so that hydrodynamic drag to the surrounding fluid occurs just as in the non-electrophoresis case. In this circumstance, the dynamics of the rod is dominated by the simple hydrodynamic interactions, *i. e.* $U_{//}^e \approx 2U_{\perp}^e$. However, when $\kappa_D a$ becomes large, there won't be any difference $U_{//}^e$ and $U_{\perp}^e$ because the Debye screening effect takes the dominant role. Under our experimental conditions, $\kappa_D a \approx 1$, the relationship $U_{//}^e \approx 2U_{\perp}^e$ holds approximately.

The calculation of the position specific diffusion coefficient $\mathbf{D}^{\mathbf{d}}(\mathbf{r})$ and the electrophoretic mobility $\mathbf{U}^{\mathbf{e}}(\mathbf{r})$ using relationships (5.20) through (5.23) relieves one from determination of a lot of parameters such as effective charge q , friction coefficients $\zeta_{//}^e$, $\zeta_{\perp}^e$, $\zeta_{//}^d$ and $\zeta_{\perp}^d$, *etc.*

5.4 Effect of the electro-osmotic flow on anisotropic transport

In the presence of electro-osmotic flow, the electrophoretic mobility of DNA molecules has to be determined from the velocities induced by two different forces. First, the velocity induced by electrostatic force is

$$\mathbf{v}(\mathbf{r}) = \bar{\mathbf{U}}^{\mathbf{e}}(\mathbf{r})\nabla\Phi(\mathbf{r}) . \tag{5.24}$$

Second, the velocity caused by the friction force of the fluids with electro-osmotic flow is

$$\mathbf{v}_{eeo}(\mathbf{r}) = U_{eeo}\nabla\Phi(\mathbf{r}) , \tag{5.25}$$

with U_{eeo} denoting the mobility of the electro-osmotic flow.

Thus the velocity of the DNA rod is the sum of these two,

$$\mathbf{v} = \left(\bar{\mathbf{U}}^{\mathbf{e}}(\mathbf{r}) + \mathbf{I}U_{eeo} \right) \nabla \Phi(\mathbf{r}) . \tag{5.26}$$

This means that the effective electric mobility is $\left(\bar{\mathbf{U}}^{\mathbf{e}}(\mathbf{r}) + \mathbf{I}U_{eeo} \right)$ in the presence of the electro-osmotic flow. In this circumstance, $\bar{\mathbf{U}}^{\mathbf{e}}(\mathbf{r})$ in Eq. (5.2) has to be replaced by this effective electrophoretic mobility in the calculation.

5.5 Integration of master transport equations

Given the electric field $\nabla\Phi$, orientational entropy S, and the transport parameters $\mathbf{D}^{\mathbf{d}}$, $\mathbf{U}^{e}$ and U^{S}, the migration of DNA in the channel of the nanofilter array can be obtained by integration of Eq. (5.3), such that

$$\mathrm{C}(\mathbf{r},t) = \mathrm{C}_0(\mathbf{r}) - \int_0^t \nabla \cdot \mathbf{J}(\mathbf{r},t')dt', \tag{5.27}$$

where $\mathrm{C}_0(\mathbf{r})$ is the initial distribution of the concentration.

As the analytical expressions for the flux and the concentration are not available for three-dimensional analysis, numerical methods are employed to discretize the problem domain and perform the necessary integration. Although the running of such numerical simulations requires a significant amount of computations, it is much faster than the stochastic models because no random variables are involved in the current continuum model. The detailed description of the numerical methods is given in the next chapter.

6 Numerical method for discretization and integration

This thesis uses Smoothed particle hydrodynamics (SPH) method to discretize the problem domain and the master transport equations. SPH discretizes the hydrodynamic equations using a set of particles that follow the flow field. Since its invention in 1977 (Lucy, 1977), these methods have been successfully applied in many areas such as astrophysics, fluid flows, material modeling and other multi-disciplinary fields (Liu and Liu, 2003; Monaghan 2005; Kum et al., 2005). SPH methods discretize the problem domain and control differential equations using a set of particles. An arbitrary continuous field function $A(r)$ and its derivatives $\partial A(r)/\partial r$ are approximated as the weighted summation over the neighboring particles through a smoothing function $W(r)$ and its derivative $dW(r)/dr$. The main idea of SPH is illustrated in Fig. 6.1. The function value at particle i, $A(r_i)$, is approximated by the weighted summation of the function values of its neighbors (j). The weight function $W(r)$, which is referred to as kernel function, is designed to satisfy the following requirements: (1) $W(r)$ is continuous function which decreases with increasing distance r; (2) $W(r)$ is non-zero only within a local domain (supporting domain), beyond which it becomes zero; and (3) The integration of $W(r)$ in the supporting domain is equal to 1.

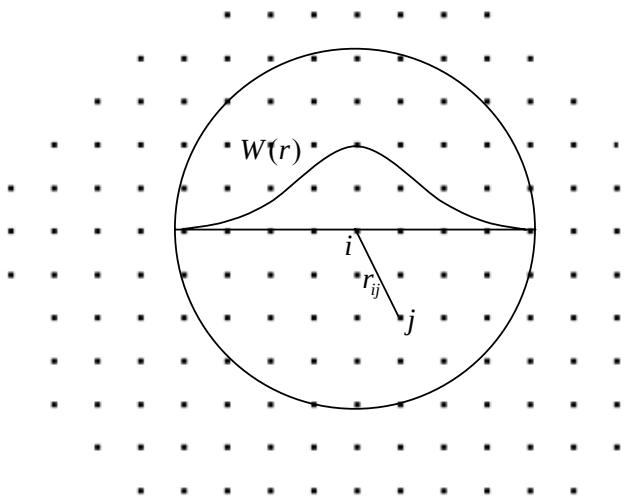

Fig. 6.1. SPH approximations of the function value at a particle by weighted summation of the function values at all the particles within its supporting domain (shown as circle). The kernel function $W(r)$ takes non-zero values only within the supporting domain. Particles outside the supporting domain do not affect particle i directly.

As all the calculations in SPH are performed in a local supporting domain and the time-integration is done explicitly, they are very efficient. This localized formulation also enables one to simulate a multiple-repeated nanochannel using structural data of only one repeat. As shown in Fig. 6.2, calculation in *nth* repeat requires only the state variables in the *nth* repeat and those in the shadowed regions of the two neighboring repeats. Other regions of the nanofilter (no matter how long the nanofilter is) do not affect the *nth* repeat directly. Therefore in the implementation, only the concentration is required to be stored for the whole multiple-repeated structure. Other data, including the electric field, tensors of diffusion coefficients and the electric mobility, the entropy etc., are all calculated and stored in a single repeat. In calculation of the flux and the changes of the concentration, the single repeat structure shown in gray (along with the shadowed region) is used to represent any repeat of the nanofilter by assigning the appropriate respective concentrations in the nanofilter. Avoiding discretization of large-scale structure reduces the scale of the problem significantly.

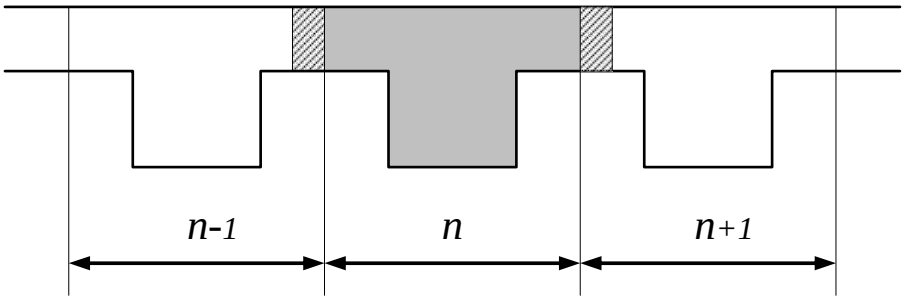

Fig. 6.2. Representation of a multiple-repeated structure using only one repeat (n). The structure shown in gray, including the shadowed extended regions (represented by virtual particles) to both sides of it, is used to represent any one of the multiple-repeated channel. The state variables of the virtual particles in the shadowed regions are taken from the neighboring repeats to provide correct supporting domain for particles near the junctions of two repeats.

6.1 Basic equations of SPH

In SPH, an arbitrary continuous field function $f(\mathbf{r})$ and its derivatives $\partial f(\mathbf{r})/\partial \mathbf{r}$ at point $\mathbf{r} = (x, y, z)$ are approximated as the weighted summation over the neighboring particles through a smoothing function $W(r)$ and its derivative $dW(r)/dr$. For a given particle centered at point $\mathbf{r_i}$, the function value and the gradient can be evaluated as

$$f(\mathbf{r_i}) = \sum_{j=1}^{N} \upsilon_j f(\mathbf{r_j}) W_{ij} \; ; \tag{6.1}$$

$$\frac{\partial f(\mathbf{r_i})}{\partial \mathbf{r_i}} = \sum_{j=1}^{N} \upsilon_j \left[f(\mathbf{r_j}) - f(\mathbf{r_i}) \right] \nabla_i W_{ij} \; , \tag{6.2}$$

where N is the number of particles in the supporting domain of particle i, $r_{ij} = |\mathbf{r}_i - \mathbf{r}_j|$ is the distance between particle j and i, υ_j is the volume of space represented by particle j. The expressions W_{ij} and $\nabla_i W_{ij}$ are given by

$$W_{ij} = W(r_{ij}) \tag{6.3}$$

and

$$\nabla_i W_{ij} = \frac{\mathbf{r}_i - \mathbf{r}_j}{r_{ij}} \frac{\partial W_{ij}}{\partial r_{ij}}, \tag{6.4}$$

respectively.

The kernel function $W(r)$ may take many forms as discussed in (Liu and Liu, 2003). In this work, the kernel function and its derivative are chosen as,

$$W(r) = \begin{cases} \frac{105}{16\pi h^3}(1+3\frac{r}{h})(1-\frac{r}{h})^3, & r < h \\ 0 & r \geq h \end{cases} \tag{6.5}$$

and

$$\nabla W(\mathbf{r}) = -\mathbf{r}F(r) = \begin{cases} -\mathbf{r}\frac{315}{4\pi h^5}(1-\frac{r}{h})^2 & r < h \\ 0 & r \geq h \end{cases}, \tag{6.6}$$

respectively. A lot of other kernel functions can be found in Liu and Liu (2003).

6.2 SPH equations for flux and concentration evolution

Substituting Eqs. (6.1) through (6.4) to Eq. (5.2), the components of flux of electrolytes in the coordinate direction $\alpha = x, y, z$ at $\mathbf{r_i}$ can be rewritten in the following form

$$\begin{aligned} J_i^{\alpha} = & -\sum_{j=1}^{N} \upsilon_j (C_j - C_i) D_j^{\alpha\beta} \frac{\partial W_{ij}}{\partial r_i^{\beta}} \\ & -\sum_{j=1}^{N} \upsilon_j (\Phi_j - \Phi_i) C_j U_j^{\alpha\beta} \frac{\partial W_{ij}}{\partial r_i^{\beta}} \cdot \\ & +\sum_{j=1}^{N} U^s T \upsilon_j (S_j - S_i) C_j \frac{\partial W_{ij}}{\partial r_i^{\alpha}}. \end{aligned} \tag{6.7}$$

Here $D_j^{\alpha\beta}$ and $U_j^{\alpha\beta}$ are $\alpha\beta$ - components of tensors $\mathbf{D}^{\mathbf{d}}(\mathbf{r_j})$ and $\mathbf{U}^{\mathbf{e}}(\mathbf{r_j})$ respectively. The summations over different directions are represented by the repeated index β $(=x, y, z)$. An example expansion of such summations is as follows

$$D^{\alpha\beta}\frac{\partial W_{ij}}{\partial r_i^{\beta}} = D^{\alpha x}\frac{\partial W_{ij}}{\partial x_i} + D^{\alpha y}\frac{\partial W_{ij}}{\partial y_i} + D^{\alpha z}\frac{\partial W_{ij}}{\partial z_i}. \tag{6.8}$$

After obtaining the fluxes, the evolution of concentration Eq. (5.3) acquires its SPH form as,

$$\frac{\partial C_i}{\partial t} = -\sum_{j=1}^{N} \upsilon_j (J_j^{\beta} - J_i^{\beta})\frac{\partial W_{ij}}{\partial r_i^{\beta}}. \tag{6.9}$$

Once again, the repeated index β represents the summations over all the coordinate directions.

Using the rate of concentration $\partial C_i / \partial t$ at time t, the concentration of particle C_i at time $t + \Delta t$ is updated from its value $C_i(t)$ according to

$$C_i(t + \Delta t) = C_i(t) + \Delta t \frac{\partial C_i}{\partial t}. \tag{6.10}$$

6.3 SPH formulation of no-flux boundary conditions

SPH suffers from the problems of particle deficiency near the boundary (Liu and Liu, 2003). For particles near the boundary, they have incomplete supporting domains as there are no particles outside the boundaries of the problem domain. Calculation of function values and derivatives would be problematic without special treatments. To apply no-flux boundary conditions on the channel wall, a set of virtual particles are introduced to construct a symmetrical scenario about the boundary surface (Libersky et al. 1993; Randles and Libersky, 1996). If the state variables are set such that they

are symmetric about the boundary, there would be no exchange of the materials across it.

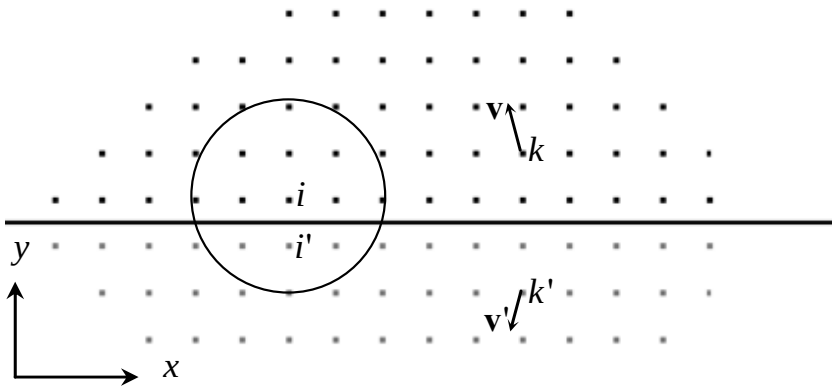

Fig. 6.3. No-flux boundary conditions in SPH. The supporting domain of particle i near the solid boundary (thick solid line) is incomplete. To facilitate SPH calculation, virtual particles (gray dots) are introduced by reflecting the real particles (black dots) against the boundary. Examples of virtual particles are i' and k' being reflection of real particles i and k respectively. The scalar field variable of a virtual particle is set the same as its corresponding real particle, while the vector variables are set such that the virtual particle has a value $\mathbf{v}'$ being reflection of that of the real particle $\mathbf{v}$.

As shown in Fig. 6.3, virtual particles i' and k' are generated from real particles i and k respectively. If, for example, the no-flux boundary surface lies in $xz-$plane, the scalar field variables at particle i' are set as

$$\begin{aligned} C_{i'} &= C_i \\ \Phi_{i'} &= \Phi_i \\ S_{i'} &= S_i \end{aligned} . \qquad (6.11)$$

In the calculation of concentration change, the values of the flux at the virtual particle are set as the reflected vector against the no-flux boundary in the $xz-$plane, such that

$$\begin{Bmatrix} J_{i'}^{x} \\ J_{i'}^{y} \\ J_{i'}^{z} \end{Bmatrix} = \begin{Bmatrix} J_{i}^{x} \\ -J_{i}^{y} \\ J_{i}^{z} \end{Bmatrix} \tag{6.12}$$

Such treatments permit one to calculate variables for the particles near the boundary in the same way as those for the interior particles. Meanwhile the no-flux boundary conditions are satisfied automatically.

6.4 Periodic boundary conditions

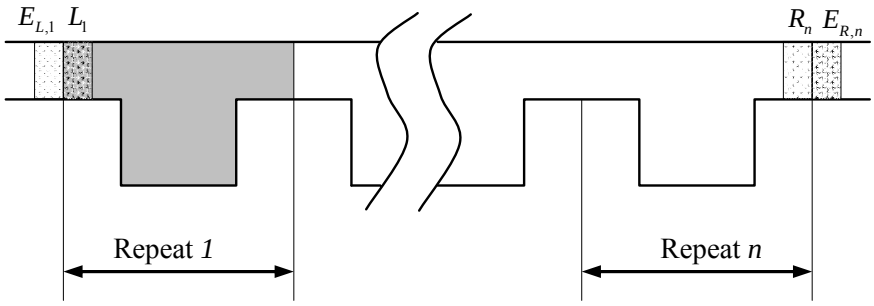

Fig. 6.4. Periodic boundary conditions for multiple-repeated nanofilter array. Periodic boundary conditions are implemented through virtual particles in two extended regions by duplicating the state variables of real particles in L_1 to the corresponding virtual particles in $E_{R,n}$ and those in R_n to $E_{L,1}$.

Our model nanofilter array contains up to 20 repeats for the purpose of the numerical simulation. However, the actual nanofilter arrays contain tens of thousands repeats. Without appropriate treatment, the model channel is unable to describe the dynamics of DNA molecules in long channels. The flux is heavily dependent on the state at the two openings of the channel. One commonly adopted method is to apply periodic boundary conditions, in which the rightmost portion of the structure is interacting which the leftmost portion of the next structure that is identical to itself. If some

molecules flow out from the right end of the channel, the same amount of molecules enter the system from the left end. This guarantees mass conservation of the molecules in the system and incorporates of the effects of other repeats that are not described in the model.

Owing to the fact that SPH simulation runs on a local domain, the treatment of repeated boundary conditions is very simple. As shown in Fig. 6.4, in calculation for the repeat 1, the state variables of the virtual particles in region to the left of the repeat ($E_{L,1}$) are copied from the right most portion of the repeat *n* (R_n as shown in fine dots). Similarly the state variables in the extended virtual particle region of repeat *n* ($E_{R,n}$) is copied from the left most portion of repeat 1 (L_1). As long as the widths of these virtual extended regions are larger than the radius of the supporting domain, the results for the real particles representing repeat *1* and repeat *n* are correct. If the peak width of the concentration is less than the half of the channel length (which guarantees that head of the peak does not catch up the end of it from the back), the dynamics of molecules in this model system is the same as that in the infinitely long channel.

6.5 Simulation of nanofiltration using SPH

In our simulation, a 20-repeat model structure is used to analyze the evolution of concentration of the DNA molecules in the channel space. Each unit cell of nanofilter is discretized with an assembly of 6000 particles, every one of which represents a fraction of DNA solution within the nanoarray. All the field functions including DNA concentration, electric field, orientational entropy, flux density *etc.* are calculated at the centers of these particles. Periodic boundary conditions are applied to this 20-

repeated structure in order to simulate effects of the neighboring repeats and ensure the conservation of mass in the system. At the beginning, the concentration at particles at the entrance of the first repeat is set to 1 (arbitrary unit), while the concentration at other particles as are 0. Flux and concentrations at later time steps are calculated according to master transport equations and the field variables at the current time. Evolution of the concentrations of DNA molecules in this model nanofilter array is therefore obtained. The results will be given in the next chapter.

7 Results and discussions

In an experiment conducted earlier in MIT (Li et al. 2008), the migration of DNA molecules of 50bp, 150bp and 300bp across the nanofilter array was studied under the electric field strengths of 57, 29 and $14 V/cm$ respectively. The specifications of the nanofilter cell are $d_s = 60\,\text{nm}$, $d_d = 240\,\text{nm}$, and $l_s = l_d = 500\text{nm}$. The total length of the nanochannel is $\tilde{L} = 1$ cm, corresponding to a repeat number of $n = 10000$. Mobilities and dispersions are measured, against which our simulation results will be compared. As the input parameters of the numerical simulation, the free-solution mobilities for 50bp, 150bp and 300bp DNA molecules are 3.38×10^{-4}, 3.6×10^{-4}, and $3.72\times10^{-4}\ cm^2V^{-1}s^{-1}$ respectively. The free-solution diffusion coefficients of these molecules are calculated using Eq. (2.2). For numerical simulations, the spatial domain is discretized by particles of size $5\text{nm}\times5\text{nm}$. Electric fields, configurational entropies, concentrations and fluxes are evaluated at centers of these particles. Simulation results of evolution times and dispersions will be compared with the experimental data.

7.1 The electric field

The electric potential is calculated through solving the Laplace's equation Eq. (5.4) with boundary conditions described by Eqs. (5.5). The profile of the nonuniform electric field is shown in Fig. 7.1. From these electric fields, the effect of inhomogeneous field lines on the distribution can be estimated. Because the

orientation dependent electric potential difference ($\left|\frac{(\Phi_A+\Phi_B)q}{2}-\Phi_C q\right|$) at any orientation (direction of the rod's x') is at least three orders smaller than k_BT at any point within the nanochannel for the DNA lengths and electric fields studied here, the effect of inhomogeneous field lines on the orientational distribution of DNA is negligible compared to that caused by the rotational diffusion. As a result, even under these inhomogeneous electric fields, the assumption of the uniform orientational distribution is still valid even when the DNA.

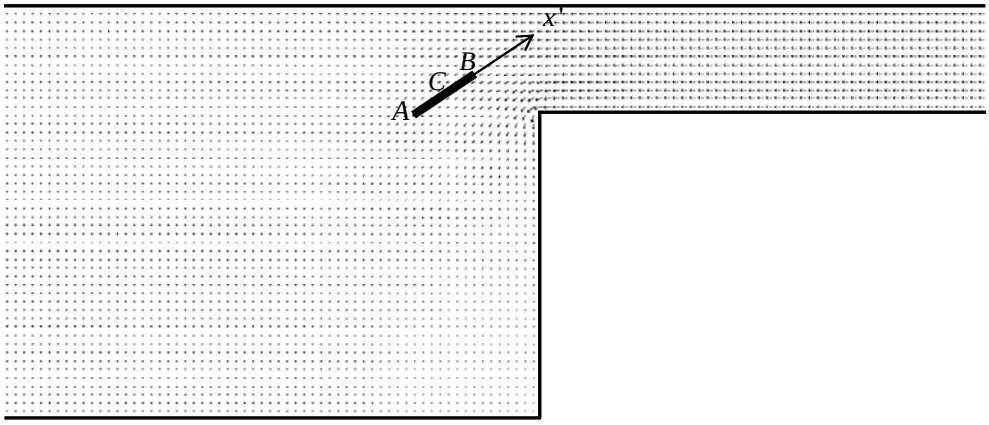

Fig. 7.1. The inhomogeneous distribution of electric field in space of the nanofilter.

7.2 Orientational entropy, diffusion coefficient and the electrophoretic mobilities in the nanochannel

When a DNA molecule is located in the confined space of a nanochannel, some of its orientations are forbidden due to the presence of the channel wall. This induces an orientational entropy that is given by Eq. (3.5). In the calculation of $S(\mathbf{r})$, the values of $\rho_\Theta(\mathbf{r})$ are determined numerically by enumerating all possible values of $\mathbf{\Theta}$ and checking their hindrances at position $\mathbf{r}$. As an example, the gradient of entropy of

15nm DNA rods in a nanofilter is shown Fig. 7.2. These gradients pointing to the internal region of the channel constitute an entropic force that drives the DNA molecules to the internal region of the channel.

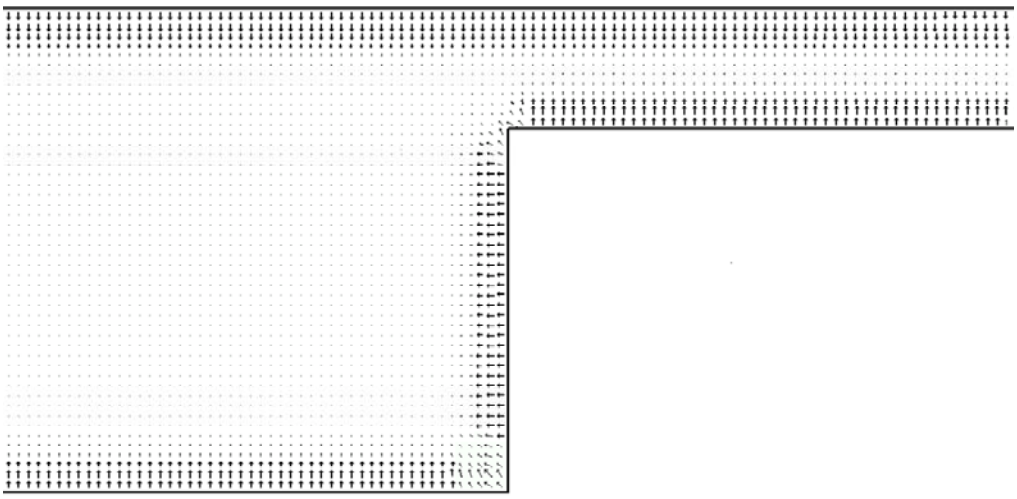

Fig. 7.2. The gradient of configurational entropy of a 150bp DNA rod in space of the nanofilter. A DNA rod has higher entropy in the internal region than that near the channel wall. This entropy difference forms an effective force that drive DNA molecules near the boundary to the internal region of the nanochannel.

When a DNA rod loses some of its orientation freedom due to confinement by the channel wall, its translational diffusion and entropic mobility would be affected. In this case, the probability that DNA molecules are aligned in the direction of channel axis (x-axis) is much higher than that in direction of depth ($y-$axis) if the dimension of the nanofilter is comparable to the length of the DNA. As a result, components of the electrophoretic mobility and diffusion coefficient in x-direction are larger than their counterparts in $y-$direction. The longer the rod is, the higher these differences are. In order to evaluate the effect of this spatial confinement on the transport parameters, tensors of translational diffusion coefficient and electrophoretic mobility for each particle are calculated using (5.13) and (5.14), respectively. Then a relative

diffusion coefficient and a relative electrophoretic mobility are defined as the ratio of their values in confined space to their respective isotropic free-solution values, *i. e.*

$$\mathbf{D}' = < \mathbf{D^d} > / \bar{D}^d, \tag{7.1}$$

and

$$\mathbf{U}' = (< \mathbf{U^e} > + U_{EEO}) / (\bar{U}^e + U_{EEO}), \tag{7.2}$$

respectively, where the bracket $< \cdot >$ represents the average over all the particles in a specific domain (the well or the slit of the nanofilter). Among all the components in the tensor $\mathbf{D}'$ and $\mathbf{U}'$, D'_{xx} and U'_{xx} have the most significant effect as the external force are applied in this direction and the motions in other directions are confined or canceled by each other.

Fig. 7.3 shows the values of D'_{xx} and U'_{xx} of DNA rods of different sizes in deep and shallow regions of the nanoarray. It could be seen that the relative diffusion coefficient D'_{xx} is close to 1.0 at all conditions, indicating that the spatial confinement does not affect the diffusion coefficient significantly. On the contrary, the relative electrophoretic mobilities are affected by the electroosmotic flow and may induce very large changes in U'_{xx}. In the cases where $U_{EEO} \sim -\bar{U}^e$, a small deviation in $< U^e_{xx} >$ from $\bar{U}^e$ yields a much larger U'_{xx}, which will change the final mobility significantly. For the studied experimental conditions here, the effective electrophoretic mobility is increased by ~40% for a 300bp DNA in the shallow region in *x*-direction compared with free-solution value, while the increase for a 50bp DNA is less than 10% based on the structure of the nanoarray under investigation.

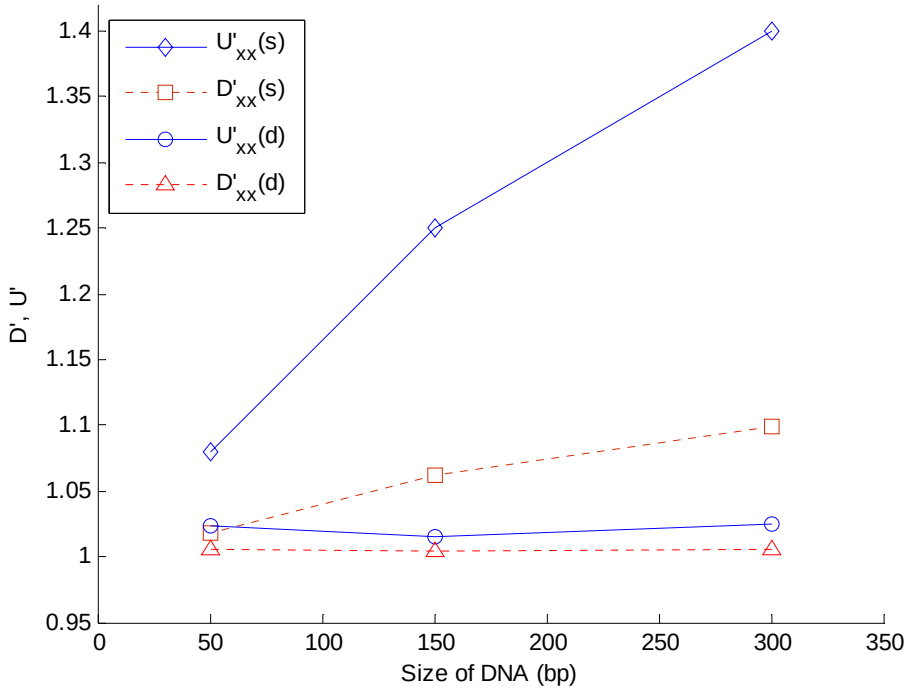

Fig. 7.3. The dependence of the relative diffusion coefficients and relative electrophoretic mobilities on the sizes of DNA molecules in deep wells (*d*) and shallow slits (*s*) of the nanofilter. Only components in the direction of channel axis (D'_{xx} and U'_{xx}) are shown because the effects of other components are much weaker due to spatial confinement in their relevant directions. The mobility U_{xx} is modified more significantly than the diffusion coefficient D_{xx} because of the presence of electroosmotic flow.

Such modification in the electrophoretic mobility may produce a totally different sequence of evolution peaks compared with that from wide channels where $\mathbf{D}^{\mathbf{d}}$ and $\mathbf{U}^{\mathbf{e}}$ are approximately isotropic. The diffusion coefficient is also affected by the constraints in the orientation space, but its magnitude is much smaller than that of the effective electrophoretic mobility.

7.3 Evolution of DNA concentration in the nanochannel

At $t = 0$, the concentration of the DNA molecule is set as 1.0 (arbitrary unit) within a

narrow band (its width is equal to the particle size) in the left side of the first repeat and the concentration in other regions is zero. For $t > 0$, the time and position dependant of DNA concentrations are obtained through integration of (5.2) and (5.3) using Eqs. (6.7), (6.9) and (6.10) with no-flux boundary conditions on the surfaces of channel walls.

$$\mathbf{J} \cdot \mathbf{n} = 0. \tag{7.3}$$

At any time, the concentration profile along the channel axis is obtained by the summation of the amount of DNA molecules in all the particles having the same coordinate along the channel axis. One example of concentration distribution along the channel axis is shown Fig. 7.4. It could be found that the concentration profiles along the channel axis are complicated because of the partitioning between the alternate wells and slits.

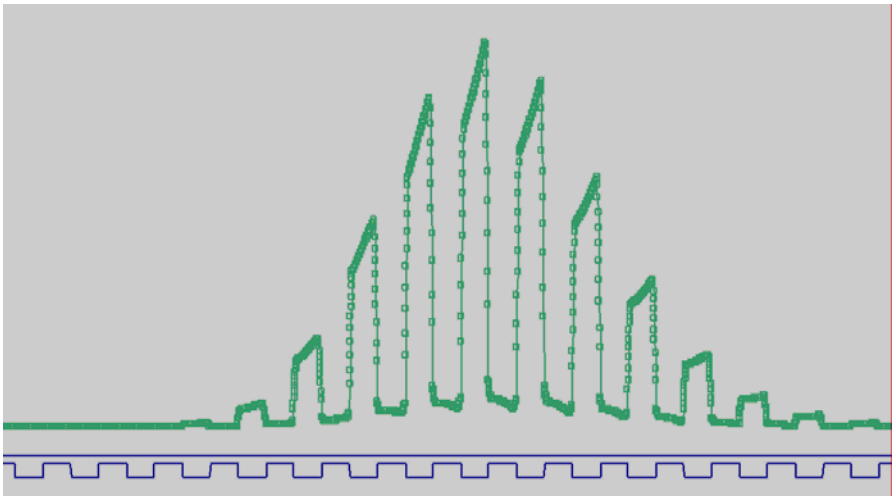

Fig. 7.4. One-dimensional distribution of DNA concentration along channel axis. The entropic trapping effect can be observed from the significantly increased amount of DNA molecules in the deep well near the entrance of the shallow slits.

Direct analysis of the concentration profiles as shown in Fig. 7.4 is quite complicated. However, when one focuses on time dependant concentration values at the end of each repeat (one example using 50bp DNA and 57V/cm filed is shown in Fig. 7.5), one can find that these values are well described by a Gaussian zone

undergoing constant translation and broadening (Giddings, 1991). In the next section, theory of one-dimensional zone evolution used to obtain the effective speed of translation and rate of zone broadening, from which the evolution time of DNA molecules over channel of any length can be estimated.

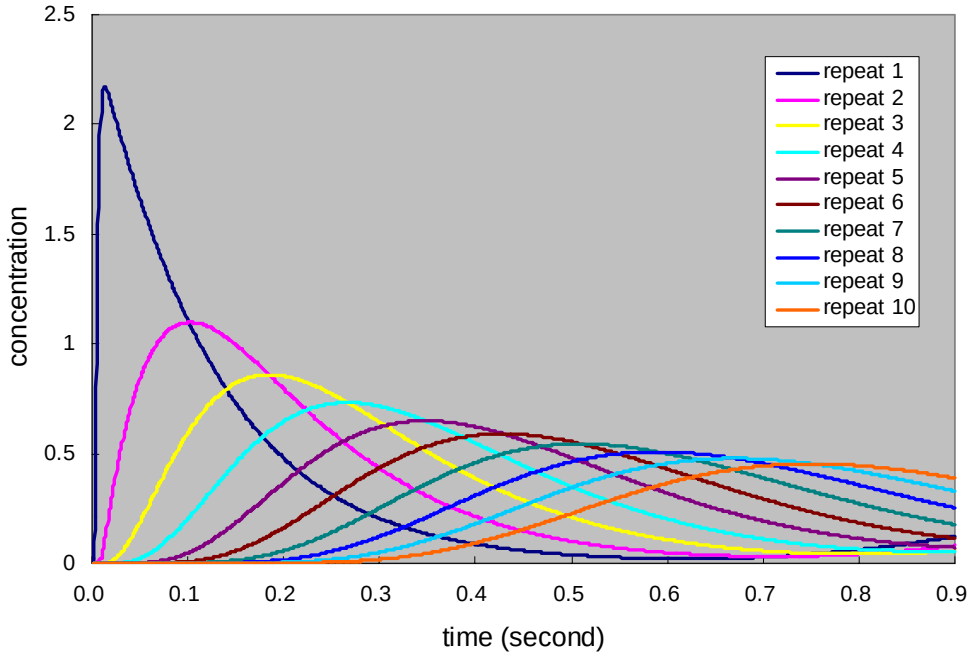

Fig. 7.5. Time dependence of DNA concentrations at the end of first 10 repeats of the nanofilter array. As DNA molecules migrate in the channel, the molecules become dispersed because of the diffusion and the trapping effect. Longer time is required for the peak to pass a detection point at farther distance from the origin. In addition, the concentration curves detected at farther distance are also broader and shorter.

7.4 Effective zone formation and evolution

Assuming that the initial peak width is zero, the shape of the zone undergoing constant spreading and translation observed at time t by a detector located at a distance $\tilde{L}$ takes the form (Giddings, 1991),

$$y(\tilde{L},t)=\frac{\tilde{n}}{\sqrt{2\pi}\sigma_T}\exp[-\frac{(\tilde{L}-\tilde{V}t)^2}{2\sigma_T^2}], \tag{7.4}$$

where $\tilde{n}$ is the amount of the DNA; $\tilde{V}$ is the apparent traveling velocity; and σ_T^2 is the spatial variance of the Gaussian zone. By assumption, σ_T^2 increase linearly with respect to t, *i. e.*

$$\sigma_T^2=\Gamma t, \tag{7.5}$$

where Γ denotes the combined zone broadening rate as the DNA molecules are passing though the filtration device. The peak passing time at distance $\tilde{L}$ is obtained from the solution of equation $\partial y/\partial t=0$,

$$t^P(\tilde{L})=\frac{-\Gamma+\sqrt{\Gamma^2+4\tilde{L}^2\tilde{V}^2}}{2\tilde{V}^2}. \tag{7.6}$$

From our simulation results, one can obtain the peak passing time $t^p(\tilde{L}_i)$ at the end of each repeat $\tilde{L}_i=i\cdot p,\ \ i=1,2,\ldots,n$. Parameters $\tilde{V}$ and Γ are estimated from curve fitting using Eq. (7.6). Once Γ and $\tilde{V}$ are known, evolution time and dispersion of the DNA at the end of channel of any length can then be calculated accordingly.

This expression of peak passing time in Eq. (7.6) approaches the widely adopted one

$$t^P(\tilde{L})=\tilde{L}/\tilde{V}, \tag{7.7}$$

when $\tilde{L}>>\Gamma/\tilde{V}$. Therefore as long as the channel length $\tilde{L}$ is significantly larger than the plate height

$$H=\Gamma/\tilde{V}, \tag{7.8}$$

or the number of plates is significantly greater than 1, electrophoretic velocity can be estimated from

$$\tilde{V} = \tilde{L} / t^{P}(\tilde{L}). \tag{7.9}$$

However, the maximum channel length is $20\mu m$ in our model, while the plate height is about $1 \sim 9\mu m$, corresponding to the number of plates of $2 \sim 22$. Therefore, one can not estimate the parameters Γ from the peak width at half height, and $\tilde{V}$ from Eq. (7.9), which are widely adopted in experimental studies.

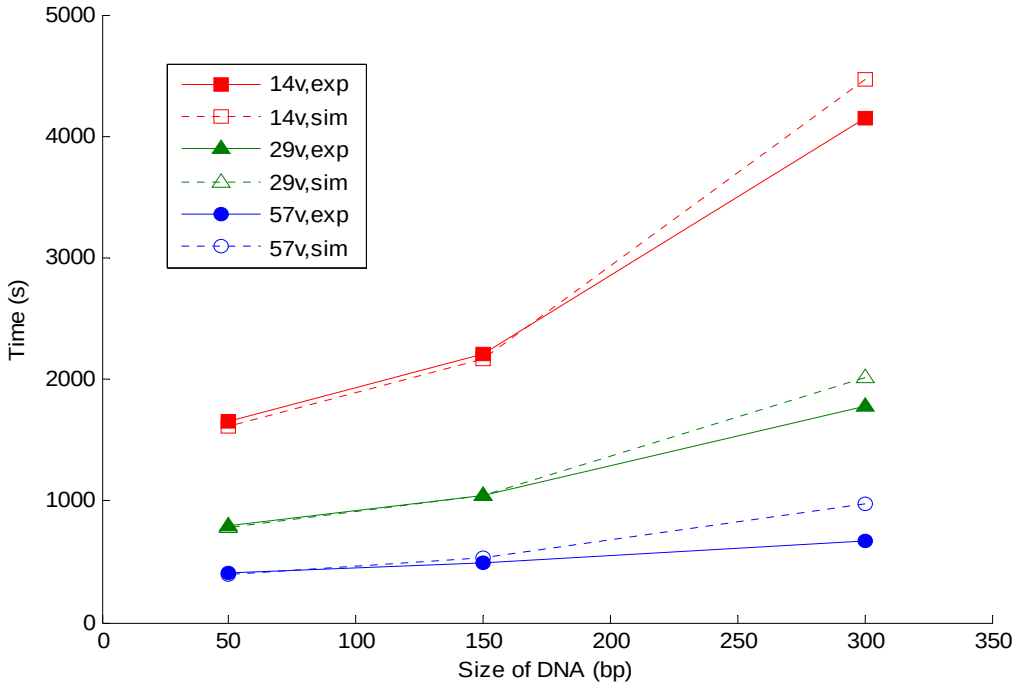

Fig. 7.6. The comparison of simulated evolution times with the experimental ones. The simulation evolution times agree well with their corresponding experimental data for 50bp and 150bp DNA molecules. For a 300bp DNA, its evolution time is overestimated in the simulation due to over-estimated entropy barrier.

The simulation and experimental results of evolution times of DNA molecules of various sizes subjected to different electric fields over 1 cm nanochannel are shown in Fig. 7.6. The simulation results are in good agreement with the experimental ones for 50bp and 150bp DNAs. However, the traveling time for 300bp DNA is overestimated in this simulation. This difference has to be attributed to the factors that are not

considered in our simulation model. As the persistence length of DNA is about 50 nm (~150bp), DNA segments of 300bp are deformable under thermal fluctuations. In our simulation, however, DNA molecules are treated as rigid rods, thereby the entropy barrier at confined region is overestimated compared with the actual deformable molecules. The result of this overestimation is that the traveling time of the 300bp DNA is longer than the experimental results.

7.5 Normalized mobility and size selectivity

The normalized mobility U^* of the DNA through the nanofilter array is defined as $U^* = \tilde{V}/(E_{av}U_{\max})$, where $U_{\max}$ is the maximum sieving free mobility. Experimentally, the maximum sieving free mobility across the nanofilter array is obtained by extrapolation of the mobility curve to a zero length (Fu et al., 2005). Size selectivity of the nanofilter device is characterized by the derivative of normalized mobility with respect to the DNA size, dU^*/dN (N is the size of DNA in bp). As shown in Fig. 7.7, the normalized mobility is dependent on both the electric fields and the DNA sizes. Low field strength leads to a steeper mobility slope, corresponding to a better size selectivity. However, reducing the electric field lengthens separation time, which will increase the dispersion and compromise the resolution of the separation. A tradeoff between the size selectivity, separation time, and peak dispersion is required to obtain optimized separation results.

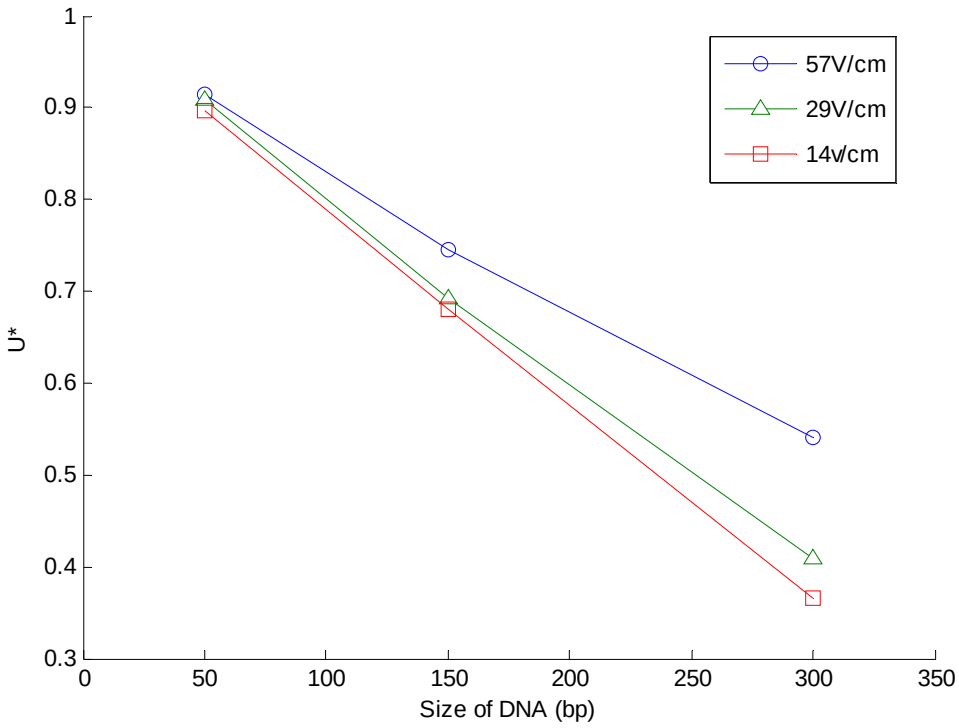

Fig. 7.7. The dependence of relative mobility on DNA sizes under different electric field strengths calculated from simulation data with consideration of electro-osmotic flow. Lower electric field leads to a higher mobility difference for DNA sizes, or a higher selectivity.

7.6 Band dispersion

As shown in Fig. 7.8, the dispersion data obtained from the simulation are generally comparable in magnitudes to the experimental data. However, the model-predicted dispersion decreases as the DNA size or electric field strength increase, while the experimental data show an almost length- and field- independent dispersion behavior. These differences are mainly due to the simplicity of our simulation model.

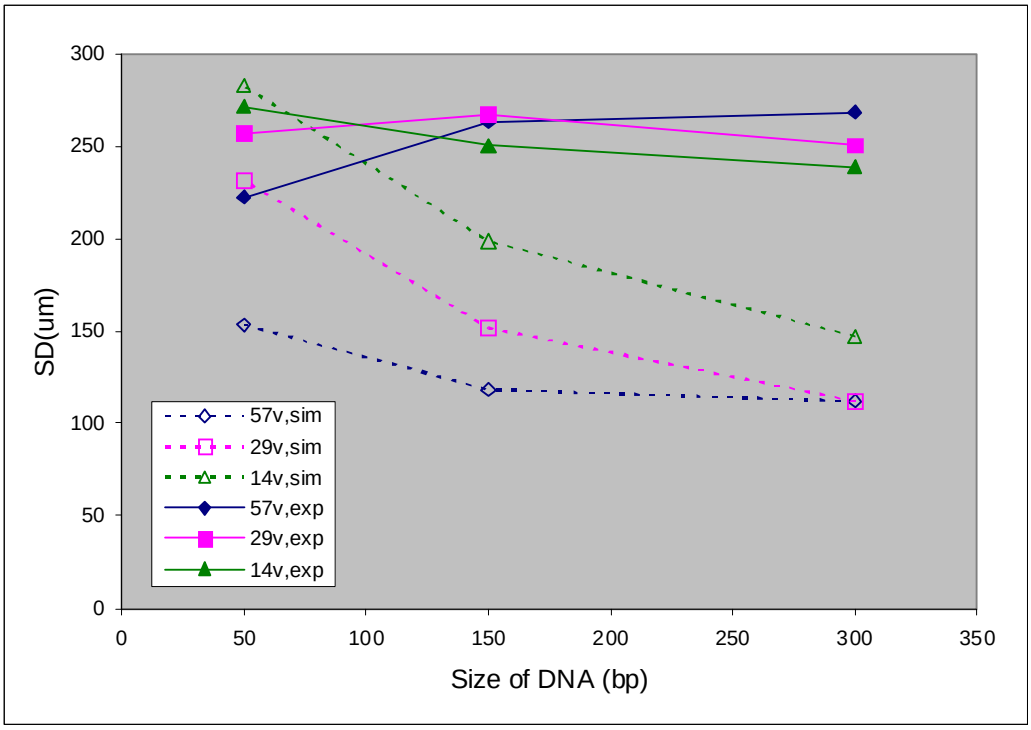

Fig. 7.8. The experimental and simulation dispersions under different electric field strengths against DNA sizes. Compared with experimental data that are generally size and field independent, variances in simulation are dependent on both factors. The deviation between the experimental and simulation data is due to the simplicity of this model, in which only the diffusive dispersion and convective dispersion are considered. Other unconsidered factors that might contribute to dispersion may include inter-molecule interactions, flexibility of molecules, stochastic nature of dye attachment *etc.*

The band broadening in this simulation model is caused by several mechanisms. The diffusive dispersion is induced by the random Brownian motion of the DNA molecules. The convective dispersion is due to the exponential decaying of the concentration with time as DNA molecules are travelling from one deep well to the next one (crossing the energy barrier in the shallow slits). In addition, there is another dispersion arising from the field non-uniformity (which provides different field lines for the molecules to take) in the deep well of the device. Our method models all the above-mentioned dispersion mechanisms appropriately. Among the three dispersion mechanisms discussed above, diffusive dispersion would be more severe for shorter

DNA molecules, while the convective dispersion would be independent of the DNA length.

Other factors that are not considered in this thesis might include the intermolecular interactions, the stochastic dye attachment, the flexibility of DNA molecules, and Joule heating *etc*. Non-uniform dye labeling will definitely contributes to the dispersion (width of peak) because it causes the DNA molecules in the experiment to have slightly different free-solution electrophoretic mobility. Any modification of the electrophoretic mobility may cause significant alteration in the effective electrophoretic mobility in the presence of electro-osmotic flow (because these two terms are similar in magnitude and have opposite signs), which gives rises to the band widths. Also inter-molecular interactions, especially the repulsion between the charged molecules surely contribute to dispersion. In addition, flexibility of the DNA molecules is certainly a factor that contributes to the mismatch between the experimental results and the simulation data. It has been observed that the fitting is getting worse as the length of the chain increases, where the flexibility of the DNA increases. However, it is unbelievable that Joule heating is a factor in our experiments, simply because the nanochannels in the device are too thin (less than 500nm, even in 'deep' region). Therefore the amount of current going through the system is tiny compared with other standard microfluidic systems. Any temperature shift in this system caused by Joule heating would be negligible (Fu et al., 2005; Fu et al., 2006).

One should note that the selectivity of the nanofilter sieving systems is more straightforward to simulate, compared with dispersion behavior. In most of previous modeling of nanofilters and entropic trapping device (Doyle and Underhill, 2005; Fan et al., 2006; Duong-Hong et al. 2008), such as Brownian dynamics and dissipated participle dynamics, the selectivity is obtained by simulating the dynamics of a single

DNA molecule through one nanofilter, while the absolute value of the electrophoretic mobility is usually one of the fitting parameters. Under such formulation, the physics that are neglected in the model are accounted for by the modifications in the (free-solution) electrophoretic mobility. However, such a method does not work for calculation of dispersion. For these reasons, most of previous modeling studies focus mainly on the selectivity, not the dispersion. Our simulation model is developed to predict the dispersion, as well as the mobility, by solution of the continuum transport equation for a collection of molecules in a non-steady state condition. The magnitude of electro-osmotic flow is the only adjustable parameter (which is estimated as $\sim 4/5$ of the DNA's free-solution electrophoretic mobility) that is used to fit the selectivity. Although dispersions in some cases are underestimated due to omission of some factors mentioned above, they are largely comparable in size. Based on the correctly predicted mobility and approximately estimated dispersion, a practical evaluation of the quality of a nanofilter array is still achievable.

The deviations between the simulation data and the experiment ones may also be due, in part, the non-ideal shape of the nanochannel devices. Our simulation is based on the ideal, square-shaped device structure, while the actual nanofilter devices have rather sloped sidewalls between nanochannels and deep wells (Fu et al., 2006). In fact, micro/nanofluidic channel sidewalls are rarely ideal as shown in Fig. 1.2, which could have a significant impact on the separation of the molecules in the system, leading to modified sieving/dispersion characteristics.

8 Conclusions and future work

8.1 Concluding remarks

This thesis proposes a theoretical model based on continuum transport theory for analysis of electrophoretic traveling of the rod-like DNA molecules over repeated regular nanofilter arrays. Unlike computationally expensive, stochastic methods such as BD and DPD, this method focuses on the behavior of group of DNA molecules rather than a single one. It is therefore capable of investigating large time and length scale macroscopic phenomena. It can also provide the estimation of peak dispersion, which is often computationally prohibitive for the current stochastic modeling techniques.

Through the theoretical and simulation studies, it is established that the orientational entropy barrier in shallow slits plays a major role in the electrophoretic partitioning of the rod-like DNA molecules of different sizes across nanofilter arrays. In addition, the steric constraint in the shallow region increases the mobility of longer rod-like DNAs. This modification affects the separation results significantly if the mobility of electroosmotic flow is comparable in amplitude to the DNA's free-solution electrophoretic mobility. It may helps to explain the complex experimental data of short DNA electrophoresis over flat nanochannels observed by Pennathur *et al.,* (2007) and Cross *et al.,* (2007). These findings are critically important in design and optimization of nanofiltration devices for the separation of the rod-like electrolytes and charged particles of other geometrical shapes.

The most important contributions of this thesis to the field of nanofiltration are highlighted as follows:

(1) It is shown that the macroscopic continuum model is suitable for description of Ogston sieving process in nanochannels, as long as the microscopic physics, such as loss of orientational freedom in confined space, are properly incorporated into to continuum transport equations. This finding permits one to study this kind of nanofiltration problems without running extremely time-consuming stochastic simulations.

(2) Analytical formulas for the mobility and dispersion in such systems are obtained through a simplified one-dimension model. Physical mechanisms of entropic trapping are elucidated explicitly. Based on these formulas, a method for assessing and optimization of task-specific nanofilters and strength of electric fields is proposed. These methods and formulas are extremely important to the experimentalists

(3) The effect of the rotational diffusion on the partition of anisotropic particles are realized and quantified (through the mobility corresponding to the entropic force). This knowledge has significant consequences in our understanding of many processes involving transport of anisotropic particles in nanochannels.

8.2 Recommendation for future work

This thesis investigates the processes of nanofiltration from a totally different view. It can be extended in many aspects as described below:

A direct extension of the current work is to analyze nanofilters with sloped walls. Actual devices often have rather sloped sidewalls between shallow channels and deep

wells. This slop of the sidewall may affect the result of separation significantly. Although it is expected that the slope may produce a higher mobility, very little is known about its overall effects on the final outcome of the separation.

In the current work, the interactions between the charged biomolecules are ignored. This assumption is valid when the concentration of molecules is extremely dilute. Because all the molecules are charged, the repulsion between the molecules may play a significant role when the concentration of molecules becomes higher. This effect will give rises to the dispersion, which will provide a better description on the dispersion dynamics.

Another very important extension of this work is to model a ratchet structure. For example, one may consider a nanofilter array that has sloped sidewalls on one side and vertical walls on the other side. Such device may produce very high resolution of separation if nonsymmetrical voltages are applied.

From the physics point of view, deformation of polyelectrolytes should be considered because even the ~200bp DNA molecules are not strictly rigid rods in aqueous solutions. As the DNA molecules to be separated frequently are normally a few hundred base pairs in length, the mode of deformations for these molecules is comparably simple compared with very long ones. Consideration of deformation, even very approximately, can improve the quality of analysis. This can be achieved by inclusion of another potential energy term in calculation orientation-dependent parameters and variables.

The electrokinetic flow poses a lot of complications in the electric field driven nanofiltration system. This thesis circumvented this problem through introduction of an electroosmotic flow which is assumed to be directly proportional to the electric

field. This assumption is valid in cases of high ionic strength, where the Debye layer is significantly thinner than channel depth. However, this assumption may become invalid when the depth of the channel is in the order of nanometers. An extension of the current model with consideration of electrostatic energy and nonuniform electroosmotic flow in Debye layer may solve this problem.

Last but not least, the description of dispersions in this thesis is still far from complete. The dispersions considered in this thesis include only the diffusive dispersions and the convective dispersion caused by the trapping effect (induced by the energy barrier). A more detailed description may include the effect of nonuniform electric field, more complex osmotic flow etc.

References

1. Ajdari, A. and J. Prost. Free-flow electrophoresis with trapping by a transverse inhomogeneous field. Proc. Natl. Acad. Sci. USA, 88, 4468-4471. 1991.

2. Aksimentiev, A., J. B. Heng, G. Timp and K. Schulten. Microscopic kinetics of DNA translocation through synthetic nanopores. Biophys. J., 87, 2086-2097. 2004.

3. Allison, S. A. and S. Mazur. Modeling the free-solution electrophoretic mobility of short DNA fragments. Biopolymers, 46, 359-373. 1998.

4. Allison, S. A., Z. Li, D. Reed and N. C. Stellwagen. Modeling the gel electrophoresis of short duplex DNA by Brownian dynamics, cubic gel lattice with direct interaction. Electrophoresis, 23, 2678-2689. 2002.

5. Arvanitidou, E. and D. Hoagland. Chain-length dependence of the electrophoretic mobility in random gels. Phys Rev Lett., 67, 1464-1466. 1991.

6. Baumgartner, A. and M. Muthukumar. A trapped polymer chain in random porous media, J. Chem. Phys., 87, 3082-3088, 1987.

7. Berg, H. C., Random walks in biology, expanded edition, Princeton: Princeton University Press. 1993.

8. Bird, R. B., Dynamics of Polymeric Liquids, Vol. 2: Kinetic Theory, New York : John Wiley and sons. 1987.

9. Brenner, H., Taylor dispersion in systems of sedimenting nonspherical Brownian particles, J. Colloid Interface Sci., 71, 189-208. 1979.

10. Carrington A. and A.D. McLachlan, Introduction to magnetic resonance. pp. 187-189, New York: Harper & Row. 1967.

11. Chou, C. F., R. H. Austin, O. Bakajin, J. O. Tegenfeldt, J. A. Castelino, S. S. Chan, E. C. Cox, H. G. Craighead, N. Darton, T. A. J. Duke, J. Han and S. W. Turner, Sorting biomolecules with microdevices, Electrophoresis, 21, 81-90. 2000.

12. Cooper, K., E. Jakobsson and P. Wolynes. The theory of ion transport through membrane channels. Prog. Biophys. Mol. Biol., 46, 51-96. 1985.

13. Cross, J. D., Strychalski, E. A., Craighead, H. G., Size-dependent DNA mobility in nanochannels, J. Appl. Phys., 102, 024701. 2007.

14. Cummings, E. B., S. K. Griffiths, R. H. Nilson and P. H. Paul, Conditions for similitude between the fluid velocity and electric field in electroosmotic flow, Anal. Chem., 72, 2526-2532. 2000.

15. Debye, P., Polar molecules, New York: The Chemical Catalog Company. 1929.

16. Dorfman, K. D. and H. Brenner, Modeling DNA electrophoresis in microfluidic entropic trapping devices, Biomed. Microdevices, 4, 237-244. 2002.

17. Doyle, P. S. and P. T. Underhill, Brownian dynamics simulations of polymers and soft matter, In S. Yip, (ed.), Handbook of Materials Modeling, Springer, 2619-2630. 2005.

18. Duong-Hong, D., J.-S. Wang, G. R. Liu, Y. Z. Chen, J. Han and N. G. Hadjiconstantinou, Dissipative particle dynamics simulations of electroosmotic flow in nano-fluidic devices, Microfluidics and Nanofluidics, 3, DOI 10. 1007/s10404-007-0170-7. 2008.

19. Eimer, W. and R. Pecora, Rotational and translational diffusion of short rod-like molecules in solution, oligonucleotides. J. Chem. Phys., 94, 2324-2329. 1991.

20. Einstein, A., Zur Theorie der Brownschen Bewegung, Ann Phys-Berlin, 19, 371 –381. 1906.

21. Español, P. and P. Warren, Statistical mechanics of dissipative particle dynamics Europhys. Lett., 30, 191-196. 1995.

22. Español, P., Dissipative Particle Dynamics, in: V. M. Harik and M. D. Salas (ed.), Trends in Nanoscale Mechanics:. Analysis of Nanostructured Materials and Multi-Scale Modeling, Netherlands: Kluwer Academic Publishers. 2003.

23. Fan, X. J., N. Phan-Thien, S. Chen, T. Y. Ng and X. H. Wu, Simulating DNA molecular suspension flow using dissipative particle dynamics. Physics of Fluids, 18, 063102. 2006.

24. Fu, J., J. Yoo and J. Han, Molecular sieving in periodic free-energy landscapes created by patterned nanofilter arrays. Phys. Rev. Lett., 97, 018103. 2006.

25. Fu, J., P. Mao and J. Han, A nanofilter array chip for fast gel-free biomolecule separation. Appl. Phys. Lett., 87, 263902. 2005.

26. Fu, J., R. B. Schoch, A. L. Stevens, S. R. Tannenbaum and J. Han, A patterned anisotropic nanofluidic sieving structure for continuous-flow separation of DNA and proteins. Nature Nanotechnology, 2, 121-128. 2007.

27. Giddings, J. C., E. Kucera, C. P. Russell and M. N. Myers, Statistical theory for the equilibrium distribution of rigid molecules in inert porous networks. Exclusion chromatography, J. Phys. Chem., 72, 4397-4408. 1968.

28. Giddings, J. C., Unified Separation Science, New York: John Wiley & Sons. 1991.

29. Groot, R. D. and P. B. Warren, Dissipative particle dynamics, bridging the gap between atomistic and mesoscopic simulation, J. Chem. Phys., 107, 4423-4435. 1997.

30. Han, J. and H. G. Craighead, Separation of long DNA molecules in a microfabricated entropic trap array, Science, 288, 1026-1029. 2000.

31. Han, J., S. W. Turner and H. G. Craighead, Entropic trapping of long DNA molecules at submicron size constriction. Phys. Rev. Lett., 83, 1688-1691. 1999.

32. Han, Y., A. M. Alsayed, M. Nobili, J. Zhang, T. C. Lubensky and A. G. Yodh. Brownian motion of an ellipsoid, Science, 314, 626-630. 2006.

33. Happel, J. and H. Brenner, Low Reynolds Number Hydrodynamics. The Netherlands: Kluwer Academic Publishers. 1991.

34. Heng, J. B., A. Aksimentiev, C. Ho, P. Marks, Y. V. Grinkova, S. Sugar, K. Schulten and G. Timp. The electromechanics of DNA in a synthetic nanopore. Biophys. J., 90, 1098-1106. 2006

35. Hogan, M. E., N. Dattagupta and D. M. Crothers, Transient electric dichroism of rod-like DNA molecules. Proc. Natl. Acad. Sci. USA, 75, 195-199. 1978.

36. Hur, J. S., E. S. G. Shaqfeh and R. G. Larson, Brownian dynamics simulations of single DNA molecules in shear flow, J. Rheol., 44, 713-742. 2000.

37. Hur, J. S., E. S. G. Shaqfeh, H. P. Babcock and S. Chu, Dynamics and configurational fluctuations of single DNA molecules in linear mixed flows, Phys. Rev. E, 66, 011915. 2002.

38. Kihm, K. D., A. Banerjee, C. K. Choi and T. Takagi, Near-wall hindered Brownian diffusion of nanoparticles examined by three-dimensional ratiometric total internal reflection fluorescence microscopy (3D R-TIRFM), Experiments in Fluids, 37, 811-824. 2004.

39. Kocherginsky, N. and Y. K. Zhang, Role of standard chemical potential in. transport through anisotropic media and asymmetrical membranes, J. Phys. Chem. B, 107, 7830-7837. 2003.

40. Kramers, H. A., The Behavior of Macromolecules in Inhomogeneous Flow, J. Chem. Phys., 14, 415-424. 1946.

41. Kratky, O. and G. Porod, Röntgenuntersuchung gelöster Fadenmoleküle, Rec. Trav. Chim. Pays-Bas., 68, 1106-1123. 1949.

42. Kuhn, W. and F. Grün, Relationships between elastic constants and stretching double refraction of highly elastic substances, Kolloid-Z., 101, 248–271. 1942.

43. Kum, O., W. G. Hoover and H. A. Posch, Viscous conducting flows with smooth particle applied mechanics. Phys. Rev. E, 52, 4899-4908. 1995.

44. Laachi, N., C. Declet, C. Matson and K. D. Dorfman, Nonequilibrium transport of rigid macromolecules in periodically constricted geometries. Phys. Rev. Lett., 98, 098106. 2007.

45. Lavalette, D., C. Tetreau, M. Tourbez, and Y. Blouquit. Microscopic viscosity and rotational diffusion of proteins in a macromolecular environment. Biophys. J. 76, 2744-2751. 1999.

46. Larson, R. G., Principles for coarse-graining polymer molecules in simulations of polymer fluid mechanics, Mol. Phys., 341-351, 2004. 102.

47. Larson, R. G., The rheology of dilute solutions of flexible polymers: Progress and problems, J. Rheol. 49, 1-70. 2005.

48. Larson, R. G., H. Hu, D. E. Smith and S. Chu, Brownian dynamics simulations of DNA molecules in an extensional flow field. J. Rheol., 43, 267–304. 1999.

49. Levine, A. J., T. B. Liverpool and F. C. MacKintosh, Mobility of extended bodies in viscous films and. membranes., Phys. Rev. E, 69, 021503. 2004.

50. Li ZR, Liu GR, Chen YZ, Wang JS, Bow H, Cheng Y, Han J (2008), Continuum transport model of Ogston sieving in patterned nanofilter arrays for separation of rod-like biomolecules, Electrophoresis, 29(2): 329-339.

51. Libersky, L. D., A.G. Petschek, T. C. Carney, J. R. Hipp and F. A. Allahadi, High strain Lagrangian hydrodynamics, J. Comput. Phys., 109, 67-75, 1993.

52. Liu, G. R., Liu, M. B., Smoothed particle hydrodynamics: a mesh-free particle method, Singapore: World Scientific. 2003.

53. Locke, B. R. and S. H. Trinh, When can the Ogston-Morris-Rodbard-Chrambach model be applied to gel electrophoresis, Electrophoresis, 20, 3331-3334. 1999.

54. Locke, B. R., Electrophoretic transport in porous media: a volume-averaging approach, Ind. Eng. Chem. Res., 37, 615-625. 1998

55. Lucy, L. B., A numerical approach to the testing the fission hypothesis, Astron. J., 83, 1013-1024. 1977.

56. Lukacs, G. L., D. Lechardeur, P. Haggie, N. Freedman and A. S. Verkman. Size-dependent DNA mobility in the cytoplasm and the nucleus. J. Biol. Chem. 275, 1625-1629. 2000

57. Lumpkin, O., Electrophoretic mobility of a porous sphere through gel-like obstacles, Hydrodynamic interactions, J. Chem. Phys., 81, 5201-5205. 1984.

58. Marko, J. F. and E. D. Siggia, Stretching DNA. Macromolecules, 28, 8759-8770. 1995.

59. Mercier, J.-F. and G. W. Slater, Universal interpolating function for the dispersion coefficient of DNA fragments in sieving matrices, Electrophoresis, 27, 1453–1461. 2006.

60. Monaghan, J. J., Smoothed particle hydrodynamics, Rep. Prog. Phys., 68, 1703-1759. 2005.

61. Morris, C. J. O. R., in: Peeters, H. (Ed.), Protides of the Biological fluids, Vol. 14, Elsevier, New York, pp. 543-551. 1966.

62. Muthukumar, M. and A. Baumgartner, Effects of entropic barriers on polymer dynamics. Macromolecules, 22, 1937-1941. 1989.

63. Muthukumar, M. and C. Y. Kong, Simulation of polymer translocation through protein channels. Proc. Natl. Acad. Sci. USA, 103, 5273-5278. 2006.

64. Muthukumar, M., Dynamics of polyelectrolyte solutions. J. Chem. Phys., 107, 2619-2635. 1997.

65. Muthukumar, M., Mechanism of DNA transport through pores, Annu. Rev. Biophys. Biomol. Struct., 36, 435-450. 2007.

66. Muthukumar, M., Polymer translocation through a hole. J. Chem. Phys., 111, 10371-10374. 1999.

67. Nkodo, A. E., J. M. Garnier, B. Tinland, H. Ren, C. Desruisseaux, L. C. McCormick, G. Drouin and G. W. Slater, Diffusion coefficient of DNA

molecules during free-solution electrophoresis, Electrophoresis, 22, 2424-2432. 2001.

68. Ogston, A. G., The spaces in a uniform random suspension of fibres. Trans. Faraday Soc., 54, 1754-1757. 1958.

69. Ohshima, H., Henrys function for electrophoresis of a cylindrical colloidal particle, J. Colloid Interface Sci., 180, 299-301. 1996.

70. Pennathur, S. and J. G. Santiago, Electrokinetic transport in nanochannels. 1. Theory. Anal. Chem., 77, 6772-6781. 2005a.

71. Pennathur, S. and J. G. Santiago, Electrokinetic transport in nanochannels. 2. Experiments. Anal. Chem., 77, 6782-6789. 2005b.

72. Pennathur, S., F. Baldessari, J. G. Santiago, M. G. Kattah and J. B. Steinman, Free-solution oligonucleotide separation in nanoscale channels, Anal. Chem., 79, 8316-8322. 2007.

73. Randles P.W. and L. D. Libersky, Smooth particle hydrodynamics: some recent improvements and applications, Comp. Meth. Appl. Mech. Eng, 139, pp. 375-408, 1996.

74. Rodbard, D. and A. Chrambach, Estimation of molecular radius, free mobility, and valence using acrylamide gel electrophoresis. Anal. Biochem., 40, 95-134. 1971.

75. Rodbard, D. and A. Chrambach, Unified theory of gel electrophoresis and gel filtration. Proc. Natl. Acad. Sci. USA, 65, 970-977. 1970.

76. Rouse, P. E. J., A theory of the linear viscoelastic properties of dilute solutions of coiling polymers. J. Chem. Phys., 21, 1272–1280. 1953.

77. Slater, G. W., S. Guillouzic, M. G. Gauthier, J. F. Mercier, M. Kenward, L. C. McCormick and F. Tessier, Theory of DNA electrophoresis. Electrophoresis, 23, 3791–3816. 2002.

78. Smith, D. E., T.T. Perkins and S. Chu, Dynamical scaling of DNA diffusion coefficients. Macromolecules. 29, 1372 (1996)

79. Smith, S. B., L. Finzi and C. Bustamante, Direct mechanical measurements of the elasticity of single DNA molecules by using magnetic beads, Science, 258, 1122-1126. 1992.

80. Sorlie, S. S. and R. Pecora. A dynamic light-scattering study of four DNA restriction fragments. Macromolecules. 23, 487-497. 1990.

81. Stellwagen, E., and N. C. Stellwagen, Determining the electrophoretic mobility and translational diffusion coefficients of DNA molecules in free solution, Electrophoresis, 23, 2794-2803. 2002.

82. Stellwagen, E., Y. J. Lu and N. C. Stellwagen, Unified description of electrophoresis and diffusion for DNA and oilier polyions, Biochemistry, 42, 11745-11750. 2003.

83. Stellwagen, N. C., C. Gelfi, and P. G. Righetti, The free-solution mobility of DNA. Biopolymers, 42, 687-703. 1997.

84. Stockmayer, W. H., Dynamics of Chain Molecules, in: Molecular Fluids, ed by R. Balian and G. Weill, London: Gordon & Breach. 1976.

85. Stokes, G. G., On the effect of the internal friction on the motion of pendulums, Trans. Camb. Phil. Soc., 9, 8-106. 1856.

86. Tinland, B, L. Meistermann, and G. Weill, Simultaneous measurement of

mobility, dispersion and orientation of DNA during steady state gel electrophoresis? Phys. Rev. E, 61, 6993-6998. 2000.

87. Tirado, M. M., C. L. Martinez and J. Garcia de la Torre, Comparison of theories for the translational and rotational diffusion coefficients of rod-like macromolecules. Application to short DNA fragments, J. Chem. Phys., 81, 2047-2052. 1984.

88. Turner, S. W., A. M. Perez, A. Lopez and H. G. Craighead, Monolithic nanofluid sieving structures for DNA manipulation, J. Vac. Sci. Techn. B, 16, 3835-3840. 1998.

89. Viovy, J. L., Electrophoresis of DNA and other polyelectrolytes, physical mechanisms. Rev. Modern Phys., 72, 813-872. 2000.

90. Volkmuth, W. D. and R. H. Austin, Electrophoresis in microlithographic arrays. Nature, 358, 600−602. 1992.

91. Vologodskii, A. V., DNA extension under the action of an external force. Macromolecules, 27, 5623-5625. 1994.

92. Wedgewood, L. E., D. N. Ostrov and R. B. Bird, A finitely extensible bead-spring chain model for dilute polymer solutions, J. Non-Newtonian Fluid Mech., 40, 119-139. 1991.

93. Yuan, C., E. Rhoades, D. M. Heuer, S. Saha, X. W. Lou and L. A. Archer, Comprehensive interpretation of gel electrophoresis data, Anal. Chem., 78, 6179-6186. 2006.

94. Zimm, B. H., Dynamics of polymer molecules in dilute solution, viscoelasticity, flow birefringence and dielectric loss, J. Chem. Phys. 24, 269–278. 1956.

Publications arising from the thesis

Conference papers:

1. **Li ZR**, Liu GR, Chen YZ, Wang JS, Hadjiconstantinou NG, Cheng Y, Han J, Anisotropic transport of rod-like DNA in patterned nanoarrays, a talk presented at Singapore MIT Alliance (SMA) Workshop on BioMEMS, Micro/Nano-fluidic devices: Simulation and Experimentation, organized by Computation Engineering Programme (SMA), 25 July 2007.

2. **Li ZR**, Liu GR, Han J, Chen YZ and Wang JS, Simulation of electrophoresis of rod-like DNA in patterned nanoarrays, 4th M.I.T. Conference on Computational Fluid and Solid Mechanics Jun 13-15, 2007 MIT, USA

3. **Li ZR**, Liu GR, Chen YZ, Wang JS, Hadjiconstantinou NG, Cheng Y and Han J, Linear thermodynamics of rod-like DNA filtration, The 7th SMA Annual Symposium Jan 23-24, 2007, Nanyang Technological University, Singapore

4. **Li ZR**, Liu GR, Chen YZ, Wang JS, Hadjiconstantinou NG, Cheng Y and Han J, Modified SPH method for simulating molecular filtration in nanofluidic sieving systems, Mini Symposium on Computational Engineering for Biotechnology and Nanotechnology July 27, 2006

5. **Li ZR**, Liu GR, Han J , Wang JS, Chen YZ and Hadjiconstantinou, Simulation Study on the Effect of Orientational Entropy on the Transport of Rod-like DNA over Regular Nanofilter Arrays, presented at International Conference on Materials for Advanced Technologies (ICMAT'07), 1-6 July, Singapore.

6. **Li ZR**, Liu GR, Cheng Y, Kocherginsky N (2006), Pressure-induced transport

through planar and hollow fiber membranes without supporting structure, 1st International Conference on Computational Methods (ICCM04), DEC 15-17, 2004, Computational Methods, PTS 1 & 2: 125-130.

7. **Li ZR**, Liu GR, Cheng Y, Mi D (2006), Designability of proteins and stability analysis upon dimerization using 2D lattice model, 1st International Conference on Computational Methods (ICCM04), DEC 15-17, 2004, Computational Methods, PTS 1 & 2: 131-136.

Journal papers:

1. **Li ZR**, Liu GR, Chen YZ, Wang JS, Bow H, Cheng Y, Han J (2008), Continuum transport model of Ogston sieving in patterned nanofilter arrays for separation of rod-like biomolecules, Electrophoresis, 29(2): 329-339.

2. **Li ZR**, Liu GR, Han J, Cheng Y, Chen YZ, Wang JS, Hadjiconstantinou NG (2008), Analytical description of Ogston-regime biomolecule separation using nanofilters and nanopores, Electrophoresis (Submitted).

3. **Li ZR**, Liu GR, Cheng Y (2005), Thermodynamic analysis of protein sequence-structure relationships in monomer and dimer forms, Physica A, 354:381-392.

4. **Li ZR**, Liu GR, Mi D (2005), Quantifying the parameters of Prusiner's heterodimer model for prion replication, Physica A, 346(3-4): 459-474.

5. **Li ZR**, Han, X., Liu GR (2004), Protein designability analysis in sequence principal component space using 2D lattice model, Comp. Meth. Prog. Biomed, 76: 21-29.